



**UNIVERSITY OF  
BIRMINGHAM**

**IMPACT OF STABILISER SELECTION ON THE  
UPTAKE OF POLYESTER NANOPARTICLES BY  
HEPATIC CELLS**

by

**İLAY SEMA ÜNAL**

**A thesis submitted to the University of Birmingham  
for the degree of  
DOCTOR OF PHILOSOPHY**

**School of Pharmacy  
The Institute of Clinical Sciences  
College of Medical and Dental Sciences  
University of Birmingham  
January 2024**

UNIVERSITY OF  
BIRMINGHAM

**University of Birmingham Research Archive**

**e-theses repository**

This unpublished thesis/dissertation is copyright of the author and/or third parties. The intellectual property rights of the author or third parties in respect of this work are as defined by The Copyright Designs and Patents Act 1988 or as modified by any successor legislation.

Any use made of information contained in this thesis/dissertation must be in accordance with that legislation and must be properly acknowledged. Further distribution or reproduction in any format is prohibited without the permission of the copyright holder.

## ABSTRACT

The development of new nanomedicines remains a priority for formulation scientists everywhere. It is also becoming increasingly apparent that a clear framework is needed to inform nanocarrier design and assessment to aid translation to the clinic. This seems particularly important for polymeric nanomaterials, where many factors need to be considered, including the impact of the stabiliser used in nanoparticle (NP) manufacture, which is the focus of this project.

This study will examine how polyester nanoparticles are taken up by hepatic cells. These cells were chosen as NPs are known to accumulate in the liver after intravenous (i.v.) administration, but little is known about the specific cells responsible for uptake. To this end, polyester NPs made from either poly(D,L-lactic acid) (PDLLA) or poly(lactic-*co*-glycolic acid) (PLGA), and using either polyvinyl alcohol (PVA) and Poloxamer 407 (PXM) as stabilisers were produced, characterised and tested *in vitro*. The NPs were synthesised by nanoprecipitation and met the stated quality attributes in terms of size (150-200 nm) and size distribution (PDI<0.2). The nature of the stabiliser had an impact on zeta potential (PVA<PXM), surface hydrophobicity (PVA>PXM) but this did not impact stability or protein adsorption (tested using BCA kit) after exposure to foetal bovine or human serum. NPs were loaded with Nile Red as a hydrophobic fluorescent dye and their uptake by immortalised cells representative of the different hepatic cells was studied. No clear trend between cell types could be detected using flow cytometry and fluorescent microscopy, but this might result from difficulties in analysing uptake data because of the fluorescence difference between NPs and requires further investigation.

Lactoferrin (LCF) is one of the ligands of asialoglycoprotein receptor (ASGP-R). LCF-targeted NPs were prepared and tested in a co-culture system involving HEP-G2 hepatomas, HMEC-1 endothelial cells and DTHP-1 macrophages to assess the feasibility of targeting hepatocytes

and determine whether NP's properties such as size, charge, and surface hydrophobicity were a barrier to achieving this. Modification with LCF did not significantly affect NP properties, though hydrophilicity did increase afterwards. Results showed increased uptake of LCF-coated PLGA-PVA NPs by HEP-G2 cells (2.6-fold,  $p < 0.01$ ) which was attributed to the ASGP-R since it is found in higher levels on hepatocytes than other hepatic cell types, while uptake by macrophages was not affected as expected since it is known that macrophages do not express ASGP-R.

To further investigate NP-cell interactions, bovine serum albumin (BSA) NPs were synthesised to compare the BSA NPs uptake behaviours of different hepatic cell lines. Here, citric acid was selected as the cross-linker. NPs, with a similar size and hydrophobicity as polyester NPs were produced. Uptake studies showed increased internalisation by THP-1 monocytes and DTHP-1 macrophage cells compared to HEP-G2 and HMEC-1 cell lines because of the higher phagocytic activity of the monocytes and macrophages than endothelial and epithelial cells. The overall findings provide an insight to importance on NP surface modification on the cellular uptake behaviour of hepatic cells.

*“In everything in the world, be it material, spiritual, or for success, the most genuine guide is knowledge, science. Seeking a guide other than science is lethargy, ignorance, and deviation from the true path.”*

*1924- Mustafa Kemal Atatürk*

## ACKNOWLEDGEMENT

I am deeply indebted to the Republic of Türkiye Ministry of National Education for giving me the opportunity to do research abroad and for all their support. I could not have undertaken this journey without my supervisor Dr Marie-Christine Jones, who guided me scientifically and mentally. I am also thankful to Dr Patricia Lalor for the recommendations on co-culture systems.

Many thanks to my lab mates Manna, Ibrahim, Shahreen, Tariq, Dira and Basant for their priceless help and the fun time they gave me in the lab and office. Each one of them has a unique place in my mind. I would like to extend my sincere thanks to the microscopy and flow cytometry specialists who taught me how to deal with these very expensive instruments, and for dealing with my endless questions.

Words cannot express my appreciation to my friends who supported me psychologically during this four-year and four-month period. I am grateful and indebted to my friends Özge, Hasan, Şule, and Büşra who opened their homes to provide me with the perfect conditions to write my thesis. Irem and Merve who are more than house-mates, my fate-mates deserve a huge thanks for being with me through “all this”.

The last and the best gratitude goes to my family; *annem Şerife, babam Mustafa*, and *kardeşim Bengisu* for patiently coping with my stress throughout my educational life and for their unconditional love and support, “*seviliyorsunuz*”.

## LIST OF ABBREVIATIONS

ABBREVIATION	DEFINITION
amp	Amplitude
ANOVA	Analysis of variances
ASGP	Asialoglycoprotein
BSA	Bovine serum albumin
CO <sub>2</sub>	Carbon dioxide
DLS	Dynamic light scattering
DMEM	Dulbecco's modified Eagle's medium
DMSO	Dimethyl sulfoxide
DPBS	Dulbecco's phosphate-buffered saline
DTHP-1	Macrophages differentiated from THP-1 monocytes
EGF	Epidermal growth factor
EPR	Enhanced permeability and retention
ESE	Emulsion solvent evaporation
EtAc	Ethyl acetate
FBS	Fetal bovine serum
Fc	Crystallizable fragment
FDA	U.S. Food and Drug Administration
GRAS	Generally recognised as safe
GM-CSF	Granulocyte-Macrophage Colony-Stimulating Factor
HCC	Hepatocellular carcinoma
HEP-G2	Human liver cancer epithelial cell
HIC	Hydrophobic interaction chromatography
HMEC-1	Human microvascular endothelial cells
HSA	Human serum albumin
HS15	Kolliphor® HS15
HSC	Hepatic stellate cell
HSP	Human serum protein
Ig	Immunoglobulin
IL	Interleukin
i.v.	intravenous
KC	Kupffer cell
LCF	Lactoferrin

ABBREVIATION	DEFINITION
LDL	Low density lipoprotein
LOD	Limit of detection
LOQ	Limit of quantification
LRP-1	Lipoprotein receptor-related protein
LSEC	Liver sinusoidal endothelial cell
MPS	Mononuclear phagocyte system
NaN <sub>3</sub>	Sodium azide
NP	Nanoparticle
PCL	Polycaprolactone
PBS	Phosphate buffer saline
PdI	Polydispersity index
PDLLA	Poly lactide
PEG	Polyethylene glycol
PLGA	Poly(lactic-co-glycolic acid)
PS	Polystyrene
PVA	Polyvinyl alcohol
PVP	Polyvinylpyrrolidone
PXM	Poloxamer 407
SAT	Salt aggregation test
SD	Standard deviation
TGF- $\beta$ R	Transforming growth factor-beta receptor
TEM	Transmission electron microscopy
THP-1	Human monocytic cell line
TLR	Toll-like receptor
TNF- $\alpha$	Tumour necrosis factor-alpha



## Table of Contents

### **Chapter 1: INTRODUCTION ..... 1**

1.1	The liver and diseases .....	1
1.1.1	Liver disease .....	2
1.1.2	Liver cells .....	3
1.2	Nanoparticles .....	6
1.2.1	Polyester NPs.....	8
1.2.2	Protein NPs .....	13
1.3	Targeting the liver.....	17
1.3.1	Passive targeting.....	17
1.3.2	Active targeting .....	18
1.3.3	Targeting specific liver cells.....	19
1.4	Aims and objectives.....	23

### **Chapter 2: OPTIMISATION, MANUFACTURE, AND CHARACTERISATION OF POLYESTER NANOPARTICLES ..... 24**

2.1	INTRODUCTION .....	24
2.2	Aims and objectives.....	26
2.3	MATERIALS AND METHODS.....	27
2.3.1	MATERIALS .....	27
2.3.2	METHODS .....	28
2.4	RESULTS AND DISCUSSION .....	34
2.4.1	Preparation of Polyester NPs.....	34
2.4.2	Characterisation of Polyester NPs .....	48
2.4.3	Colloidal stability .....	50

2.4.4 Hydrophobicity of the NPs .....	55
2.5 CONCLUSION.....	59

### **Chapter 3: MONOCULTURE STUDIES OF POLYESTER NANOPARTICLES 61**

3.1 INTRODUCTION .....	61
3.2 Aim and objectives: .....	62
3.3 MATERIALS AND METHODS.....	63
3.3.1 MATERIALS .....	63
3.3.2 METHODS .....	64
3.4 RESULTS AND DISCUSSION .....	69
3.4.1 Viability studies .....	69
3.4.2 Inflammatory potential .....	76
3.4.3 Uptake studies.....	79
3.5 CONCLUSION.....	88

### **Chapter 4: ACTIVE TARGETED PLGA NANOPARTICLES ON LIVER COCULTURE SYSTEM ..... 89**

4.1 INTRODUCTION .....	89
4.2 Aim and objectives: .....	91
4.3 MATERIALS AND METHODS.....	92
4.3.1 MATERIALS .....	92
4.3.2 METHODS .....	93
4.4 RESULTS AND DISCUSSION .....	96
4.4.1 Characterisation of the LCF-coated NPs .....	96
4.4.2 Co-culture uptake assay.....	98

4.5	CONCLUSION.....	104
-----	-----------------	-----

## **Chapter 5:    BSA NANOPARTICLES OPTIMISATION AND MONOCULTURE STUDIES        105**

5.1	INTRODUCTION .....	105
5.2	Aim and objectives: .....	106
5.3	MATERIALS and methods .....	107
5.3.1	MATERIALS .....	107
5.3.2	METHODS.....	108
5.4	RESULTS AND DISCUSSION .....	110
5.4.1	Preparation techniques of BSA NPs .....	110
5.4.2	Characterisation of BSA NPs .....	114
5.4.3	Colloidal stability .....	115
5.4.4	Hydrophobicity of the BSA NPs .....	117
5.4.5	Monoculture studies with BSA NPs .....	118
5.5	CONCLUSION.....	123

## **Chapter 6:    CONCLUSION AND FUTURE WORK.....125**

6.1	Conclusion .....	125
6.2	Future works .....	127

## **Chapter 7:    REFERENCES.....129**

## **Chapter 8:    SUPPLEMENTARY FIGURES.....148**

## LIST OF FIGURES

Figure 1.1 Schematic representation of the structure of liver (5).....	1
Figure 1.2 Schematic representation of the cellular structure of the liver (18) .....	3
Figure 1.3 Chemical structures of the common polysters.. .....	9
Figure 1.4 Emulsion solvent evaporation method for preparing polyester nanoparticles .....	10
Figure 1.5 Nanoprecipitation method for preparing polyester nanoparticles.....	10
Figure 1.6 Salting-out method for preparing polyester nanoparticles. ....	11
Figure 1.7 Dialysis method for preparing polyester nanoparticles.....	12
Figure 1.8 Supercritical fluid technology for preparing polyester nanoparticles. ....	12
Figure 2.1 Molecular structures of used stabilisers. ....	25
Figure 2.2 Standart curve for PXM .....	30
Figure 2.3 Standart curve for PVA.....	31
Figure 2.4 Colloidal stability of polyester NPs.. .....	41
Figure 2.5 Chemical and surface charge stability of polyester NPs.....	43
Figure 2.6 Impact of stabiliser concentration on NP properties. ....	46
Figure 2.7 Residual stabiliser quantification.. .....	48
Figure 2.8 Characterisation of polyester NPs.....	49
Figure 2.9 TEM images of the NPs. ....	50
Figure 2.10 NPs colloidal stability at (A) 4°C, (B) RT and (C) 37°C. ....	52

Figure 2.11 NPs zeta potential as a function of time.....	53
Figure 2.12 Stability of NPs after incubation in a 0.5 mg/mL BSA solution.....	54
Figure 2.13 Hydrophobicity assessment of the NPs. (A) SAT, (B) HIC index.....	56
Figure 2.14 BSA adsorption study. ....	57
Figure 2.15 HSP adsorption onto NPs.....	58
Figure 3.1 Stabilisers toxicity.....	70
Figure 3.2 Cytotoxicity of polyester NPs on J774 cells. ....	73
Figure 3.3 Cytotoxicity of polyester NPs on human cell lines.....	75
Figure 3.4 Inflammatory potential of polyester NPs.. ....	78
Figure 3.5 Uptake on NPs by HEP-G2 cells. ....	81
Figure 3.6 Uptake on NPs by HMEC-1 cells.. ....	82
Figure 3.7 Uptake on NPs by DTHP-1 cells. ....	83
Figure 3.8 Uptake on NPs by THP-1 cells. ....	84
Figure 3.9 Impact of NP coating on uptake.....	85
Figure 3.10 PVA:PXN MFI ratio for NPs. ....	86
Figure 4.1. Hepatic sinusoid structure.....	90
Figure 4.2 Preparation of co-cultures. ....	95
Figure 4.3 SAT of passively- and actively-targeted NPs. ....	98
Figure 4.4 Uptake of coated and uncoated PLGA NPs in receptor inhibition condition .....	100

Figure 4.5 Kinetics of PLGA-PVA NP diffusion through the naked insert. ....	101
Figure 4.6 The uptake of LCF-PLGA NPs and PLGA NPs.....	103
Figure 5.1 Impact of citric acid concentration on BSA NPs properties. ....	113
Figure 5.2 Characterisation of BSA NPs.....	114
Figure 5.3 TEM analysis of BSA NPs.....	115
Figure 5.4 Colloidal stability of BSA NPs. ....	116
Figure 5.5 Hydrophobicity assessment of BSA NPs.....	117
Figure 5.6 Cytotoxicity of BSA NPs. ....	119
Figure 5.7 Impact of BSA NPs on cytokine release.. ....	121
Figure 5.8 Cellular uptake of BSA NPs.. ....	123

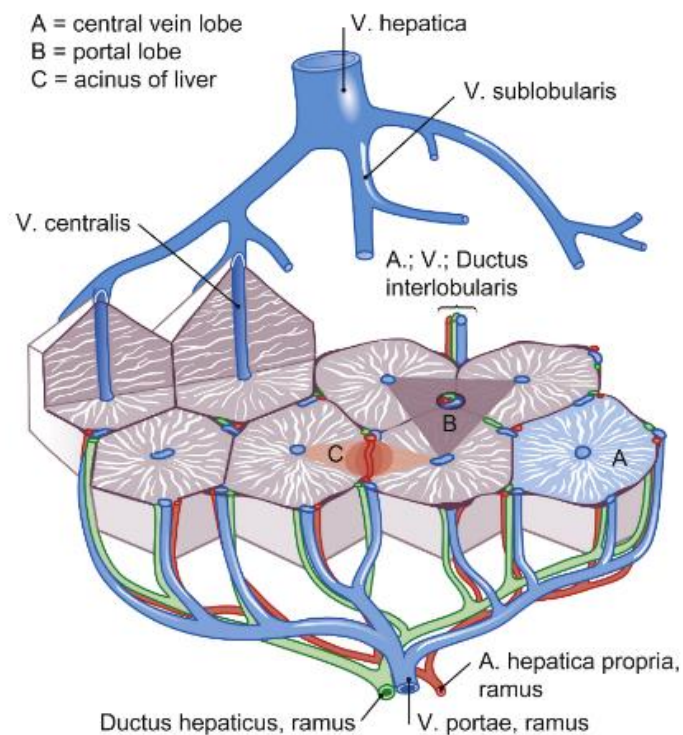
## LIST OF TABLES

Table 1.1 Polyester nanoparticle preparation method comparison.....	13
Table 2.1 Solvent properties s and solubility of polyesters and stabilisers. ....	35
Table 2.2 PCL NPs optimisation studies using EtAc. (n=1) .....	36
Table 2.3 PCL NPs optimisation studies using Chloroform. (n=1) .....	37
Table 2.4 Size and size distribution of polyester NPs prepared by ESE. ....	39
Table 2.5 Selected stabiliser concentrations for each polymer. ....	40
Table 3.1 Cytokine concentration calculation factors .....	67
Table 4.1. Impact of active targeting on NPs properties. (n=3, mean± SD) .....	96
Table 5.1 Kinetics of formation for BSA NPs prepared by by the denaturation technique (n=1) .....	111

# Chapter 1: INTRODUCTION

## 1.1 THE LIVER AND DISEASES

The liver is the body's largest gland and sits in the abdominal cavity, just below the rib cage. This highly-perfused organ play a crucial role in maintaining homeostasis and protecting the body from toxins (1-4). Hepatic tissue is comprised of a network of cells intertwined with bile ducts and blood vessels (**Figure 1.1**) (1). Blood flows at a speed of 1350 mL/min through the liver *via* the portal vein, enabled by low resistance to blood flow (4).



**Figure 1.1** Schematic representation of the structure of liver (5).



The liver has several crucial functions. The liver metabolizes and processes carbohydrates, fat, and proteins and contribute to energy reserves by storing glucose as glycogen. As an exocrine gland, the liver secretes 500 ml/day of bile to aid the digestion of fats into fatty acids, carbohydrates, and ketone bodies. The liver also contributed to the synthesis of cholesterol, phospholipids, and lipoproteins. As an endocrine gland, the liver produces vitamin D, insulin-like growth factor 1, and angiotensinogen, directly (6). It also synthesizes proteins, especially albumin, coagulation factors, and C-reactive proteins (opsonin) which have a crucial role in the body, influencing the pharmacokinetics of drugs and nanomedicines. More importantly, the liver plays a major role in the metabolism of xenobiotics and is the main site of distribution for passively-targeted nanomedicines (4). Owing to the presence of Kupffer cells (KCs), the liver also plays an important role in innate immunity (1, 4, 6).

### **1.1.1 Liver disease**

Liver diseases is an umbrella term that covers a variety of conditions from viral hepatitis to hyperbilirubinemia, fatty liver disease, liver fibrosis, cirrhosis, or hepatocellular carcinoma (HCC).

Hyperbilirubinemia, also known as jaundice, is a condition in which tissues turn yellow due to the accumulation of bilirubin (7, 8). Fatty liver disease is the accumulation of excess fat in hepatocytes, commonly related to obesity, diabetes, or excessive alcohol consumption (9).

Viral hepatitis is the inflammation of the liver caused by viral infections (hepatitis A-G), leading to liver dysfunction, cirrhosis, and liver failure (10). Liver fibrosis is the excessive accumulation of fibrous connective tissue in the liver because of chronic inflammation (11). This scar tissue prevents normal liver function and increase the risk of portal hypertension and liver failure (12); over time fibrosis can progress to cirrhosis (11, 12).

HCC originates in hepatocytes and is the most common type of liver cancer, accounting for 70-85% of primary liver cancers worldwide (13). In 2020, there were nearly 905,677 new cases of HCC and 830,180 deaths. Liver cancer is the third most common cause of cancer-related deaths in the world, after lung, and colorectal cancers (14) but only second to lung cancer in men (15). HCC can be primary or secondary to metastases or results from the progression of non-malignant liver disease.

Liver diseases causes nearly 2 million death every year (15). Additionally, over 1 million liver cancer cases are expected by 2025 (16) and prognosis is often poor (17). Therefore, the treatment of liver diseases is an area of high priority.

### 1.1.2 Liver cells

The liver is comprised of different cell types, namely hepatocytes, endothelial cells, phagocytic cells, lymphocytes, and fat-storing cells (4) each with distinct location and roles (**Figure 1.2**).

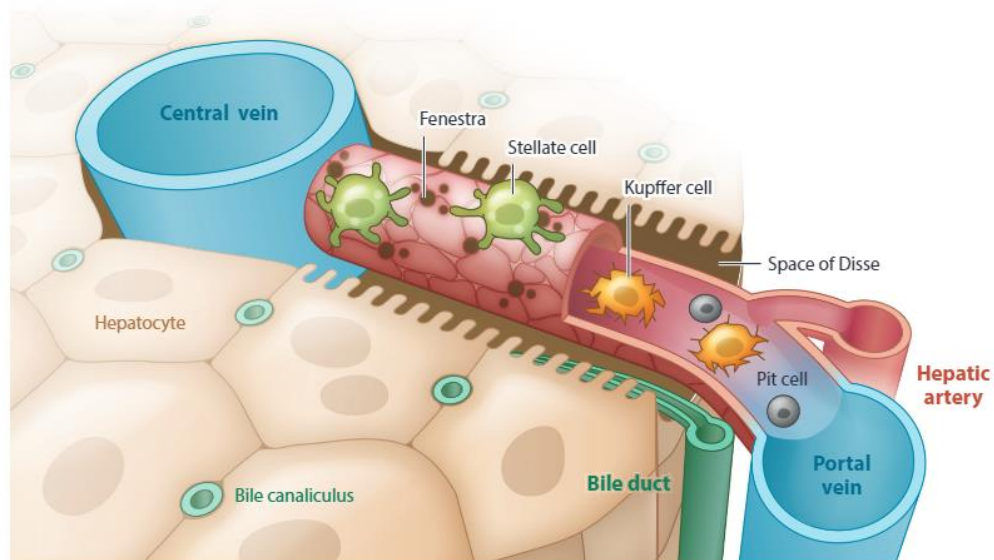


**Figure 1.2** Schematic representation of the cellular structure of the liver (18) “Figure adapted with permission from Erlich et al. (1999); *Annual Review Of Biomedical Engineering, Annual Reviews.*”

Hepatocytes are parenchymal cells and makes up ca. 70% of the liver. The remaining 30% is composed of non-parenchymal cells: liver sinusoidal endothelial cells (LSECs, 15%), KCs (6%), pit cells (lymphocytes; 5%), biliary cells (<5%), and hepatic stellate cells (HSCs, <1%) (19, 20). Each cell type is unique in terms of properties and functions.

### ***Hepatocytes***

Hepatocytes, the primary functional cells in the liver, regulate various cellular processes related to digestion, immunity, detoxification. Hepatocytes secrete lipoproteins and bile acid and play a role in storing glucose as glycogen. Many receptors are expressed by hepatocytes, including insulin receptors (21), progesterone receptors (22), immunoglobulin A (IgA) receptors (23), glycyrrhetic acid receptors (24, 25), and scavenger receptors which reflect the many functions these cells play (24, 26, 27). Importantly hepatocytes also express the ASGP-R which binds to galactose, hyaluronic acid, lactose, lactobionic acid, LCF and pullulan and hepatocytes have been targeted in nanomedicine development (24, 25, 28). Low density lipoprotein (LDL) receptor has been used for the same purpose (29, 30).

### ***Liver sinusoidal endothelial cells***

LSECs are located next to hepatocytes and are walls of the blood vessels irrigating the liver. Their strategic position allows these cells to fulfil their role contributing to exchange of nutrients, hormones and waste products. They possess unique structural features in the form of fenestrations, the diameter of which can change reach 100-200 nm in response to change in their environment (20, 31). These fenestrations allow chylomicron-like particles (75-300 nm) to reach hepatocytes (32), where they play a crucial role in lipid metabolism. These fenestrations can play a role in the accumulation of nanomedicines in the liver (33) and require careful consideration when designing new formulations.

LSECs have specific receptors designed to recognise and bind to low-density lipoprotein, known as lipoprotein receptor-related protein (LRP-1) (34). Scavenger receptors on LSECs include SR-B1, CD36, Lox-1, mannose receptor, and contribute to stabilin uptake and waste removal (24, 35). FcγRIIb are antibody mediated receptors that bind to Ig-Gs (31, 36) and Toll-like receptors (TLR) play a role in immune response by clearance of pathogens (28, 31).

### ***Kupffer cells***

KCs are the resident phagocytes of the liver and the main macrophages population in the body (37). KCs are on endothelial cells and are able to migrate quickly to the site of disease, inflammation or infection (20). KCs play vital roles in the body, including the clearance of endotoxins and foreign particles through an endocytosis process, the promotion of cell death in cancer and infection by producing (tumour necrosis factor- $\alpha$ ) TNF- $\alpha$ . Expectedly, KCs, like all macrophages express several surface receptors, including scavenger receptors that contribute to clearance of lipoproteins and cell debris (24, 37, 38), mannose receptors (35), Fcγ receptors and complement receptors CR1, CR3, and CR4 to identify antibody or complement coated particles and perform phagocytosis (37, 38), CD14 receptors (38), TLR (e.g. TLR4) to help pathogen clearance (38, 39). KCs can internalise nanoparticles (NPs) through a variety of pathways and mechanisms (e.g. phagocytosis, macropinocytosis, clathrin-mediated endocytosis and caveolin-mediated endocytosis) (33). Clathrin-mediated processes are responsible for the uptake of 100-350 nm NPs, whereas caveolin contribute to the uptake of smaller particles internalises 20-100 nm particles. Macropinocytosis and phagocytosis favour the uptake of larger NPs (0.5-5  $\mu$ m).

Uptake of nanomedicines by KC is influenced by NP size (>200 nm), charge (positive charge), hydrophobicity and shape as these factors can contribute to opsonisation of nanomedicines in the systemic circulations which earmarks them for capture by phagocytes including KCs (40).

### *Pit cells, biliary cells, hepatic stellate cells*

Pit cells (lymphocytes) are in the sinusoidal lumen and attached to LSEC. Their primary role is to act as the local natural killer (NK) cells (35, 41). NKG2D, CD16 and NKR-P1 receptors are expressed by pit cells, which are involved in antibody dependent cellular cytotoxicity (42, 43). Biliary cells are the epithelial cells of bile ducts (20) while HSC also known as Ito cells or fat storing cells are present in the perisinusoidal space (20) and contribute to retinoid storage and sustain the sinusoidal extracellular matrix. In the event of an injury or inflammation, HSC are activated, synthesise protein and deposit collagen which may cause fibrosis (24). HSC express a variety of receptors including TLR4, CD14, MD2, transforming growth factor-beta receptor (TGF- $\beta$ R) and mannose-6-phosphate receptor which induce fibrinogenic activity and extracellular matrix protein synthesis (44), while epidermal growth factor receptor (EGFR) increase the proliferation of the HSCs (45).

In addition to its role in maintaining normal body function, and to some extent, because of these roles, the liver is an important organ to consider when developing new drugs and treatments, including nanomedicines.

## **1.2 NANOPARTICLES**

NPs are solid colloidal systems characterised by dimensions in the range of 1 to 1000 nm. In the field of pharmaceutical sciences, NPs are considered promising options for the formulation of therapeutic and imaging agents (46) due to their unique properties, in particular their high surface-to-volume ratio (47). This feature contributes to enhanced biological or chemical reactivity, a factor that can be strategically utilised for improved solubility and encapsulation but that also requires careful consideration to minimise potential toxicity (47).

In drug formulation, nanomedicines offer a convincing way of overcoming challenges such as poor aqueous solubility, susceptibility to degradation and the need to modulate pharmacokinetics to achieve targeted accumulation and controlled release (48). Achieving these goals requires careful design and detailed characterisation. NPs should be large enough to avoid renal elimination, but small enough to avoid capture by the cells of the mononuclear phagocyte system (MPS), which includes KCs, and prevent blocking smaller blood vessels (49, 50). For example, large NPs (>500 nm) may pose a risk of pulmonary embolism, while particles in the 10-50 nm range may accumulate in renal tissue (51, 52). Unmodified NPs with a size between 15 and 200 nm tend to accumulate in the liver or spleen, depending on their surface properties (51, 53). The work of Arnida *et al.* (50) also highlights the importance of particle shape in addition to size, showing that both factors influence accumulation in tumour tissue, uptake by macrophages and circulation times, as observed by the distribution patterns of spherical and rod-like NPs. They showed that rod-like NPs are less taken up by macrophages than spherical NPs because the contact area is less and engulfment by macrophages is more difficult for rod-like NPs.

In general, nanomedicines can be categorised based on their composition; organic and inorganic. Organic NPs including lipid-based NPs, micelles, polymeric NPs, protein NPs and dendrimers. Polymeric NPs can be further categorised as nanospheres and nanocapsules (54-56). Polymeric nanospheres are solid matrix NPs, while nanocapsules are characterised by a liquid core (water or oil) surrounded by a polymeric shell. Protein-based NPs can be made of natural proteins such as albumin, silk fibroin, or casein and are produced by triggering the physical or chemical aggregation of the raw protein material (57). NP albumin-bound paclitaxel (nab-paclitaxel, Abraxane®) is a protein-based NPs available in the clinic. Dendrimers are naturally-spherical arborescent polymeric structures, sometimes used for gene therapy (58).

Lipid-based NPs include liposomes, lipid nanocapsules and solid lipid NPs and are the most common nanomedicines with many formulations reaching the clinic (59). Micelles are spherical structures resulting from the self-assembly of low or high molecular weight amphiphiles in a selective solvent (60). Inorganic NPs include quantum dots, metallic NPs (e.g. iron, gold or silver), carbon-based and silica nanomaterials.

Regardless of composition, all NPs must meet biocompatibility standards, which favours the use of raw materials that are generally recognised as safe (GRAS). GRAS standards have been developed by the U.S. Food and Drug Administration (FDA) for oral use. Since pharmaceuticals can be administered via intravenous (i.v.), inhalation or dermal route other than orally, the safety of these materials must still be assessed by various tests. While inorganic NPs find applications outside the medical field, such as in electronics and chemical synthesis (61), organic NPs are mainly used for medical purposes, though some are also included in cosmetics (62, 63). In this work, two different types of NPs will be manufactured and assessed: polyester and albumin NPs both of which are organic.

### **1.2.1 Polyester NPs**

Polyesters is a general term to describe any polymer where the repeating units are bound by an ester group. When used for biomedical applications, hydrophobic, biodegradable and biocompatible polyesters [e.g. polycaprolactone (PCL), polylactide (PLA) and poly(lactic-co-glycolic acid) (PLGA) (**Figure 1.3**)] are the preferred option due to their ability to interact safely with biological systems, degrade harmlessly over time, and provide controlled release of substances (60, 64, 65). By controlling composition and molecular weight, it is possible to tailor the crystallinity, hydrophobicity, loading, release and degradability of the resulting NPs (60). The presence of a carboxylic end group also allows facile modification of the surface of NPs (60, 66). There is a long history of using polyesters for medical applications, e.g. absorbable

sutures and as implants for prolonged drug release (67). Despite this, polymer NPs have yet to make it to the clinic, contrary to lipid and protein-based nanomaterials.

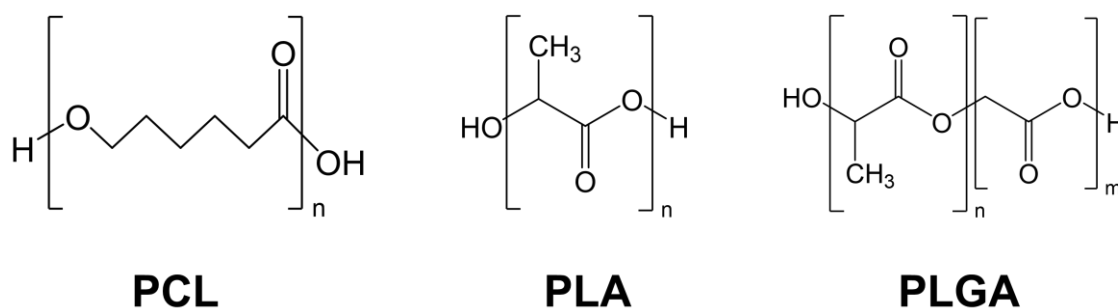


**Figure 1.3 Chemical structures of commonly used polyesters.** Polycaprolactone (PCL), polylactic acid (PDLLA), and poly(lactic acid- co-glycolic acid) (PLGA) structures.

#### *Polyester NPs preparation methods*

Different methods have been described for the manufacture of polyester NPs. The procedures mentioned below assume the use of poorly-soluble polymers to generate hydrophobic nanospheres, as will be performed in this project.

#### Emulsion solvent evaporation (ESE)

In this technique, the polymer is dissolved in a water-immiscible organic solvent (O) and added to an aqueous phase containing a suitable stabiliser (W). Then, single (O/W) or double emulsions (W/O/W) are prepared with the help of a homogeniser or sonicator. Finally, the organic phase is evaporated to generate polymeric nanocapsules dispersed in the aqueous phase (68) (**Figure 1.4**). Emulsification conditions, solvent, evaporation method and rate, and stabiliser concentration all affect the NPs size and size distribution (69) and it is not linear in every case. For example, increasing concentration of the stabiliser may result in larger or smaller NPs in different conditions (70-72). Overall, ESE is a simple, yet time-consuming method (65).



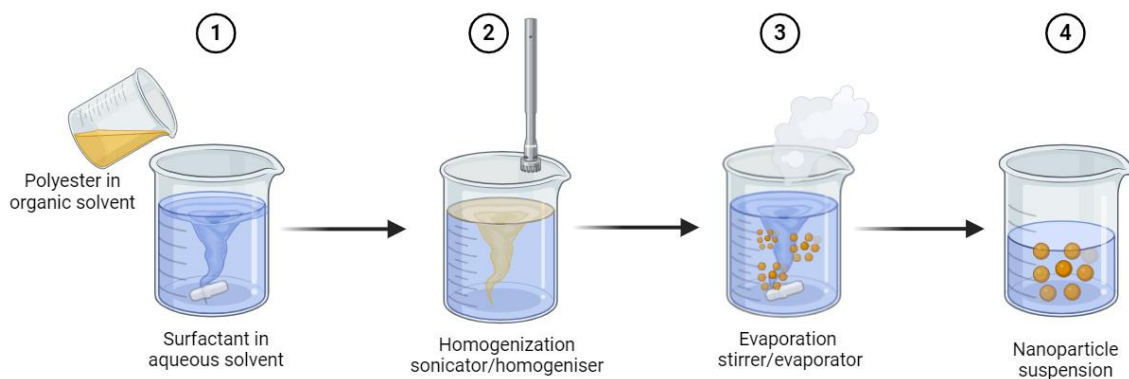


**Figure 1.4 Emulsion solvent evaporation method for preparing polyester nanoparticles.** (Created with Biorender)

### Nanoprecipitation

The polymer dissolved in a water-miscible, volatile organic solvent, is dropped into an aqueous phase containing the stabiliser, under stirring. When mixed in the aqueous phase, the organic solvent diffuses, and polymer begin to precipitate as nanospheres or nanocapsules because of the decrease in affinity for the dispersing phase (73) (**Figure 1.5**). The size and size distribution of the NPs depend on polymer concentration, organic solvent injection rate, and W:O ratio. Nanoprecipitation is a simple, economical, and fast method (48, 65).

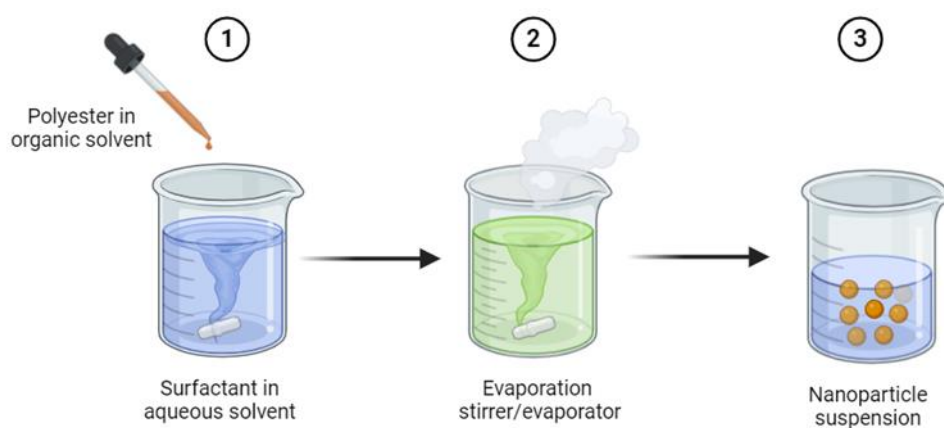


**Figure 1.5 Nanoprecipitation method for preparing polyester nanoparticles.** (Created with Biorender)

### Salting-out

The salting-out method is a variation of the emulsion-diffusion method. In this technique, an emulsion is formed by adding a solution of the polymer in a water-miscible organic solvent (acetone or tetrahydrofuran) to an aqueous phase containing a salt ( $\text{MgCl}_2 \cdot 6\text{H}_2\text{O}$  or  $\text{MgAc}_2 \cdot 4\text{H}_2\text{O}$ ) together with the stabiliser (74). Excess water is added to the dispersing phase, diluting the salt and restoring the water-miscibility of the organic solvent. Again, NPs are formed after precipitation of the polymer in a poor solvent (water) (48, 75) (**Figure 1.6**).

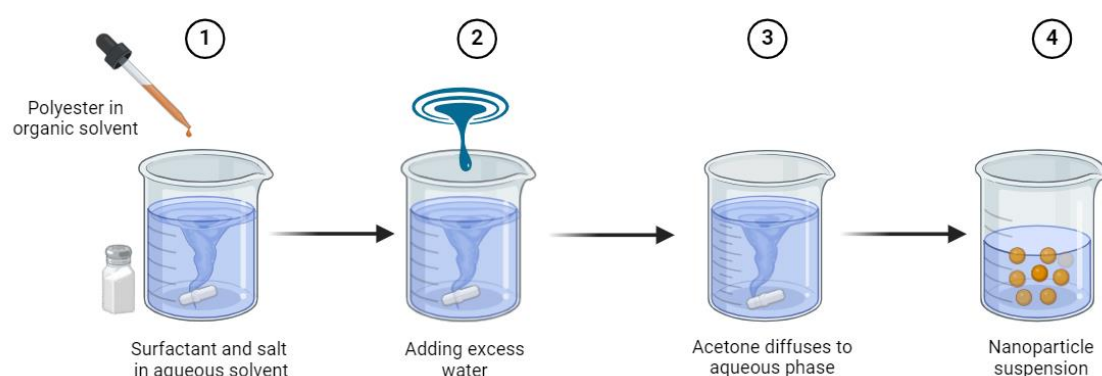


**Figure 1.6 Salting-out method for preparing polyester nanoparticles.** (Created with Biorender)

### Dialysis

The polymer is dissolved in an organic solvent and loaded into a dialysis tube with a molecular weight cut-off allowing the diffusion of water and organic solvent, but not the polymer (**Figure 1.7**). The method is based on the formation of a homogeneous NP suspension following solvent displacement in the membrane and aggregation of polymers due to low solubility (74). It has a similar mechanism to the nanoprecipitation method (76).

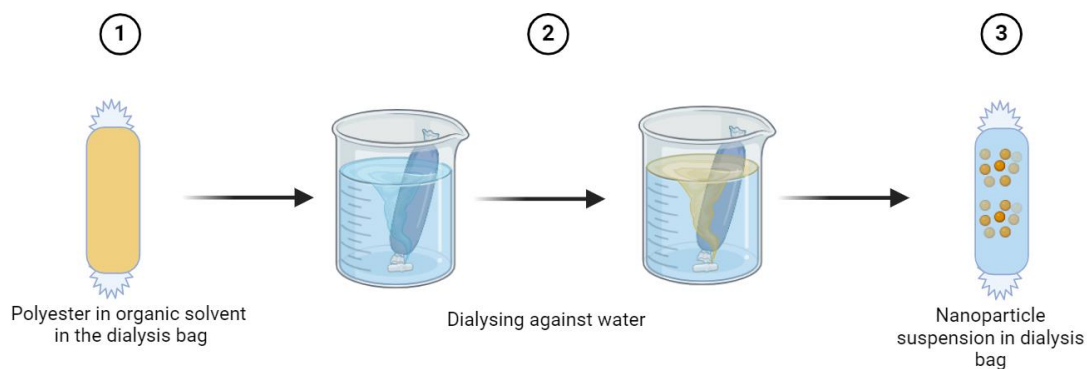


**Figure 1.7** Dialysis method for preparing polyester nanoparticles. (Created with Biorender)

### Supercritical fluid technology

The supercritical fluid method of producing polyester NPs uses a compound, usually carbon dioxide ( $\text{CO}_2$ ), in a supercritical state. A polyester is dissolved in liquid  $\text{CO}_2$  or in a solvent (chloroform, EtAc, etc.) introduced into this supercritical fluid in a special reactor. Under controlled pressure and temperature, the substance undergoes dissolution and subsequent recrystallisation, resulting in the formation of homogeneous polyester NPs (77) (**Figure 1.8**).

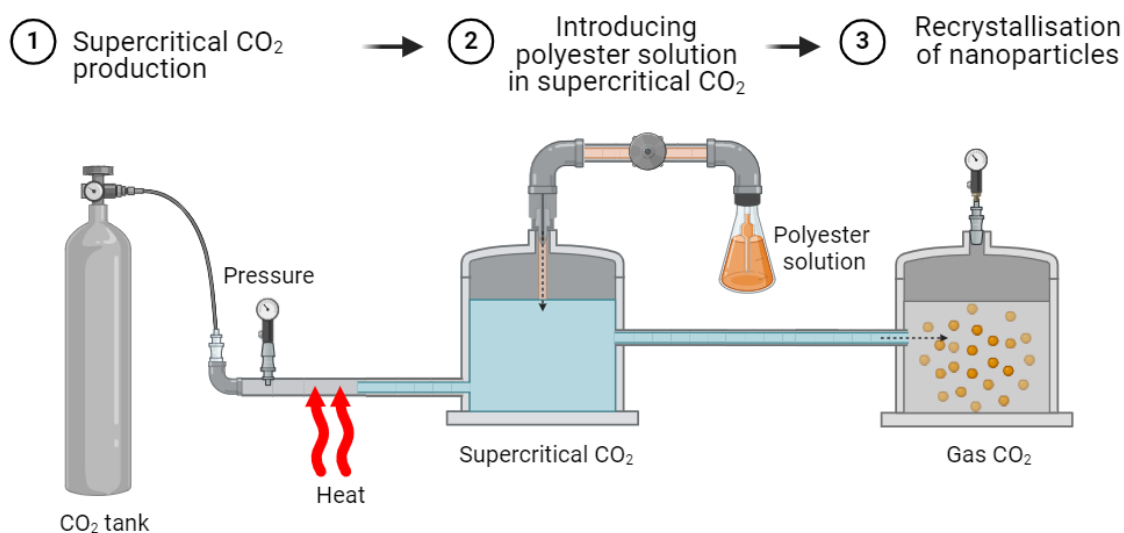


**Figure 1.8** Supercritical fluid technology for preparing polyester nanoparticles. (Created with Biorender)

The advantages and disadvantages of the mentioned methods were summarised in **Table 1.1**.

In this work, ESE and nanoprecipitation will be trialled for the manufacture of biodegradable polyester NPs since these techniques are the most used methods in the literature. BSA NPs will also be prepared and characterised for the cellular uptake studies, therefore protein NPs and their preparation techniques explained below.

**Table 1.1 Polyester NP preparation method comparison**

<b>Preparation method</b>	<b>Advantages</b>	<b>Disadvantages</b>
<b>Emulsion Solvent Evaporation</b>	<ul style="list-style-type: none"> <li>- Versatile and widely used method</li> <li>- Allows encapsulation of hydrophilic and hydrophobic drugs</li> </ul>	<ul style="list-style-type: none"> <li>- May require toxic organic solvents</li> <li>- Requires high shear rate</li> <li>- W/O/W emulsion instability causes hydrophilic drug leakage</li> <li>- Heat or vacuum needed for evaporation</li> </ul>
<b>Nanoprecipitation</b>	<ul style="list-style-type: none"> <li>- Simple and rapid process</li> <li>- Suitable for scale up</li> <li>- Organic solvents are less toxic</li> </ul>	<ul style="list-style-type: none"> <li>- Limited control over particle size and drug loading</li> <li>- Not suitable for hydrophilic drugs</li> </ul>
<b>Salting Out</b>	<ul style="list-style-type: none"> <li>- Relatively simple and cost-effective method</li> <li>- Does not require the use of toxic organic solvents or heat</li> </ul>	<ul style="list-style-type: none"> <li>- Limited control over particle size and drug release kinetics</li> <li>- Time consuming purification process</li> </ul>
<b>Dialysis Method</b>	<ul style="list-style-type: none"> <li>- Allows for the removal of residual solvents and impurities</li> <li>- Suitable for preparing large quantities of NPs</li> </ul>	<ul style="list-style-type: none"> <li>- Slow process</li> <li>- Requires specialized equipment</li> <li>- Limited control over particle size distribution</li> </ul>
<b>Supercritical Fluid Technology</b>	<ul style="list-style-type: none"> <li>- High purity of NPs</li> <li>- Solvent is environmentally friendly</li> </ul>	<ul style="list-style-type: none"> <li>- Requires specialized equipment and expertise with high operational costs</li> <li>- Limited control over particle size distribution</li> </ul>

### 1.2.2 Protein NPs

Since proteins are natural polymers, protein NPs are often considered inherently safe and their natural ability to interact with poorly-soluble drugs, make them particularly interesting for the formulation of nanomedicines (78). Moreover, while the preparation of most polymeric NPs requires toxic solvents and emulsifying agents, there are more options to avoid toxic reagents

when making protein NPs. The fact that albumin is abundant in the plasma has caused it to be one of the most studied proteins. Because it works as a nutrient carrier to cells, albumin can be used as a drug carrier to target specific receptors or cross the blood-brain barrier (79). Abraxane® (Paclitaxel albumin-bound NPs) is the first protein-based NP and approved by the FDA to be used for breast cancer therapy. Abraxane® causes fewer side effects than conventional treatment with paclitaxel because of the tendency to accumulate only in the tumour tissue owing to its size (130 nm) (80). Abraxane® or nAb-paclitaxel is manufactured using a simple, solvent- and surfactant-free high-speed homogenisation method (81). However, this method of preparation might not be applicable to all proteins and extensive optimisation may be required to generate well-defined protein NPs without toxic cross-linkers or solvents (82).

Besides albumin (bovine or human), fibroin and collagen are the most common animal-based proteins used in the production of NPs. Fibroin is an immune-friendly protein which is hydrophobic, porous, waxy, and shapable and is acquired from silk filaments. Because of its porosity, fibroin possesses a high surface area which may be advantageous for adhesion of therapeutic molecules (79, 83). Because of its relative hydrophobicity, a variation of the nanoprecipitation method can be applied to the production of fibroin NPs but raises similar issues as organic solvents are required (84, 85). Plant-based options are also available, including gliadin, legumin, soy protein, and zein which have all shown good stability but may be poorly tolerated by patients (e.g. gliadin is a component of gluten and some legumin lectins can cause digestive issues) (78, 86).

The main concern in using protein-based NPs is the possibility of generating an immunogenic response. Animal proteins are generally more likely to produce immune responses than those of plant origin (87). However, while gliadin, a plant-derived protein, is considered non-

immunogenic, zein can cause an immune response when given intramuscularly (87). Among the animal proteins, keratin and fibrinogen are considered non-immunogenic while silk and collagen have potential immunogenicity (87). Immune response intensity may depend on the source of the collagen as is it also understood that bovine collagen causes a higher antibody response than avian collagen (88).

BSA NPs have been investigated for their biodegradable, biocompatible, non-toxic and non-immunogenic properties, with the ability to be modified by electrostatic adsorption or covalent bonding (89). Khramstov *et al.* (90) also suggested the potential of BSA NPs as carriers for intracellular and tumoral delivery. Furthermore, Maghsoudi *et al.* (91) demonstrated that BSA NPs loaded with 5-fluorouracil were able to maintain a constant release over 20 h. Similarly, Su *et al.* (92) showed that avermectin-loaded BSA NPs had a sustained release performance of 20 days, suggesting the potential for controlled drug release over an extended period. Highlighting the potential of modifiability of BSA NPs in targeted therapy, Huang *et al.* (93) developed curcumin-loaded galactosylated BSA NPs for targeted drug delivery to hepatocellular carcinoma cells. Interestingly Chen *et al.* (94) efficiently co-loaded an anti-tumour drug doxorubicin and a drug resistance inhibitor verapamil into BSA NPs, demonstrating the potential of BSA NPs in overcoming multidrug resistance. The potential of BSA NPs for drug delivery systems, targeted therapy, sustained release and enhanced therapeutic efficacy has been demonstrated by in vitro studies on drug-loaded BSA NPs. Taken together, these studies open up new avenues for advanced drug delivery applications and highlight the versatility and efficacy of BSA NPs as drug carriers.

### ***BSA NPs preparation methods***

#### ***Desolvation (nanoprecipitation, coacervation)***

The protein is dissolved in the aqueous phase. The precipitation of the protein is triggered by the addition of (ethanol, acetone). A protein nucleus is formed, and protein NPs are obtained

by aggregation. Cross-linkers (generally glutaraldehyde) can be used to improve the stability of the NPs (95, 96), however should be avoided using toxic crosslinkers (97).

#### Thermal denaturation

A BSA buffered solution (pH=6) is heated under stirring at 65°C for less than a minute. This quick heating step is sufficient to denature the protein and trigger aggregation. The size of the NPs was controllable as a function of heating time, and aggregation amount, however this method is not suitable for heat sensitive drug loading (98).

#### Emulsion solvent evaporation

An albumin solution is emulsified in an oil phase using a homogeniser in the presence of oil-soluble stabilisers (Span 80, phosphatidylcholine). Then the oil phase is removed by adding an organic solvent which allows NP formation (95). This method might cause protein degradation because of the high shear force.

#### Thermal crosslinking

Briefly, the protein is dissolved in oil and heated to initiate crosslinking and form NPs (96). However, removing oil after production can be challenging and heat sensitive drugs cannot be encapsulated safely (97).

Preparation of NPs is the first step in the application, then these NPs need to be delivered to the relevant site to achieve less toxic effect in the organism. Since hepatocyte targeting was investigated in this study, the characteristics and targeting mechanisms of liver cells are also evaluated below.

## 1.3 TARGETING THE LIVER

Drug targeting is the selective delivery of a drug to its site of action. The reason for targeting is to ensure that the drug accumulates only where it is needed and therefore, minimise off-target side effects. Drug delivery systems can be passively or actively targeted.

### 1.3.1 Passive targeting

NPs are generally administered by i.v. administration. Once in the body, NPs circulate and can accumulate in any tissues/organs with leaky vasculature, provided pore size is large enough. Tumours vasculature is characterised by the presence of large gaps between endothelial cells (99). These anatomical and physiological differences contribute to create the enhanced permeability (larger gaps) and retention (lack of lymph vessels) (EPR) effect. The EPR effect is often suggested as an explanation for the preferential accumulation of NPs at the tumour site (100). NPs do not need to be modified with a specific ligand to take advantage of the EPR effect; indeed, accumulation in diseased tissues will happen naturally based on NP properties such as their size and surface charge. NPs of a certain size, typically between 10 and 200 nanometres, are small enough to pass through endothelial cell gaps from the blood vessels of tumour tissue. Larger particles are generally retained in the bloodstream or filtered out by the liver and spleen, while smaller particles are rapidly eliminated by the kidneys. In addition, NPs with a neutral or slightly negative charge tend to circulate longer in the bloodstream than positively charged NPs, which are more likely to be rapidly cleared by the liver or sequestered by macrophages (101). However, in order to benefit from the EPR effect, NPs need to circulate in the blood for long periods of time. This means avoiding renal elimination and capture by the MPS.

Controlling hydrodynamic size is probably the best way to prevent renal filtration. (102) With regards to the MPS, a number of parameters must be considered like size and surface properties



such as charge and hydrophobicity (102, 103). For example, it has been suggested that cationic, hydrophobic and/or bigger sized NPs are more prone to be captured by MPS (24). Furthermore, controlling shape may be useful as rod-shaped NPs are said to last longer in circulation than spherical NPs though they also accumulate more in the liver, because contact area with the macrophages is less so engulfing by phagocytes is harder of rod NPs, so elimination rate is slower (51, 104).

Because most of the body's macrophages are located in the liver sinusoids (80-90%), and because NPs captured by the MPS can be taken to the spleen, a vast proportion of passively-targeted NPs (>100 nm) accumulate in these two organs after injection (105). Thus far, Attaching polyethylene glycol (PEGylation) remains the preferred method to avoid the MPS and achieve the prolonged circulations times needed to exploit the EPR effect (101, 106). Fujiura *et al.* (107) highlights that PEGylation allows NPs to evade macrophage recognition, resulting in prolonged blood retention. This mechanism involves shielding NPs from the RES, especially macrophages, thereby reducing opsonisation, mononuclear phagocyte identification and macrophage uptake, and finally increasing circulation half-life and body distribution. In addition, Perry *et al.* (108) reported that varying the PEG density on hydrogel PRINT NPs influenced protein binding, macrophage engagement, biodistribution and pharmacokinetics. Although passive targeting has some advantages, it may not be enough to achieve therapeutic levels in the target tissue/organ. Thus, active targeting, that is specific recognition of NPs by membrane receptors, is considered as an add-on strategy to promote accumulation specificity (109).

### **1.3.2 Active targeting**

Active targeting strategies are based on increasing the recognition of ligand-decorated NPs by specific receptors. Folate, mannose, glucose, monoclonal antibodies, peptides, etc. have all

been used for this purpose (110). This approach can help minimize off-target effects associated with nanomedicines (111). However, there are some limitations to consider. For example, multiple cells can express the receptor of interest making targeting more challenging, macromolecular ligands can affect the stability of the drug carriers and capture by the MPS remains possible (112). The overall instability of ligand-targeted NPs may result from the detachment of macromolecules from the NPs due to weak bonds or environmental conditions, or because of the nature of the macromolecules, such as proteins or amino acids, which cause aggregation of the NPs. This might be suitable if these organs are the site of the diseases, but NP formulation and modification with the suitable ligands can be challenging to target specific tissue or cell type.

### **1.3.3 Targeting specific liver cells**

Liver targeting can be achieved using passively- or actively-targeted nanomedicines depending on the cell type being targeted (113).

#### ***Targeting KCs***

KCs have a role in activating liver diseases and helping liver regeneration. Chronic KC activation can lead to liver failure, hepatic fibrosis, portal hypertension, etc. On the other hand, following liver resection, KCs release TNF- $\alpha$  and IL-6 (interleukin-6) to help regeneration of the liver. Also, KCs contribute to adaptive immunity and immune tolerance, for example, after liver transplantation (114).

NPs can easily be targeted to KCs. Indeed, as the drug carrier becomes larger (>100-200 nm) or less rod-like the possibility of capture by the liver KCs increases (104). Similarly, a strong negative (*e.g.* liposomes) or positive charge, (*e.g.* polymer NPs) (115) and/or a highly hydrophobic surface may all increase the risk of recognition by KCs. Passive targeting, therefore, is the easiest way to target KCs, but accumulation can be controlled better by

attaching a suitable ligand, e.g. mannose, human serum albumin (HSA) or apolipoproteins (24, 40). Active targeting of KCs is not widely studied as surface receptors are likely expressed by all macrophages. Moreover, KCs and LSECs share common receptors and in-depth knowledge of their molecular profile is needed to ensure the correct cell is targeted.

### ***Targeting LSECs***

LSECs contribute to the pathophysiology of HCC and liver inflammation by providing leucocytes into the liver tissue (116) making these cells interesting therapeutic targets (117).

As mentioned above, LSECs have pores which can reach 200 nm in size. Particles size between 200 and 150 nm have, respectively, been shown to pass through these pores and reach hepatocytes (24). Negatively charged nanocarriers are easily taken up by LSECs, which express a multitude of scavenger receptors like KCs. However, since these scavenger receptors also exist on the surface of hepatocytes and KCs, cell-specific targeting via HSA or apolipoproteins might be inconvenient (24). Alternatively, NPs could be targeted to the common lymphatic endothelial and vascular endothelial receptor (118).

### ***Targeting stellate cells***

Stellate cells are used for lipid and retinoid storage, so vitamin A can be used as targeting ligand. These cells also express mannose-6 phosphate receptors, but again, this may affect specificity as KCs also express this receptor (24). Active stellate cells have been targeted to treat liver fibrosis. Beljaars, *et al.* (119, 120) showed that BSA or HSA bound mannose-6-phosphate was internalised by receptor-mediated endocytosis in stellate cells 40%, while KCs internalised 35%, and LSECs 25%. Again, this receptor is not selective enough and similar receptors are expressed on KCs, LSECs, and quiescent stellate cells. Y. Li *et al.* (121) the use of a cyclic peptide-guided liposomes to target cell membrane integrin  $\alpha v \beta 3$  to improve accumulation in

LSEC. They have shown that cyclic peptide targeted liposomes successfully accumulated in the active HSCs and decreased in-vivo fibrinogenic response.

### ***Targeting hepatocytes***

Hepatocytes can be passively targeted using nanocarriers smaller than 200 nm (122). However, in order to reach their target, these NPs would need to avoid the MPS and all other physiological barriers standing between them and their target. Generally, positively charged NPs have higher a chance to bind the hepatocytes but will likely interact with other cells before reaching their target (24, 40). In theory, any of the receptors present on hepatocytes, can be used for targeting. The ASGP-R are very common on liver parenchymal cells and hepatic cancerous cells and bind galactose, lactose, galactosamine, lactobionic acid, hyaluronic acid, LCF, pullulan *etc.* Biessen *et al.* (123) showed that lactosylated a poly-L-lysine antiviral (5-iodo 2'-deoxyuridine) drug conjugate could be targeted to hepatocytes via this receptor. Drug accumulation in hepatocytes was increased from 3% to 85% by actively targeting this receptor (123). Other options include the glycyrrhizin/glycyrrhetinic acid receptors which bind to glycyrrhizin and glycyrrhetinic acid molecules (35). Scavenger receptors remain an option, with the caveat (similar receptor/ligand couples exist for the other liver cells) already highlighted (24). An *in vitro* study performed by Xin Guan *et al.* (124) showed that 150-200 nm PLGA NPs were taken up efficiently by HEP-G2 cells and accumulated in liver *in vivo*, while the free drug-quercetin-administered was eliminated by the kidneys. El-Naggar M. *et al* (125) prepared 117 nm curcumin-loaded, cationic PLLA-PEG-CTAB (Cetyltrimethylammonium bromide) NPs and found that the anti-inflammatory nanomedicines were more effective on inducing diabetic hepatopathy (liver inflammation) than the free drug. As shown in both examples above, in the literature it is unclear whether the NPs accumulated in hepatocytes or KCs. Taken together,

these examples show that while NPs can reach the liver cells, it may be difficult to target specific structures within the liver.

## 1.4 AIMS AND OBJECTIVES

Despite their widespread use, a comprehensive understanding of the impact of stabiliser selection on polyester NP uptake by hepatic cells is still lacking. This research aims to fill this knowledge gap by investigating the role of stabilisers in altering NP-liver cell interactions, with a particular focus on minimising macrophage interactions while enhancing hepatocyte uptake.

To achieve this goal, the following objectives were established:

1. Select and optimise a manufacture method to produce narrowly dispersed polyester and albumin NPs with a size between 150 and 200 nm
2. For polyester NPs, select suitable stabiliser to study the impact of coating on NP properties and behaviour. For albumin NP, select a suitable cross-linker
3. Characterise the resulting NPs using suitable methods to assess particle size, size distribution, morphology, zeta potential and surface hydrophobicity
4. Assess the safety of all NP in vitro by performing monitoring cell viability and pro-inflammatory potential
5. Evaluate uptake of polymer NPs in different cell lines that are relevant to the liver
6. Prepare actively targeted polyester NPs and assess their uptake in a co-culture model of liver

By systematically addressing these objectives, this research aims to improve our understanding of the impact of stabiliser selection on the interactions of polyester NPs with liver cells, providing valuable insights for optimising their biomedical applications.

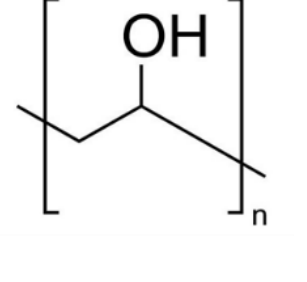
Each chapter of this thesis will cover one or more of these objectives. The first part will focus on polyester NPs (chapters 2 to 4) and the final chapter (chapter 5) will cover preliminary work on albumin NPs.

# **Chapter 2: OPTIMISATION, MANUFACTURE, AND CHARACTERISATION OF POLYESTER NANOPARTICLES**

## **2.1 INTRODUCTION**

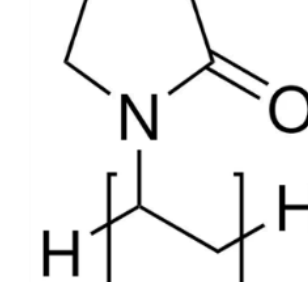
This chapter covers the optimisation, preparation, and characterisation of polyester NPs, focusing initially on the comparison between two manufacturing techniques: ESE and nanoprecipitation. These methods are the most widely used techniques in the literature due to their ease of scalability and the ability to obtain monodisperse NPs without the need of specialised equipment, and therefore these two techniques were applied in this work. The primary aim of this optimisation step was to determine which method would yield precisely sized polyester NPs within the target range of 150-200 nm. Although there were four different stabilisers in the initial trials (polyvinyl alcohol (PVA), Poloxamer 407 (PXM), polyvinyl pyrrolidone K30 (PVP), Kolliphor HS15 (HS15)), the decision was to do further trials with just PVA and PXM. Once a manufacturing method was selected, PLGA and PDLLA NPs were produced using PVA and PXM as stabilisers as the main NPs used throughout this work. This was because it was expected that these two stabilisers would provide the greatest difference in surface properties due to the difference in hydrophilicity in their molecular structure (**Figure 2.1**). PXM has a triblock polymer structure with hydrophilic PEG chains at each end and a hydrophobic poly(propylene glycol) segment in the middle. The hydrophobic core of PXM interacts with polyesters to facilitate the formation of NPs. Meanwhile, the PEG chains extend outwards into the aqueous medium and act as steric stabilisers, hindering interactions between NPs and preventing their aggregation. PVA, on the other hand, has a lower hydrophilic nature

**A**



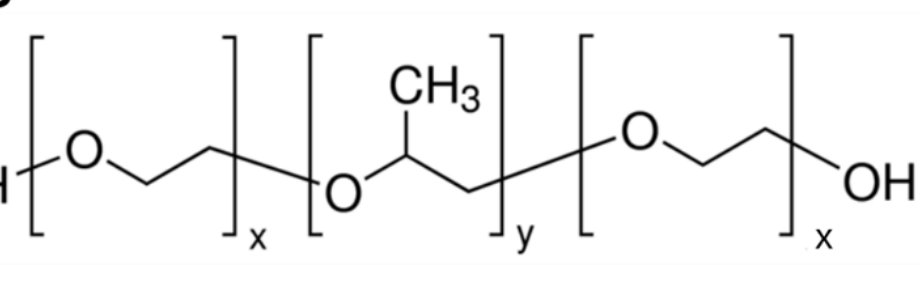
Chemical structure of the repeat unit of poly(2-propanol). It consists of a three-carbon chain with a hydroxyl group (OH) attached to the central carbon. The chain is enclosed in brackets with a subscript  $n$ .

**B**



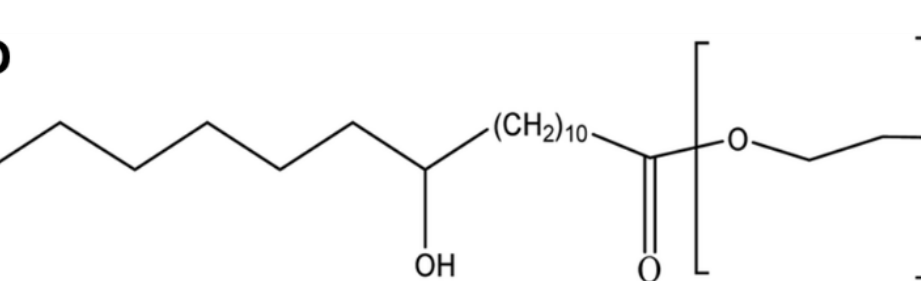
Chemical structure of the repeat unit of poly(2-(1-oxo-2-pyrrolidinyl)ethyl). It features a pyrrolidine ring (a five-membered ring with one nitrogen atom and a carbonyl group) attached to a two-carbon chain. The chain is enclosed in brackets with a subscript  $n$ .

**C**



Chemical structure of a triblock copolymer. It consists of three blocks: a poly(2-oxaethyl) block (H-O-CH<sub>2</sub>-CH<sub>2</sub>-O-), a poly(2-methoxyethyl) block (O-CH(CH<sub>3</sub>)-CH<sub>2</sub>-O-), and a poly(2-oxaethyl) block (O-CH<sub>2</sub>-CH<sub>2</sub>-OH). The blocks are connected by ether linkages and are enclosed in brackets with subscripts  $x$ ,  $y$ , and  $x$  respectively.

**D**



Chemical structure of a functionalized copolymer. It features a long alkyl chain (CH<sub>2</sub>)<sub>10</sub> attached to a hydroxyl group (OH) and a carbonyl group (C=O). The carbonyl group is part of a poly(2-oxaethyl) block, which is enclosed in brackets with a subscript  $n$ .



## 2.2 AIMS AND OBJECTIVES

The main aim of the work presented in this chapter was to prepare NPs varying in terms of the polymer core and stabiliser with a suitable method selected from ESE and nanoprecipitation and to characterise them prior to *in vitro* studies.

Objectives:

1. NPs were prepared using ESE and nanoprecipitation methods.
2. Dynamic light scattering (DLS) and transmission electron microscopy (TEM) were used to assess particle size, size distribution (as the polydispersity index (PdI)) and morphology.
3. Stability tests were carried out under three different conditions: water (4°C), phosphate buffered saline (PBS) at room temperature, and cell culture media (Dulbecco's modified Eagle's medium (DMEM) at 37°C.
4. Surface hydrophobicity of the NPs was investigated using hydrophobic interaction chromatography (HIC), salt aggregation test (SAT) and a protein adsorption test.

These assays provided valuable insights into the surface properties of the NPs, which are essential for understanding their behaviour in biological systems.

## 2.3 MATERIALS AND METHODS

### 2.3.1 MATERIALS

Ammonium thiocyanate ( $\text{NH}_4\text{SCN}$ ) was purchased from Merck, BSA lyophilised powder, ethyl acetate (EtAc), chloroform (anhydrous,  $\geq 99\%$  purity, contains 0.5-1.0% ethanol as a stabilizer), Dulbecco's modified Eagle's medium (DMEM), methanol (MeOH), acetone, and PBS tablets, poly(D, L-lactide) (PDLLA, molecular weight (MW): 10,000-18,000), poly(D, L-lactide-*co*-glycolide) (PLGA, 75:25 monomer ratio lactic: glycolic acid; MW:4000-15000), poly(caprolactone) (PCL, MW:14,000), poly(vinyl alcohol) (PVA; MW ~13,000-23,000; 98% hydrolysed), poly(vinylpyrrolidone) K30 (PVP, MW:10,000), Poloxamer® 407 [PXM, poly(ethylene glycol)<sub>101</sub>-*b*-poly(propylene glycol)<sub>56</sub>-*b*-poly(ethylene glycol)<sub>101</sub>; MW: ~9,840-14,600], were purchased from Merck (Gillingham, Dorset, UK). Kolliphor® HS15 (HS15, polyethylene glycol<sub>660</sub> 12-hydroxy stearate; MW: 344.5 g/mol) were generous gifts from BASF (Ludwigshafen, Germany). Normal human serum (HSP) was purchased from Jackson Immuno Research Labs (Ely, Cambridgeshire, UK). Boric acid, iodine, potassium iodide, hydrochloric acid (HCl, 1 N) and sodium hydroxide (NaOH, 1 N), Pierce™ BCA protein assay kit, ethanol absolute ( $\geq 99.0\%$  purity), dimethyl sulfoxide (DMSO), polystyrene latex (PS) NPs (0.20 micron, 2.5 wt%) and Triton X-100 were purchased from Thermo Fisher Scientific (Loughborough, Leicestershire, UK). Ferric chloride anhydrous ( $\text{FeCl}_3$ ) obtained from Scientific Laboratory Supplies Ltd. (Wilford, Nottingham, UK) ultrapure water with a resistivity of 18.2 M $\Omega$ .cm was used for all experiments. All the solvents were of analytical grade and used without further purification.

### 2.3.2 METHODS

#### *Preparation of polyester NPs*

##### Solvent selection

Appropriate volatile solvent for the manufacture of NPs was selected by visual assessment -no particulate residue- of the solubility of all polyesters (PLGA, PLLA, PCL) in selected organic solvents, and of both stabilisers (PVA, PXM, PVP, HS15) in aqueous solvents, heating the preparation as needed up to 60 minutes. The solvent selection was based on suitable solubility and viscosity to allow filtration through a 0.22 µm syringe filter. The tried solvents were EtAc, chloroform, acetone, methanol, ethanol for polyesters, and water and PBS for stabilisers. Once the solvent was selected, NPs were prepared by ESE or nanoprecipitation.

##### NP preparation- ESE

All polyesters (PCL, PDLLA or PLGA) were dissolved in chloroform at a concentration of 0.1% (w/v). Aqueous solutions of the stabilisers (PVA, PXM, HS15 or PVP) were prepared separately at concentrations between 0.01- 1.00% (w/v). All aqueous solutions were filtered (0.45 µm, cellulose acetate) before use. For NP preparation, the polyester solution (1 mL) was added (0.5 mL/min rate) to 20 mL of the stabiliser solution under vigorous stirring (5,000 rpm). The dispersion was left to stir for a further 5 min at the same speed before sonication (Probe sonicator, QSonica LLC, USA, 60% amplitude (amp) on an ice bath for 10 min). The preparation was left to stir (500 rpm) under the fume cupboard overnight to remove the chloroform. Finally, the NP suspension was centrifuged (50,000 RCF; 40 min) three times and the pellet was washed with ultrapure water to remove excess stabiliser and concentrate the NP dispersion.

##### NP preparation- nanoprecipitation

A modified nanoprecipitation method was used to prepare PDLLA and PLGA NPs (73). Briefly, 100 mg polyester (and 0.1% Nile red for imaging and flow cytometry studies) was

dissolved in 10 mL acetone, then added to 40 mL of an aqueous stabiliser solution (1% (w/v); PVA or PXM) at a 1 mL/min rate, under stirring (400 rpm). Acetone was evaporated over 4 h under the fume cupboard. The formulations were then centrifuged and washed as described above. The NPs are dispersed in relevant media (either water, PBS, or cell culture media according to the test conditions) at 16 mg/mL concentration for the following tests. In this thesis untargeted NPs will be named as X-Y, where X is the polyester used (PCL, PDLLA or PLGA) and Y is the stabiliser (PXM, PVA, PVP, HS15).

### ***Residual stabiliser detection***

#### **Residual PXM quantification**

The supernatant (100  $\mu$ L) of PXM-stabilised NPs was collected after centrifugation (5,433g; 10 min) and added to a mixture chloroform (1.2 mL) and ammonium ferro thiocyanate solution (16.2 mg/mL ferric chloride and 30.4 mg/mL ammonium thiocyanate in water; 1.2 mL). The biphasic system was incubated for 30 min, under gentle shaking, in the dark at room temperature. The absorbance of the chloroform layer was measured at 510 nm (126) on UV-vis spectroscopy (Shimadzu UV-2600; Kyoto, Japan). The study investigated the linearity of the detection method over a concentration range of 0-10 mg/L PXM. The linear range was found to be between 0.2-1 mg/mL (**Figure 2.2**). The equation for the line of best fit was  $y = 1.2686x - 0.0923$  and the regression coefficient ( $R^2$ ) was 0.999. The limit of detection (LOD) and limit of quantification (LOQ) were determined based on a signal-to-noise (S/N) ratios of 3 and 10, respectively. LOD is calculated as follows;  $LOD = 3 \times (\text{Standard deviation of blank response}) / (\text{slope of the standard curve})$ . The LOD was calculated to be 0.042 mg/mL and the LOQ was determined to be 0.128 mg/mL.

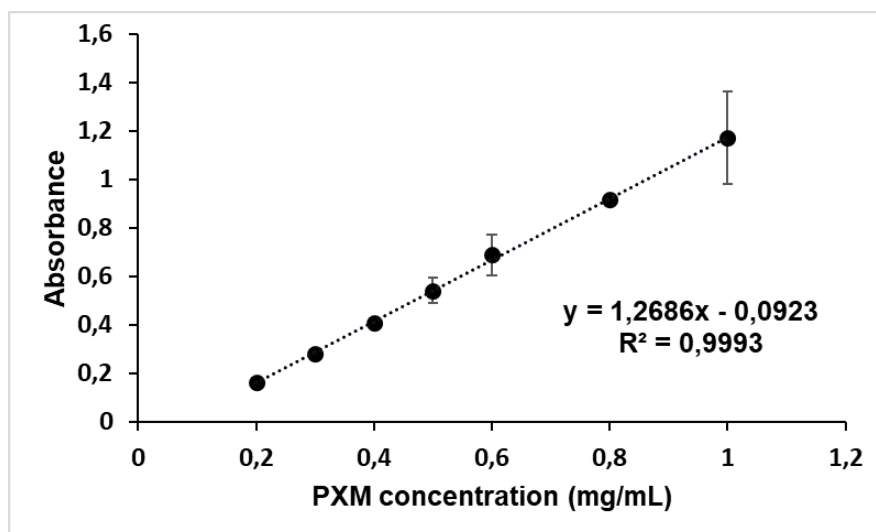


**Figure 2.2** Standart curve for PXM (n=3)

#### Residual PVA quantification

NP dispersions (1 mg/mL) were centrifuged (5,433 g; 10 min), and the supernatant was incubated in 0.5 M NaOH<sub>aq</sub>, at 60°C. After 15 min, 0.9 mL of 0.1 M HCl<sub>aq</sub> was added, and the volume was adjusted to 5 mL with ultrapure water. 0.65 M boric acid (3 mL), ultrapure water (1.5 mL) I<sub>2</sub>:KI (0.05 M:0.15 M; 0.5 mL) solution were added to the supernatant and incubated for a further 15 min at room temperature, in the dark. The absorbance of the aqueous solution was measured at  $\lambda_{\text{max}}$ =690 nm on UV-vis spectroscopy (Shimadzu UV-2600; Kyoto, Japan) (69, 127). The linear range was found to be between 0.006-0.2 mg/mL (**Figure 2.3**). The equation for the line of best fit was  $y = 13.525x - 0.0076$  with  $R^2 = 0.997$ . The LOD and LOQ were found to be 0.015 and 0.048 mg/mL, respectively.

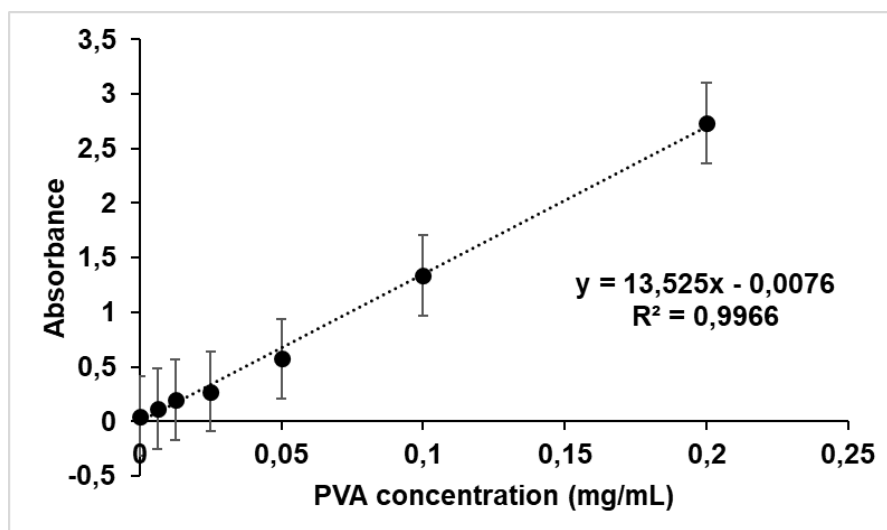


**Figure 2.3** Standart curve for PVA. (n=3)

### *Characterisation of Polyester NPs*

#### *Size and zeta potential measurements*

Particle size was measured by DLS on a Nanosizer ZS (Malvern Panalytical Ltd, Malvern, Worcestershire, UK) at 25°C, and a 173° back-scatter measurement angle; three measurements were taken for each sample. NP dispersions were filtered through a 0.45 µm syringe filter (cellulose acetate) and diluted with ultrapure water at a 1:9 (NP: water) ratio before size measurements. Zeta potential measurements were carried out in 0.8X PBS, to provide sufficient ionic strength, on the same instrument.

#### *TEM*

NPs were imaged by TEM (Jeol 1400 Bio TEM, Jeol, Japan) to assess their morphology and size. All NPs were dispersed in water (0.2-1 mg/mL). For the measurement, 10 µL of each NP dispersion was dropped onto a 200-mesh copper grid and left to dry at room temperature for 5 min. NPs were imaged under an 80.03 kV beam. The size and size distribution of the polyester NPs were processed using ImageJ Fiji (LOCI, University of Wisconsin) (128). Gaussian smoothing was applied to decrease the background noise.

### ***Colloidal stability testing***

The size, size distribution and pH of PCL, PDLLA, and PLGA NPs prepared by the ESE were measured over time before and after storage at 4°C. NPs produced by nanoprecipitation, particle size and distribution (PDI) were measured at regular intervals over 30 days. NP dispersions (1 mg/mL) in deionised water were stored at 4°C while dispersions in PBS were stored at room temperature. Stability in the presence of proteins was studied by adding NP dispersions (1 mg/mL) to an aqueous BSA solution (0.5 mg/mL) and monitoring particle size and size distribution over 30 min at 37°C. The stability of the NPs under cell culture condition was also assessed for dispersions prepared in DMEM containing 10% FBS stored at 37°C. These stability test conditions have been developed taking consideration the conditions under which NPs are stored, tested and used in *in vitro* assays.

### ***Hydrophobicity of the NPs***

Prepared polyester NPs by nanoprecipitation method and commercial PS NPs (200 nm) were used for the hydrophobicity tests. PS NPs were used as a positive control group.

### **Hydrophobic interaction chromatography (HIC)**

The ÄKTA start protein purification system (Cytiva, Sheffield, UK) was used for the HIC study (129-132). NP dispersion in PBS (1 mg/mL; 1 mL) was introduced on a Butyl FF column (Cytiva, Sheffield, UK). Flow rate was set at 1 mL/min and NPs were eluted using PBS then Triton X (0.1%) as the mobile phase samples (1 mL) for a total of 30 min (15 min in each mobile phase). NP turbidity signal was monitored by spectrophotometry ( $\lambda_{\text{max}} = 450 \text{ nm}$ ). The same process was repeated for Phenyl FF (HS) and Octyl FF columns. The area under the curve (AUC) of a plot of the absorbance as a function of time was determined to calculate retention (R) (Eq. 2.1) and the HIC index (Eq.2.2).

$$\text{Eq.2.1 Column retention\% (R\%)} = \frac{AUC_{TritonX}}{AUC_{PBS} + AUC_{TritonX}} * 100$$

$$\text{Eq.2.2 HIC index} = \frac{[(R_{butyl}\% * \log P_{butyl}) + (R_{phenyl}\% * \log P_{phenyl}) + (R_{octyl}\% * \log P_{octyl})]}{(\log P_{butyl} + \log P_{phenyl} + \log P_{octyl})}$$

The logP values used for Butyl FF, Phenyl FF (HS), and Octyl FF are 0.47, 0.94, and 2.05, respectively (130).

#### Salt aggregation test

NPs (1 mg/mL) were added to NaCl solutions in water to achieve a final salt concentration between 0.1-5 M. The aim was to test the NP aggregation in different salt concentrations. Particle size was assessed by DLS at 37 °C for 30 min to observe the aggregation rate (133).

#### Protein adsorption assay

Protein adsorption was assessed by monitoring alterations in NP diameter and PDI using DLS. Briefly, 0.5 mg/ml NPs were mixed with BSA (0.125, 0.25, 0.5, 1 mg/mL) and HSP (0.625, 1.25, 2.5, 5 mg/mL) solutions under gentle shaking in a 37°C incubator for 2 h. Samples were collected at 0, 15, 30, 60 and 120 min then, centrifuged to obtain NP-free supernatants. A BCA (bicinchoninic acid) kit which utilises reduction of Cu<sup>2+</sup> to Cu<sup>+</sup> by protein in an alkaline medium was used to determine the concentration of free albumin in the supernatant following the manufacturer's instructions. The BCA assay can detect protein concentrations ranging between 20 and 2,000 µg/mL. The assay uses two components: a carbonate buffer that includes the BCA reagent, and a cupric sulphate solution. These components are mixed to form a working solution that is green on preparation and turns purple after incubation at 37°C for 45 minutes in the presence of protein, and the absorbance of final reactant read at 562 nm (134). The concentration of protein adsorbed on NPs was calculated as the difference between the initial albumin concentration and the albumin concentration detected in the supernatant.



## 2.4 RESULTS AND DISCUSSION

### 2.4.1 Preparation of Polyester NPs

#### *Solubility testing of polyesters and stabilisers*

An experiment was performed to decide the most suitable solvent to use to dissolve the hydrophobic polyesters and stabilisers (**Table 2.1**). Five organic solvents and two aqueous phases were considered for the polyesters and stabilisers, respectively. The organic phase was selected considering factors such as water miscibility, and volatility. Acetone, ethanol and methanol are all miscible with water, making them suitable for nanoprecipitation; while chloroform (0.79% w/w) and EtAc (8.7% w/w) have limited solubility and are immiscible with water (135), making them more suitable for ESE (**Table 2.1**). All the organic solvents selected are volatile, but have different vapour pressures: acetone (30 kPa), chloroform (26 kPa), methanol (16.9 kPa), EtAc (14 kPa) and ethanol (12.4 kPa) (136). Higher the vapour pressure is easier the removal from the formulation, and it is important to not to have residues of solvent in the final product of NP suspension. All solvents are generally safe to use when good laboratory practices are followed, according to the “Pfizer solvent selection guide” (135). The International Council for Harmonisation of Technical Requirements for Pharmaceuticals for Human Use (ICH) has developed guidelines for acceptable limits of residual solvents in pharmaceutical products. The oral and *i.v.* concentration limit for chloroform and methanol is 60 ppm, 3000 respectively and lower than 5000 ppm for acetone and ethanol (137).

EtAc and chloroform were used for the ESE method while acetone was chosen for the nanoprecipitation method. Acetone is miscible with water and has a higher volatility than methanol and ethanol, therefore its removal is expected to be easier.

**Table 2.1 Solvent properties s and solubility of polyesters and stabilisers.**

	Solvents Polymers	EtAc	Chloroform	Acetone	Methanol	Ethanol	Water	PBS	Tg °C
Polyester	PCL <sup>a</sup>	h+	+	+	-	-	-	-	-60 <sup>h</sup>
	PDLLA <sup>b</sup>	h+	+	+	-	-	-	-	50-80 <sup>i</sup>
	PLGA <sup>c</sup>	+	+	+	-	-	-	-	28-46 <sup>j</sup>
Stabilisers	PVA <sup>d</sup>	-	-	-	-	+	H+	H+	85 <sup>k</sup>
	HS15 <sup>e</sup>	-	-	-	-	+	+	+	na
	PXM <sup>f</sup>	-	-	+	+	+	+	+	na
	PVP <sup>g</sup>	-	+	-	+	+	+	+	161 <sup>m</sup>

(+): soluble without heating, (H+); dissolves after heating at 80°C for 60 min., (h+); dissolves after heating at 30°C for 5 min., (+): slightly soluble(138), (-): non-soluble. [references a-m:(138-149)]

The stabilisers were all soluble in water and PBS, however, PVA needed heating at 80°C to dissolve. Since the heating temperature was below its Tg (85°C), heating is not expected to affect PVA's physical properties or stability (150).

### ***NP preparation - ESE***

Preliminary evaluation of ESE as a method for NP production, included three polyesters as starting materials. Tests were carried out to prepare PCL NPs with different concentrations of stabilisers considering the previous studies (151-153). The effect of different solvents, homogenisation speeds and sonication durations on size and distribution was also investigated. The results are presented in the **Table 2.2 and 2.3**. Analysis of the results showed that PCL NPs prepared with 0.1% PCL dissolved in chloroform tended to be <200 nm in size and more homogeneous. Combinations of low stabiliser concentrations (0.01% or 0.05%) and high-speed

homogenisation (5000 rpm for 10 min in an ice bath), resulted in 130-212 nm PCL NPs (PdI=0.2-0.3) (Table 2.3; lines 23-26).

Table 2.2 *PCL NPs optimisation studies using EtAc. (n=1)*

Line	PCL wt.% volume (mL)	PCL solvent	Polymer stabiliser % volume (mL)	homogenising rpm	Ultrasonication	evaporation rpm	d.nm	PdI
1	0.05% - 1 mL	EtAc	0.7% HS15- 20 mL	5000 rpm	10 min	300 rpm	375.1	0.46
2	0.05% - 1 mL	EtAc	0.7% HS15- 20 mL	5000 rpm	5 min	300 rpm	942.16	0.83
3	0.05% - 1 mL	EtAc	0.05% HS15- 20 mL	5000 rpm	10 min*	300 rpm	164.6	0.364
4	0.05% - 1 mL	EtAc	0.01% HS15- 20 mL	5000 rpm	10 min*	300 rpm	175.6	0.272
5	0.10% - 1 mL	EtAc	0.05% HS15- 20 mL	5000 rpm	10 min*	300 rpm	213.7	0.377
6	0.10% - 1 mL	EtAc	0.01% HS15- 20 mL	5000 rpm	10 min*	300 rpm	221.8	0.372
7	0.10% - 1 mL	EtAc	0.5% HS15- 20 mL	3000 rpm	10 min	300 rpm	x	x
8	0.125% - 0.5 mL	EtAc	1% PVP-10 mL	500 rpm		500 rpm	x	x
9	0.125% - 0.5 mL	EtAc	1% PXM-10 mL	500 rpm		500 rpm	500	0.4
10	0.25% - 0.5 mL	EtAc	1% PVP-10 mL	500 rpm		500 rpm	149	0.2
11	0.5% - 0.5 mL	EtAc	1% PVP-10 mL	500 rpm		500 rpm	x	x
12	0.5% - 1 mL	EtAc	0.1% HS15- 20 mL	3000 rpm	10 min	300 rpm	477.5	0.6
13	0.5% - 1 mL	EtAc	0.5% HS15- 20 mL	3000 rpm	10 min	300 rpm	308.4	0.6
14	0.5% - 1 mL	EtAc	1% HS15- 20 mL	3000 rpm	10 min	300 rpm	124.1	0.4
15	0.5% - 0.5 mL	EtAc	8% PVA-10 mL	500 rpm	-	500 rpm	101.7	1
16	0.5% - 0.5 mL	EtAc	1% PVP-10 mL	500 rpm		500 rpm	x	x
17	1% - 1 mL	EtAc	0.5% HS15- 20 mL	3000 rpm	10 min	300 rpm	380.1	0.6

\*: Sonication was progressed on an ice-bath. x:NP formation did not observed

Table 2.3 *PCL NPs optimisation studies using Chloroform. (n=1)*

line	PCL wt.% volume (mL)	PCL solvent	Polymer stabiliser % volume (mL)	homogenising rpm	Ultrasonication	evaporation rpm	d.nm	PdI
18	0.05% - 0.2 mL	Chloroform	0.5% HS15- 20 mL	5000 rpm	10 min	300 rpm	299.5	0.5
19	0.05% - 1 mL	Chloroform	0.5% HS15- 20 mL	5000 rpm	10 min	300 rpm	194.6	0.6
20	0.05% - 1 mL	Chloroform	0.05% HS15- 20 mL	5000 rpm	10 min*	300 rpm	167.1	0.4
21	0.05% - 1 mL	Chloroform	0.01% HS15- 20 mL	5000 rpm	10 min*	300 rpm	249.7	0.4
22	0.10% - 1 mL	Chloroform	0.5% HS15- 20 mL	3000 rpm	10 min	300 rpm	157.5	0.5
23	0.10% - 1 mL	Chloroform	0.05% HS15- 20 mL	5000 rpm	10 min*	300 rpm	212.3	0.3
24	0.10% - 1 mL	Chloroform	0.01% HS15- 20 mL	5000 rpm	10 min*	300 rpm	174.7	0.2
25	0.10% - 1 mL	Chloroform	0.01% HS15-20 mL	5000 rpm	10 min*	500 rpm	130.8	0.3
26	0.10% - 1 mL	Chloroform	0.01% PXM- 20 mL	5000 rpm	10 min*	300 rpm	196.8	0.3
27	0.10% - 1 mL	Chloroform	0.01% PVP- 20 mL	5000 rpm	10 min*	300 rpm	270.8	0.2
28	0.10% - 1 mL	Chloroform	0.01% PVA- 20 mL	5000 rpm	10 min*	300 rpm	358.3	0.2
29	0.10% - 1 mL	Chloroform	0.5% HS15- 20 mL	5000 rpm	10 min	300 rpm	275.1	0.4
30	0.10% - 0.2 mL	Chloroform	0.5% HS15- 20 mL	5000 rpm	10 min	300 rpm	490.3	0.6
31	0.5% - 1 mL	Chloroform	0.1% HS15- 20 mL	3000 rpm	10 min	300 rpm	90.6	0.6
32	0.5% - 1 mL	Chloroform	0.5% HS15- 20 mL	3000 rpm	10 min	300 rpm	285.9	0.6
33	0.5% - 1 mL	Chloroform	1% HS15- 20 mL	3000 rpm	10 min	300 rpm	46.0	0.2
34	1% - 1 mL	Chloroform	0.5% HS15- 20 mL	3000 rpm	10 min	300 rpm	165.8	0.5

\*: Sonication was progressed on an ice-bath.

Therefore, these conditions were selected as for ESE in this study. Then, the same method was applied to prepare PDLLA and PLGA NPs using different stabilisers in various concentrations (Table 2.2). The method established for PCL was also used for PDLLA and PLGA. This is because PCL is more hydrophobic than PDLLA and PLGA, which would require more

challenging optimisation, and the conditions that work for PCL can be applied to PLA and PLGA.

The size of the PCL-PVA NPs decreased gradually with increasing concentration of the stabiliser. Trends were less clear for other stabilisers, though the smallest particles were typically produced when stabiliser concentration was highest, but often with a higher PDI (**Table 2.4**). The smallest particles (88 nm) were obtained when using 1% PXM, but the lowest PDI (0.15) was achieved using 0.5% PVA or 0.01% HS15. PVA produced NPs within the target size (150- 200 nm), but not the latter because of the low stabiliser concentration.

Looking at the data for PDLLA and PLGA NPs (**Table 2.4**), size and PDI fluctuated and, again, a clear trend was hard to identify. PDLLA NPs within the target range were obtained with 0.01-0.2% PXM and 0.01-0.5% HS15 with acceptable PDI ranging from 0.15 to 0.35. Finally, for PLGA NPs, particles within the 150-200 nm were obtained when using 0.01, 0.5% or 1% PXM, 0.2% PVP, 0.1% PVA or 0.1% HS15; PDI varied between 0.19 and 0.42. PLGA NPs obtained under other conditions were either too large or too small.

**Table 2.4 Size and size distribution of polyester NPs prepared by ESE.**

Stabilisers concentration (w/v)		0.01%		0.10%		0.20%		0.50%		1%	
Polyester (0.1%)	Stabilisers	size	PdI	size	PdI	size	PdI	size	PdI	size	PdI
PCL	PXM	187	0.2	212	0.3	72	0.5	207	0.4	88	0.5
PCL	PVP	313	0.3	276	0.2	148	0.3	9158	0.9	70	0.6
PCL	PVA	396	0.3	309	0.3	245	0.2	184	0.2	130	0.3
PCL	HS15	201	0.2	173	0.4	247	0.4	213	0.4	53	1.0
PDLLA	PXM	179	0.2	168	0.4	167	0.3	112	0.5	1150	0.4
PDLLA	PVP	240	0.2	214	0.2	127	0.3	51	0.6	78	0.6
PDLLA	PVA	217	0.3	279	0.4	221	0.2	142	0.3	114	0.3
PDLLA	HS15	157	0.2	152	0.2	152	0.3	166	0.4	37	1.0
PLGA	PXM	167	0.3	123	0.2	133	0.5	198	0.4	148	0.3
PLGA	PVP	410	0.5	307	0.2	200	0.2	101	0.5	144	0.5
PLGA	PVA	303	0.2	196	0.2	228	0.2	126	0.3	122	0.3
PLGA	HS15	79	0.3	155	0.2						

(n=1; NPs prepared with 1 mL polyester (0.1%) dissolved in chloroform and 0.01-1% stabiliser.)

In literature, PVA is preferred as a stabiliser for most polyester NPs and has been used at a concentration of 1% to prepare 180-240 nm ( $PdI \leq 0.1$ ) NPs from 2-4% PCL solutions in organic solvents (154, 155). PVA concentrations between 0.5-1% have been used to manufacture 160-270 nm PDLLA NP ( $PdI < 0.2$ ) (156). In most studies, the polyester solutions are more concentrated (ca. 1-5%) than those used here, which could explain the differences in the properties of the NPs obtained. After noting that the size distribution of NPs obtained using

conventional emulsification methods would be high, Wei *et al.* (157, 158) emphasised that this is an obstacle to the repeatability of NP production. Here, the results obtained support this observation. Still, it was possible to prepare NPs within the expected size and PDI. And, NPs with the promising stability were selected and studied.

#### Stability of NPs prepared by ESE

For stability studies, a single concentration of each stabiliser was used to manufacture polyester NPs. The following concentrations of the HS15, PXM, PVP, and PVA were, respectively 0.5%, 0.5%, 0.2%, 1% for PCL NPs; 0.2%, 0.1%, 0.2%, 0.5% for PDLLA NPs; and 0.1%, 0.1%, 0.5%, 0.1% for PLGA NPs (**Table 2.5**).

**Table 2.5** Selected stabiliser concentrations for each polymer.

<b>Polymer \ Stabiliser</b>	<b>HS15 (%)</b>	<b>PXM (%)</b>	<b>PVP (%)</b>	<b>PVA (%)</b>
<b>PCL</b>	0.5	0.5	0.2	1
<b>PDLLA</b>	0.2	0.1	0.2	0.5
<b>PLGA</b>	0.1	0.1	0.5	0.1

PCL NPs were prepared using 1% PVA showed good size stability in water at 4°C, but the PDI quickly increased over the target value (PDI>0.2). NPs prepared using any of the other stabilisers showed noticeable size fluctuations over the study period with PDI varying between 0.23 and 0.7 (**Figure 2.4**). PDLLA NPs generally appeared more stable and less affected by the nature of the stabiliser. PDLLA-PXM, -PVP and -PVA remained stable for 15 days, after which size and PDI fluctuated, apart for PDLLA-PVA NPs. Between day 0 and 15, PDI values did not seem to change; however, it should be noted that in most cases, PDI> 0.25 were observed. This somehow contrasts with the impact of HS15 on PLGA NP stability. The size of PLGA-HS15 NPs stayed between 150 and 155 nm (PDI< 0.2) for 15 days. Notably, PLGA-PXM NPs showed stability for two weeks, whereas 0.5% PVP- and 0.1% PVA-coated PLGA NPs showed signs

of destabilisation within the first week. It should be stressed that a single batch of each formulation was prepared in this optimisation step and more work would be needed to confirm these conclusions.

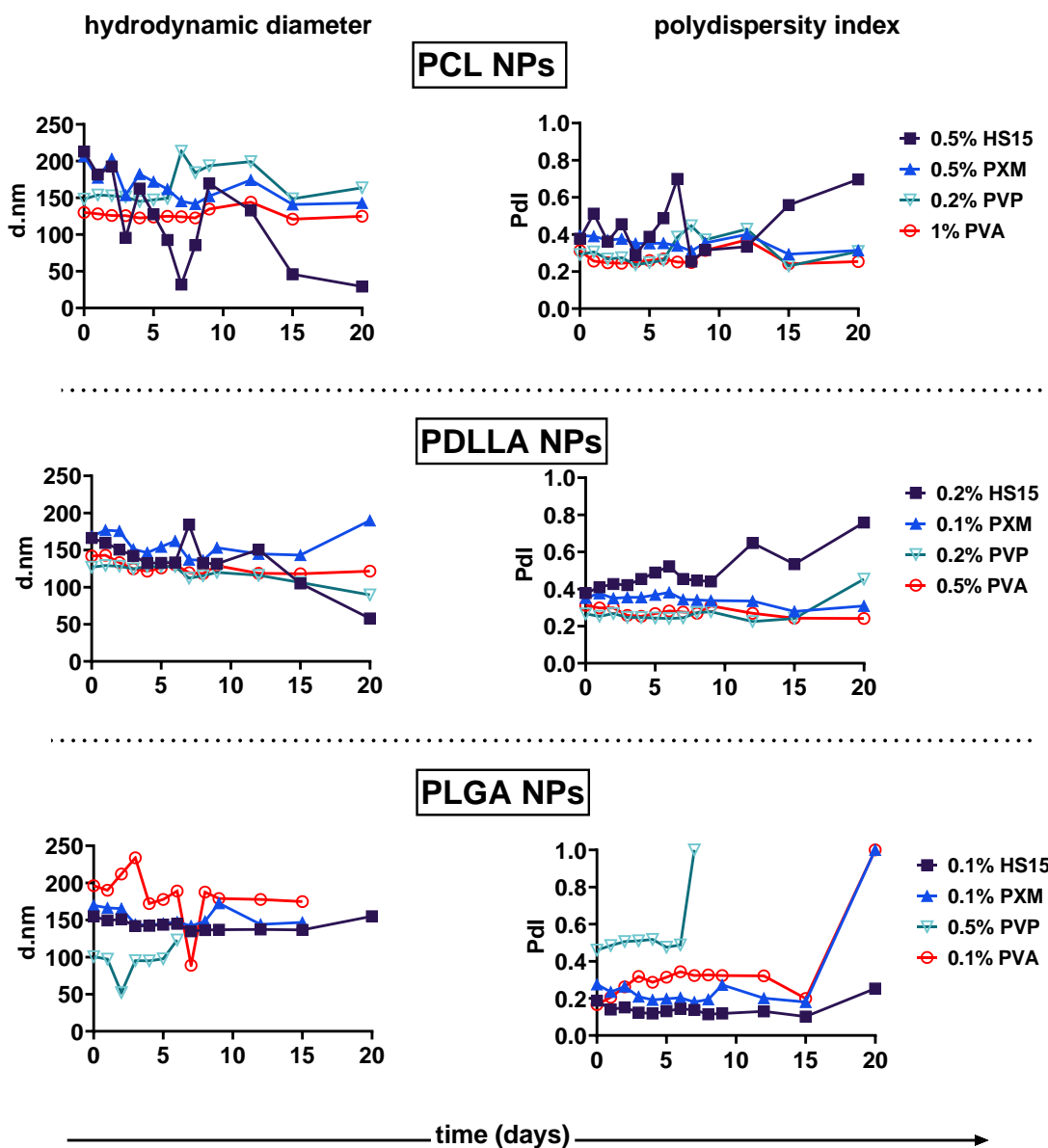


**Figure 2.4 Colloidal stability of polyester NPs.** The stability of NPs prepared by ESE method with different stabilisers was studied in water at 4°C over 20 days (n=1). PXM and PVA stabilisation worked better on PCL NPs, while HS15 was effective only on PLGA NPs. The coating had little impact on the stability of PDLLA NPs, apart when HS15 was used.



Overall, distinct stability patterns were observed for each polymer, highlighting the critical role of stabiliser selection and the polymer-specific nature of stabiliser efficacy. This study also emphasised the need for a tailored approach to stabiliser selection to achieve optimal stability. For example, the hydrolysis rate of the stabilisers should be considered based on the need of the storage duration of the NPs in water. Also, desired degradation rate or mechanism of the polyester NPs in the organism can be arranged using different polymers since polymers have different physicochemical properties. Further investigation into the underlying mechanisms of stabiliser-polymer interactions could provide valuable insights for the design and optimisation of NP formulations in pharmaceutical applications.

*Stability testing- variation of pH and zeta potential over time*

A second stability study was performed on the same formulations, under the same conditions, this time looking at changes in zeta potential and pH. The assessment of pH serves as an indicator of potential degradation. The pH patterns were similar for PCL and PDLLA NPs, with higher pH values (pH 5-6) measured for PVA-coated NPs and more acidic values (pH<4) obtained for all other preparations (**Figure 2.5**). In contrast, all PLGA NPs dispersions were more acidic (159), yet PVA stabilisation again produced marginally less acidic dispersions. The elevated acidity in PLGA suspensions, particularly in comparison to PDLLA, is attributed to the presence of glycolic acid. Studies have confirmed that an increased ratio of glycolic acid causes a reduction in the pH of NP dispersions, as it dissociates more readily in water (160, 161). The pH variations between stabilisers, although less clear, may be due to various interactions between the polyester and the stabiliser, presence of impurities from the polymer source, synthesis process or excess stabiliser in the NP suspension. Notably, the pH of the NP dispersion remained stable even when the NPs were destabilised (**Figure 2.4**).

Stabilisers play a crucial role in preventing particle aggregation. In this study, non-ionic macromolecules were used, which act primarily through steric stabilisation, rather than electrostatic repulsion.

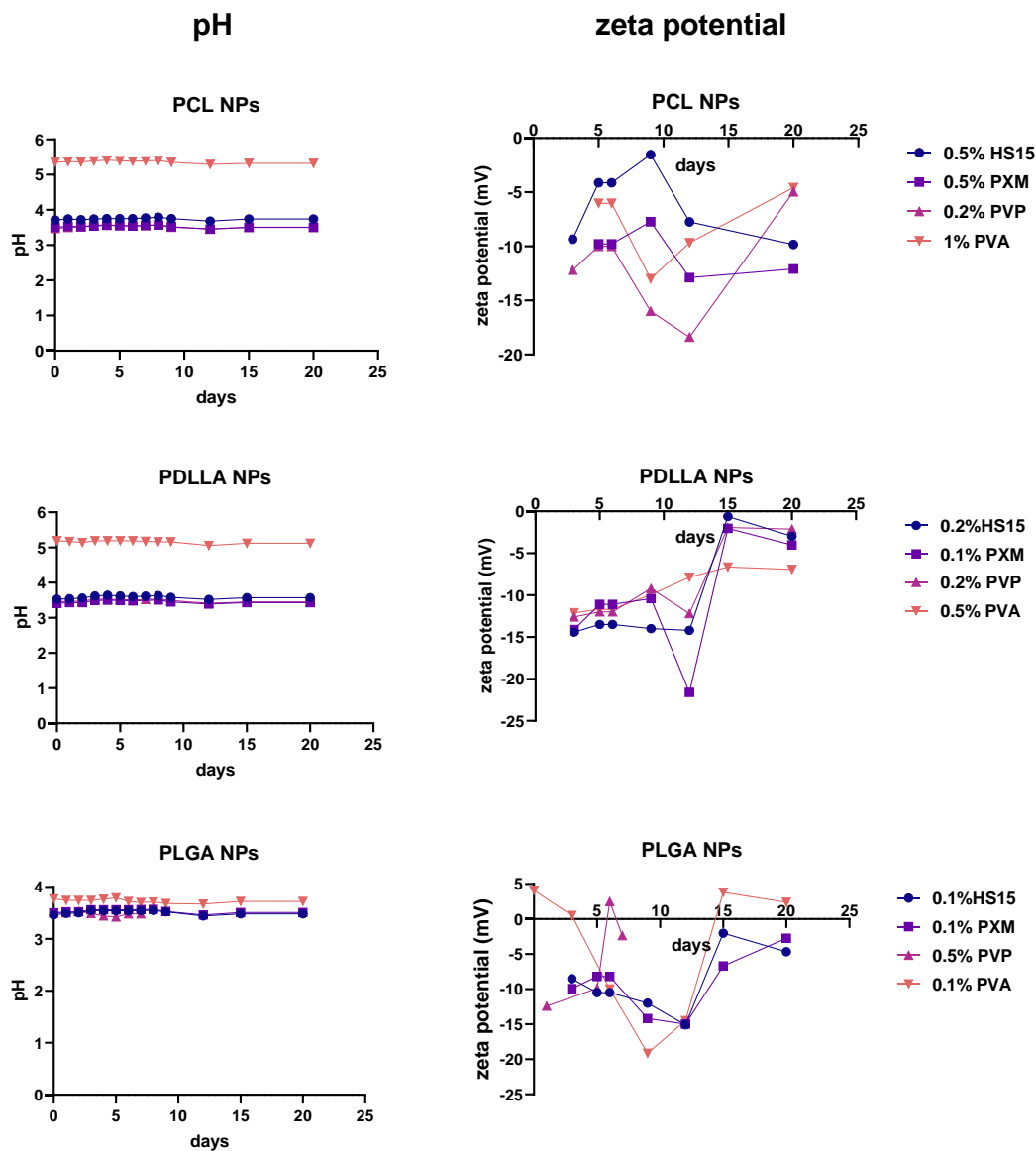


**Figure 2.5 Chemical and surface charge stability of polyester NPs.** PCL, PDLLA, and PLGA NPs were prepared using ESE method. pH and zeta potential were recorded for 20 days (n=1). The pH of the NP dispersions did not change over the study period, while zeta potential fluctuated.

However, polyesters have a carboxylic end group, which is known to provide an anionic surface charge. While most of the literature reports zeta potentials ca. -20 to -30 mV (70, 71), our observations rarely recorded values below -20 mV and in some cases, zeta potential approached neutrality.

Ekinci *et al.* (162) also obtained a neutral zeta potential ( $-0.88 \pm 0.45$  mV) for 182 nm PDLLA-PVA NPs. Zeta potential is also dependent on the stabiliser used and its effectiveness in masking the polymer charge. Also, it is reported that NP surface charge may change depending on the volatility of the solvent used during manufacture and how quickly it is removed (163, 164). Differences in the conductivity of the diluent used for zeta potential measurements can also alter results (165).

Overall, the ESE technique did not allow the production of NPs with the correct quality attributes. This method requires numerous variables to be controlled both during emulsion preparation and organic solvent removal (166, 167). For instance, the speed, duration of stirring or homogenisation, the type of sonicator and the amp, and duration of sonication must be optimised. Similarly, solvent selection, duration of solvent evaporation or the use of a rotary evaporator, must be individualised depending on the desired NP properties.

Nawaz *et al.* (168) studied PCL-PVA NPs and showed the effect of PCL concentration and stirring speed during homogenisation on the size and PdI of the NPs. While high concentration of the polyester cause increase in size, higher homogenisation speeds led to decrease in size and PdI, as expected (168). In another study, it was reported that increasing probe sonication time from 120 to 300 seconds resulted in an increase in size from 187 to 232 nm while increasing stabiliser concentration resulted in a decrease in size from 227 to 148 nm, when sonication conditions were kept constant (70) which is also observed in our study for many of the

stabilisers. Yet, the impact of changing stabiliser concentration is not always linear (**Table 2.4**), making it hard to predict the impact of changes made (71, 72).

Conducting experiments based on the considerations such as non-linearity of size changes based on concentration or sonication duration proved to be time-consuming in the attempt to produce NPs of the appropriate size and stability for our study. Therefore, it was decided to stop the ESE manufacturing and explore nanoprecipitation as a method for NP manufacture. At the same time, the decision was made to focus on PLGA and PDLLA only as PCL with the correct properties could not be produced (data not shown). PVA and PXM were used as the stabilisers since the molecular structure of these two stabilisers differs in terms of hydrophobicity and it is thought that it affects the final surface characteristics of the prepared polyester NPs.

#### ***NP preparation- nanoprecipitation***

PDLLA and PLGA NPs were prepared by nanoprecipitation using acetone as the solvent. Acetone was preferred for this method because of its volatility, which allows easy removal from dispersions without the need for dialysis (169-171). PVA is one of the most commonly used stabilisers in the literature for the preparation of NPs, so PVA was chosen as the first stabiliser for the preparation of NPs. As the aim is to prepare polyester NPs with different surface properties for cellular uptake testing, the molecular structures of the stabilisers were taken into account when deciding on the stabilisers. PXM is a surfactant with a hydrophobic core and PEG ends on both sides of the polymer chain, which was expected to give the NPs a more hydrophilic feature. PVA and PXM were therefore chosen as stabilisers.

In previous studies, 1% has been suggested as a suitable PVA or PXM concentration (172-174). Here, the impact of stabiliser concentration on size and PDI was systematically investigated for the optimisation studies.

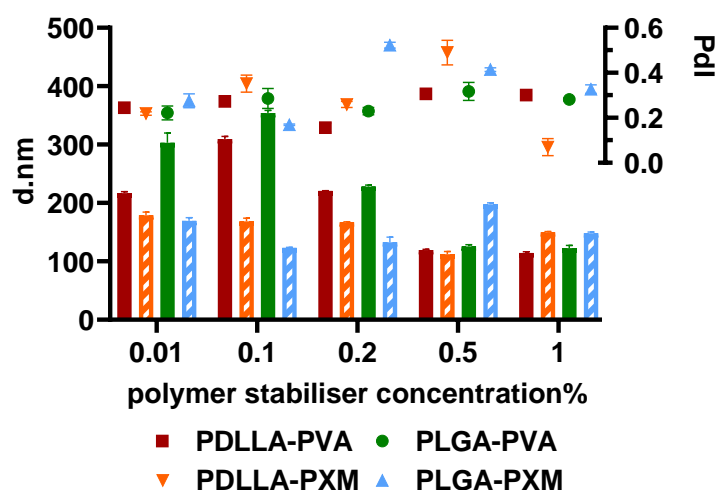


**Figure 2.6 Impact of stabiliser concentration on NP properties.** Results are presented as the mean $\pm$ SD (n=3).

The effect of polymer and stabiliser concentration on the size of PDLLA and PLGA NPs is illustrated in **Figure 2.6**. The diameter of PDLLA- and PLGA-PVA NPs decreased with increasing concentration of the stabilisers, while PdI did not show a gradual decrease as PVA did. It should be noted that this trend is only observed for PVA concentrations  $\geq 0.1\%$  (**Figure 2.6**) These results agree with previous reports that increasing PVA concentration leads to a decrease in NP size (175, 176) probably because the high concentration of stabilisers helped the polyesters not to aggregate during NP formation and finally created NPs with smaller core. Surprisingly, Maaz *et al.* (177) observed an enlargement in PDLLA-PVA NPs diameter with increasing stabiliser concentration (147 to 302 nm; 0.1 to 0.4%), possibly due to an increase in the thickness of the stabiliser layer.

The impact of PXM is less striking with NPs mostly staying within a narrow size range, independently of PXM concentration. Sharma *et al.* (178) reported that an increase in the concentration of PXM from 0.2-1.5%, resulted in a decrease in PLGA-PXM NP size from 205 nm to 177 nm. In contrast, others have reported that changing PXM concentration has limited

impact on PLGA NP size with the increasing concentration of stabiliser from 0.05% to 2% , but with only 10 nm change in the NP size (179), somewhat similar to results obtained here (177). The reason of PXM did not affect the size might be because of its surfactant nature and the used concentrations are already over critical micelle concentration ( $2.8 \times 10^{-6}$  M) (180). Since the PXM molecules are already in micellar form, further increasing the concentration may not significantly impact the stabilization of NPs or affect their size.

Interestingly, PVA-stabilised NPs exhibited larger sizes at low stabiliser concentrations compared to PXM-stabilised NPs. At low PXM concentrations, the hydrophobic segment (poly(propylene oxide)) (**Figure 2.1-C**) of PXM may facilitate more effective interactions with the hydrophobic core of the polyesters NPs, thus, improving coverage and stabilisation of the NPs (181). Based on this optimisation study, a stabiliser concentration of 1% was chosen as this allowed the production of PDLLA and PLGA NPs with the correct quality attributes (i.e. 150-200 nm and PDI (<0.2)).

#### Residual stabiliser detection

The residual stabiliser concentration was determined for both types of NPs (**Figure 2.7**). The results indicated some difference in the interaction between stabiliser and the polymer cores. Higher residual stabiliser concentrations were detected in the supernatant of PDLLA-NPs compared to PLGA-based NPs, suggesting better coverage for the latter NPs.

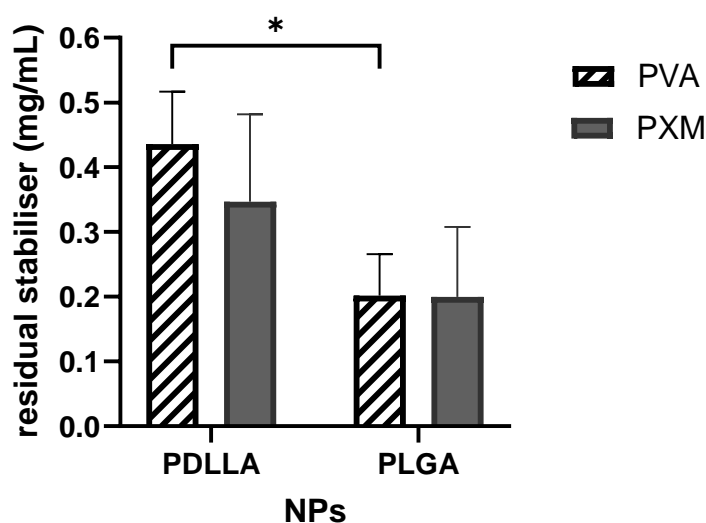


**Figure 2.7 Residual stabiliser quantification.** PDLA and PLGA NPs were prepared by nanoprecipitation using 1% PXM or PVA and residual stabiliser concentrations were measured using colorimetric techniques. Stabiliser coverage was better on PLGA, and PVA coverage was significantly greater on PLGA than that of PDLA. Data is presented as mean $\pm$ SD, n=3, two-way ANOVA, Bonferroni test for multiple comparison, \*p<0.05).

## 2.4.2 Characterisation of Polyester NPs

### *Size and zeta potential measurements*

PDLA and PLGA NPs with a 140-170 nm size and low PDI (0.07-0.16) were obtained. Notably, PXM-coated NPs tended to be larger compared to their PVA-coated counterparts (**Figure 2.8**).

PDLA-PVA NPs and PLGA-PVA NPs exhibited zeta potentials of  $-30\pm 12$  mV and  $-17\pm 7$  mV, respectively, which were more negative than those observed for PDLA-PXM NPs ( $-4\pm 3$  mV) and PLGA-PXM NPs ( $-9\pm 5$  mV) (**Figure 2.8**). Clearly, the PVA-coated NPs exhibited a greater negative surface charge compared to their PXM-stabilised counterparts. These results differ from what was observed for NPs prepared by ESE, but lower stabiliser concentrations were used for ESE method (182, 183). These results are in agreement with values reported in the literature for PXM-stabilised PDLA or PLGA NPs (173, 178, 184, 185) and PVA-

stabilised NPs (175, 177, 184, 186, 187). The observed differences in zeta potential could be due to the different nature of the interactions facilitated by PVA and PXM (183, 188).

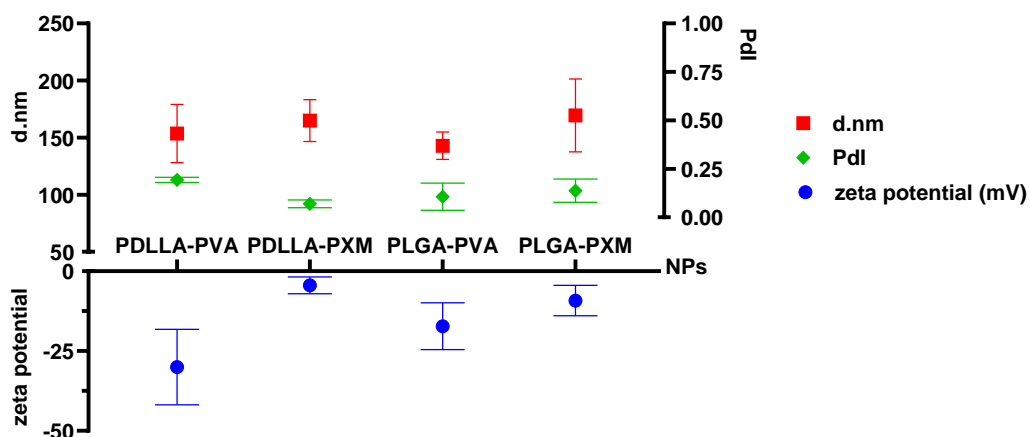


**Figure 2.8 Characterisation of polyester NPs.** The size, PDI and zeta potential of the NP suspensions measured using DLS at room temperature. PXM coated NPs were slightly larger and less anionic than PVA-coated NPs. Data is presented as mean $\pm$ SD (n=3).

Additionally, looking at the residual stabiliser data, since PVA showed better coverage on the PLGA core than on the PDLLA core (**Figure 2.7**), this may have shielded the carboxyl ends from water molecules, limiting ionisation and hence minimising the observed charge on PLGA-PVA NPs.

### TEM

NPs displayed a spherical morphology (**Figure 2.9**). The measured average diameters for P-NPs were as follows: PDLLA-PVA NPs 124 $\pm$ 29, PDLLA-PXM NPs 154 $\pm$ 10, PLGA-PVA NPs 132 $\pm$ 30, and PLGA-PXM NPs 151 $\pm$ 16 nm. PVA-coated NPs showed larger particle size distribution than PXM-coated NPs which is in agreement with the DLS results. There were small differences in the sizes determined by TEM and DLS. As expected, diameters measured by DLS were systematically 10-30 nm larger than those obtained by TEM. That difference is



attributed the hydration of stabiliser coating under the conditions used for DLS, while TEM measures dried NPs size on the copper grid (189).

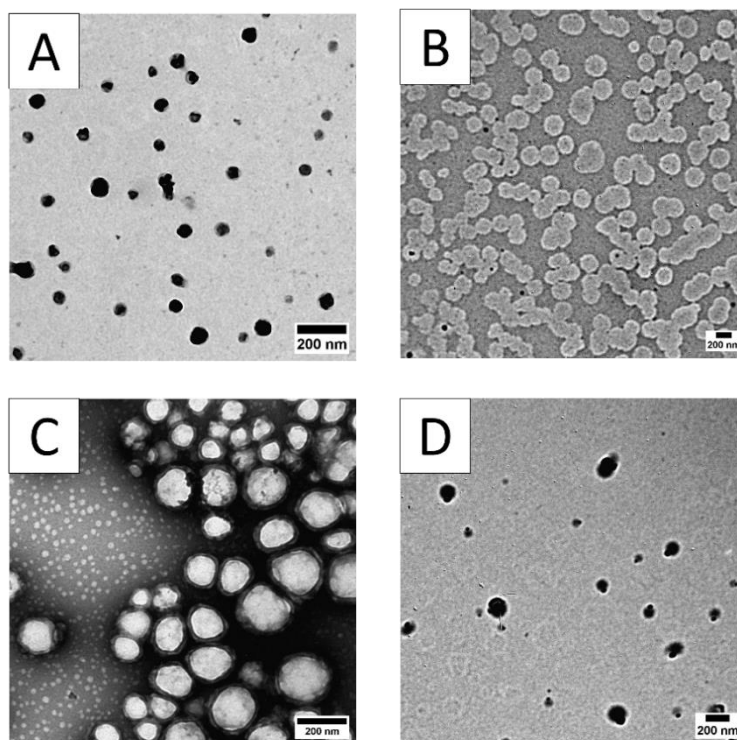


**Figure 2.9 TEM images of the NPs.** (A)PDLLA-PVA (124 nm), (B) PDLLA-PXM (154 nm), (C) PLGA-PVA (132 nm), (D) PLGA-PXM (151 nm). Bars represent 200 nm.

### 2.4.3 Colloidal stability

The physical stability of all NPs preparation was studied at three different temperatures: 4°C, room temperature (RT) and 37°C (**Figure 2.10**). All formulations (PDLLA-PVA, PDLLA-PXM, PLGA-PVA, PLGA-PXM NPs) demonstrated good colloidal stability at 4°C in deionised water for a minimum of 30 days, with particle diameters staying within the aimed 150-200 nm range and a PDI below 0.3 (**Figure 2.10-A**). Previous research by Swider *et al.* (190) focusing on PLGA-PVA NPs (200 nm) indicated their potential to maintain colloidal stability for at least two weeks in situ. In the literature, ~170 nm PLGA-PXM NPs were reported to be stable for 90

days at 25°C (178), however the PDI were not recorded. In addition, studies noted that under favourable surfactant conditions (0.1-1%), stability could extend up to 12 months on double emulsion systems (162). At RT, PDLLA and PLGA NPs sizes were maintained below 200 nm but the size of PDLLA NPs started to fluctuate after the second week. The decrease in stability may be attributed to the presence of salt ions in the PBS. PBS salts can affect the stability of NPs by influencing the ionic strength and pH of the surrounding medium, which in turn can affect the electrostatic interactions and surface charge of the NPs, leading to changes in colloidal stability and aggregation behaviour. In addition, the presence of salts can induce NP aggregation by shielding surface charges or by promoting interparticle interactions. However, the PDI remained constant ( $\leq 0.21$ ) throughout the 30-day study period. Although average sizes showed continued stability, larger error bars began to appear from day 7 of the RT and 37°C tests, indicating a reduction in some inter-batch variability. The study of NP stability at 37°C in DMEM was designed to predict the behaviour of polyester NPs under cell culture conditions. *In vitro* studies are expected to last a maximum of three days and maximum 24 h tests will be conducted with NPs in the CCM, during which time all NPs were found stable (**Figure 2.10-C**).

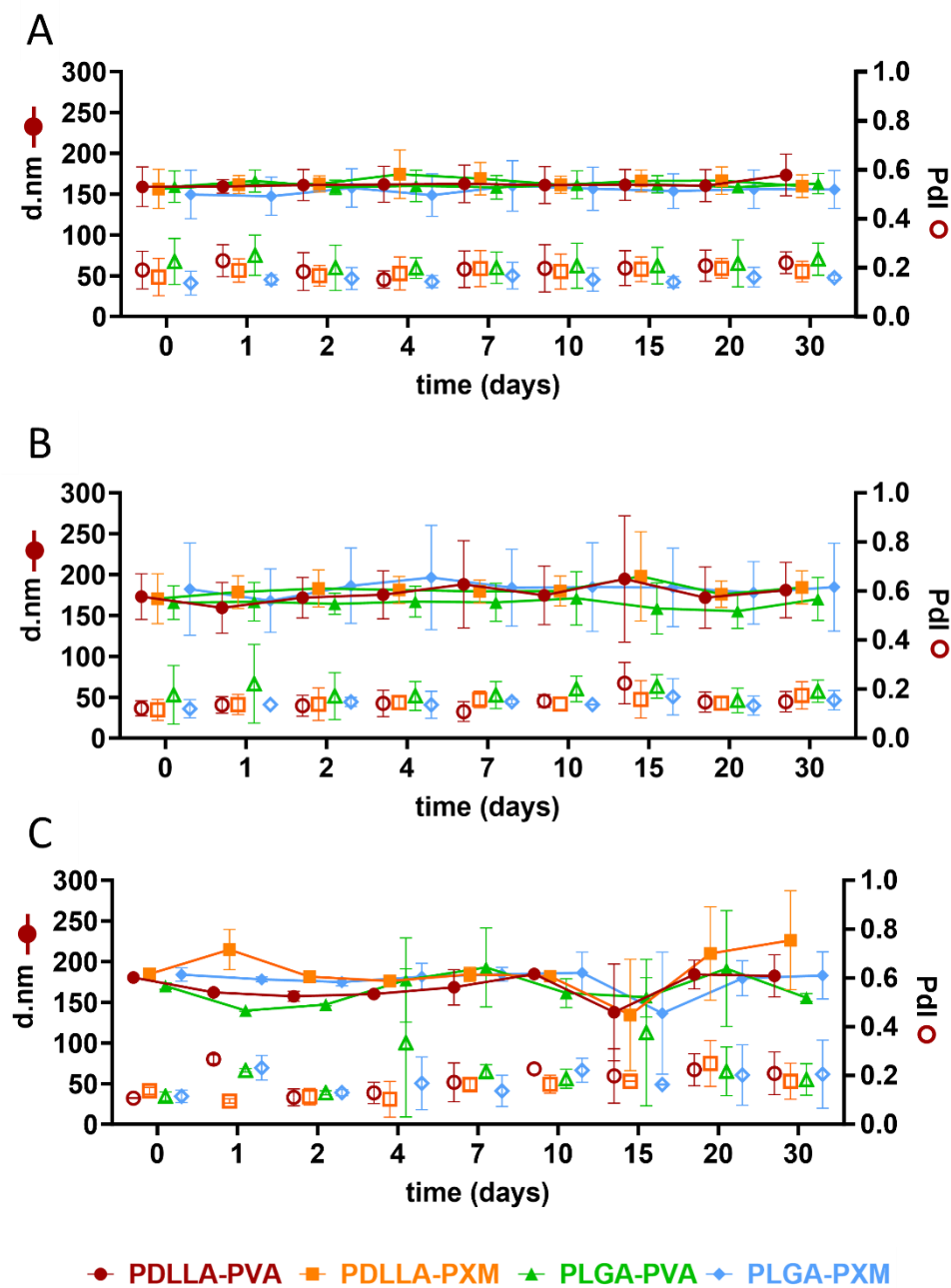


**Figure 2.10** NPs colloidal stability at (A) 4°C, (B) RT and (C) 37°C. (A-C) Particle diameter (closed symbols; left axis) and PDI (open symbols; right axis) were measured for 30 days under different conditions. NPs showed better stability at 4°C (in water) (A). While at RT (PBS) and at 37°C (in CMM) NP stability decreased (B-C). Data is presented as mean $\pm$ SD (n=3).

The zeta potential of NPs stored at 4°C in deionised water was measured over time. PVA-coated NPs had a stronger negative charge (-48 and -33 mV) than PXM-coated NPs (-3 and -14 mV)

starting from the beginning of the stability test to the 30<sup>th</sup> day (**Figure 2.11**). The values are slightly different to what was reported in **Figure 2.8**, but the trend is the same. Over the test period, PDLLA-PVA NPs surface charge increased from -48 mV to -15 mV which was a greater increase than seen for PLGA-PVA NPs. Despite a near-neutral zeta potential, PDLLA-PXM NPs did not show any aggregation for 30 days at 4°C and kept their PDI below 0.2, confirming successful steric stabilisation.

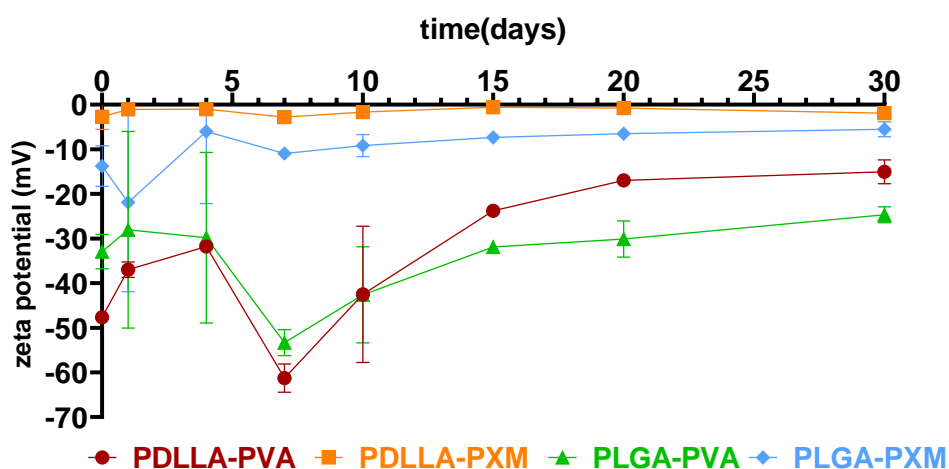


**Figure 2.11** NPs zeta potential as a function of time. Surface charge of the 4°C stored NPs for 30 days. Data is presented as mean±SD (n=3).

In these studies, zeta potential was monitored in simple aqueous solutions only. In the future, similar studies should be performed in cell culture media containing 10% FBS at 37°C as this is critical for predicting the *in vitro* and *in vivo* behaviour of NPs. This is particularly important in cases where protein adsorption can alter the zeta potential, potentially affecting the interaction between NPs and cells.

BSA is used for *in vitro* stability testing of NPs, simulating biological conditions. This provides initial information on the adsorption of proteins on the NPs and stability of the coating. Polyester NPs were exposed to 0.5 mg/mL BSA for 30 min to assess the impact of protein adsorption on size and agglomeration. PDLLA-PVA NPs showed a decrease in size of ~50 nm,

while PDLLA- PXM NPs showed a slight increase of about 30 nm. The average size of PLGA-PVA and PLGA-PXM NPs remained the same. Likely, the better coverage was achieved for PLGA NPs (**Figure 2.7**) repelled BSA and allowed NPs to maintain their size in BSA solution. Incubation for one day in FBS-containing media (**Figure 2.10-C**) or 30 min in a BSA solution at 37°C (**Figure 2.12**) had similar effect on diameter of PDLLA and PLGA NPs. Indeed, both conditions led to 1) a decrease in PLA-PVA NPs diameter, 2) an increase in PLA-PXM NPs size and 3) no change for PLGA-PXM NPs. Hence, prolonged exposure to higher albumin (50 mg/mL) or protein concentration (80 mg/mL) should be tested to understand their stability under physiological conditions.

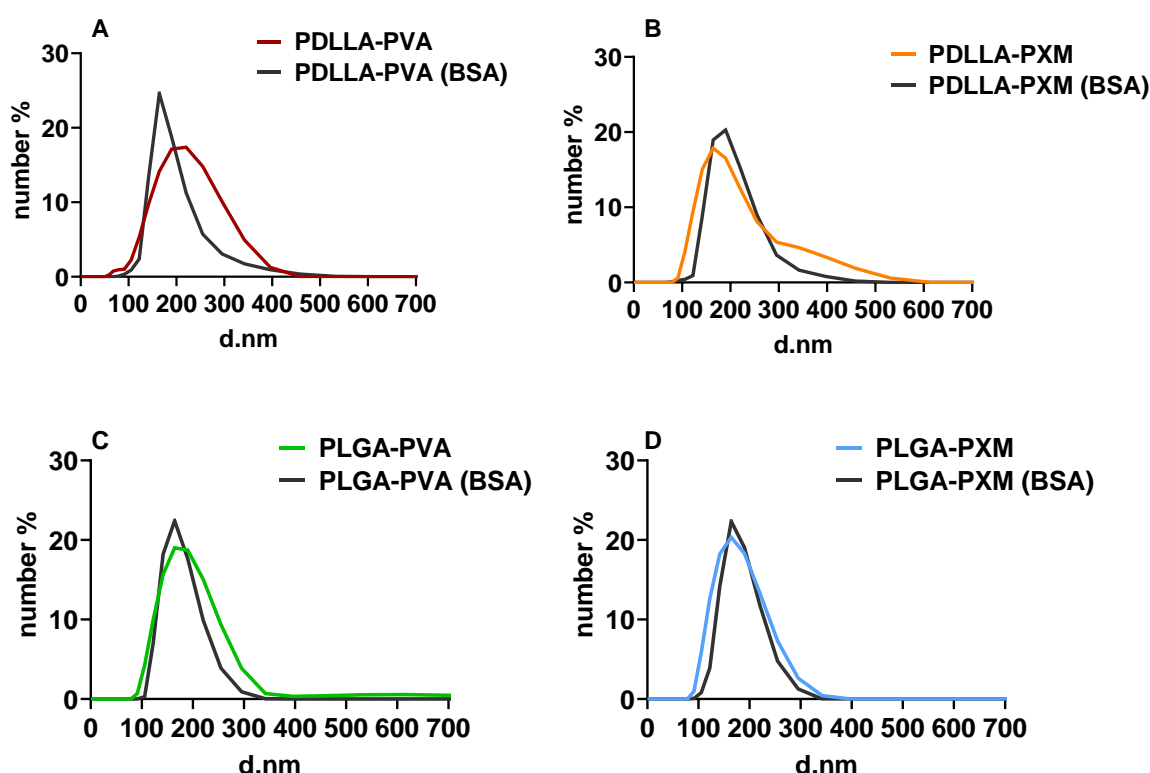


**Figure 2.12 Stability of NPs after incubation in a 0.5 mg/mL BSA solution.** Polyester NPs were treated in BSA solution at 37°C for 30 min (n=1).

One study by Oliveira *et al.* (191) reported that the size of PLGA-Poloxamer 188 NPs increased by 10 nm in a 0.4 mg/mL BSA solution at 37°C, by 50 nm in mouse plasma and by >1000 nm

in human plasma after 1 hour. It was also reported that the protein corona concentration on the NPs followed a similar pattern, reflecting differences in protein concentration between the three media. Therefore, protein adsorption assay with BSA and human serum protein (HSP) was conducted as part of the surface hydrophobicity assessment.

#### **2.4.4 Hydrophobicity of the NPs**

Three separate methods were used to assess NP hydrophobicity: SAT, HIC and protein adsorption.

SAT can be used to assess the hydrophobicity of NPs by monitoring their aggregation in the presence of increasing salt concentrations. Hydrophobic NPs tend to aggregate in the presence of salts due to reduced electrostatic repulsion as salt molecules compete for water molecules and allows hydrophobic interactions to strengthen, leading to NP aggregation (192). Therefore, the lower the salt concentration needed to trigger aggregation, the higher the hydrophobicity (133). PXM-coated NPs maintained their size even in 4 M NaCl<sub>aq</sub>, while PVA-coated NPs began to aggregate in 2 M NaCl<sub>aq</sub>. PS NPs, which were used as the positive control, aggregated at significantly lower salt concentration compared to any of the PDLLA and PLGA NPs (**Figure 2.13-A**). All NPs showed signs of aggregation in 5 M NaCl<sub>aq</sub>, but even at that high concentration, aggregation was stronger for PS NPs compared to polyester NPs. Based on the SAT results, NPs can be classified in order of increasing hydrophobicity as PDLLA-PXM < PLGA-PXM << PDLLA-PVA < PLGA-PVA <<<< PS.

HIC utilises stationary phases of varying hydrophobicity and analyses the interactions between the hydrophobic regions of the NPs and the stationary phase. Hydrophobic NPs interact more strongly with hydrophobic stationary phases, resulting in longer retention times. The hydrophobicity of NPs can then be compared by analysing these retention times (130, 132). PS NPs had higher HIC index (0.41) compared to other NPs, confirming the SAT results, which is

in agreement with the literature (130, 131). Also, the HIC index of PVA-coated NPs were higher compared to PXM-coated NPs. Based on HIC results, NPs can be classified in order of increasing hydrophobicity as PDLLA-PXM < PLGA-PXM < PLGA-PVA << PDLLA-PVA << PS-NPs (**Figure 2.13-B**). Although this order is broadly similar to what was seen in the SAT tests, the differences are less striking. Here, the HIC index of PS NPs was significantly higher than the values obtained for polyester NPs, except for PDLLA-PVA NPs. Carstensen *et al.* (132) suggested that coating PS NPs with PXM could reduce their hydrophobicity and their retention on HIC columns. Similarly, in a different study PLA-PEG NPs found to be more hydrophilic than PDLLA NPs (132).

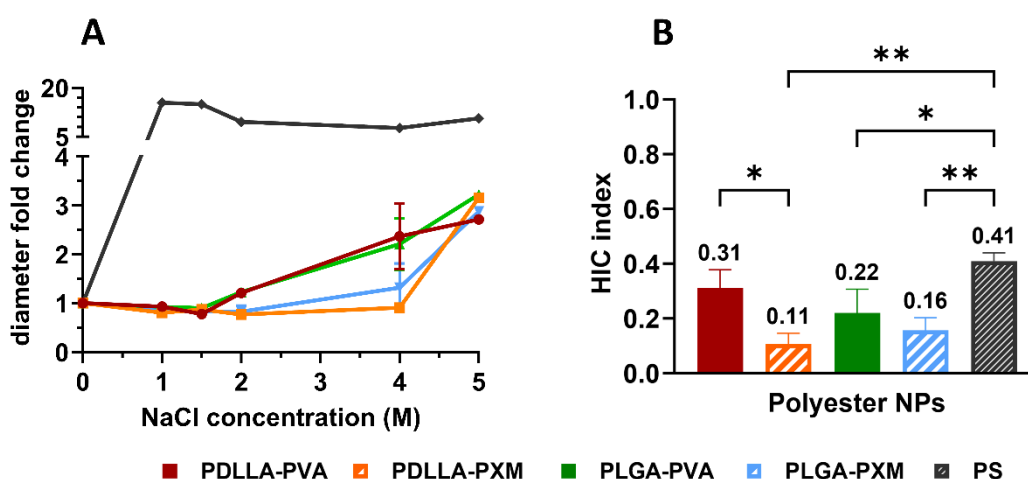


**Figure 2.13 Hydrophobicity assessment of the NPs.** (A) SAT, (B) HIC index. Results are represented as mean  $\pm$  SD (n=3). (\*p<0.05, \*\*p<0.01, one-way ANOVA with Tukey multiple comparison test)

Overall, results from SAT and HIC agreed, suggesting that PVA-coated NPs are relatively more hydrophobic. This hydrophilicity of PXM-coated NPs attributes to PEG ends, which run into water, of PXM while hydrophobic block interacts with the polyester core. Interestingly, PDLLA-PXM NPs were slightly more hydrophilic than PLGA-PXMs despite a potentially less effective stabiliser coverage as suggested by the quantification of residual stabiliser (**Figure 2.7**).

The kinetics of protein adsorption was studied in the presence of 1 mg/mL BSA (**Figure 2.14-A**) or 1.25 mg/mL HSP (**Figure 2.15-A**). After the NPs were treated in the presence of protein, the amount of protein adsorbed on the NP was calculated by measuring the amount of unabsorbed protein in the liquid phase. The adsorption was assessed by measuring the residual protein concentration in the diluent after 60- and 120-min. Initial data showed that protein adsorption did not change in the first 60 min. However, there was a marked shift over the next hour, with a two-fold increase in protein adsorption to approximately 0.25 mg/mL.

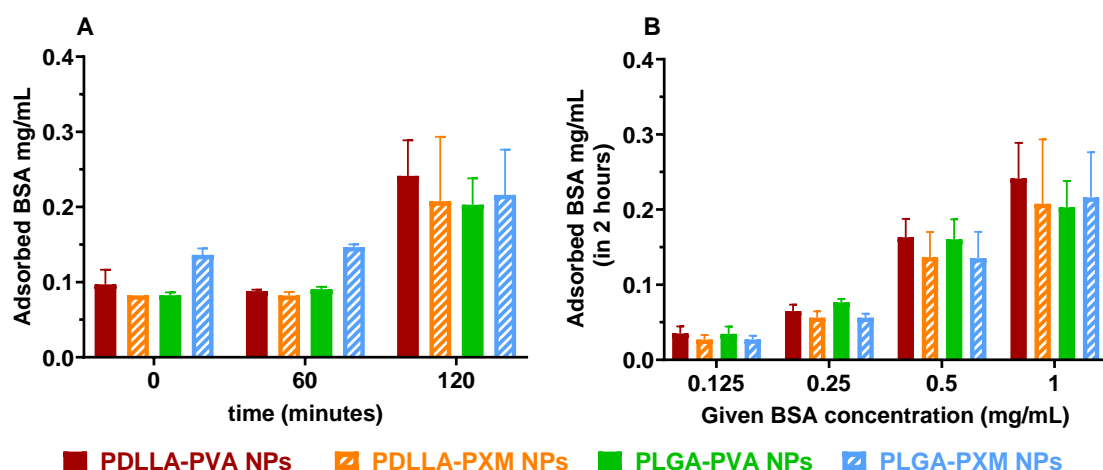


**Figure 2.14 BSA adsorption study.** A) Quantification of the BSA adsorbed on P-NPs 0, 60, and 120 min after NPs were exposed to BSA (1 mg/mL) at 37°C, (B) Impact of concentration (0.125-1 mg/mL) on BSA adsorption after 2h at 37°C. Data is presented as mean $\pm$ SD (n=3), two-way ANOVA, Tukey post-hoc test).

The study was extended to cover HSP as it would better mimic the organism. HSP differs from BSA in its protein content; HSP contains human sourced albumin, fibrinogens, coagulation factors, complement proteins, transport proteins, *etc.*, whereas BSA is only an animal albumin. HSP showed different kinetics of protein adsorption compared to BSA. In particular, the binding of HSP was faster and reached higher levels than observed for BSA. Interestingly, the adsorption of HSP showed no apparent increase over time, indicating rapid saturation on the NP surface (**Figure 2.15-A**).



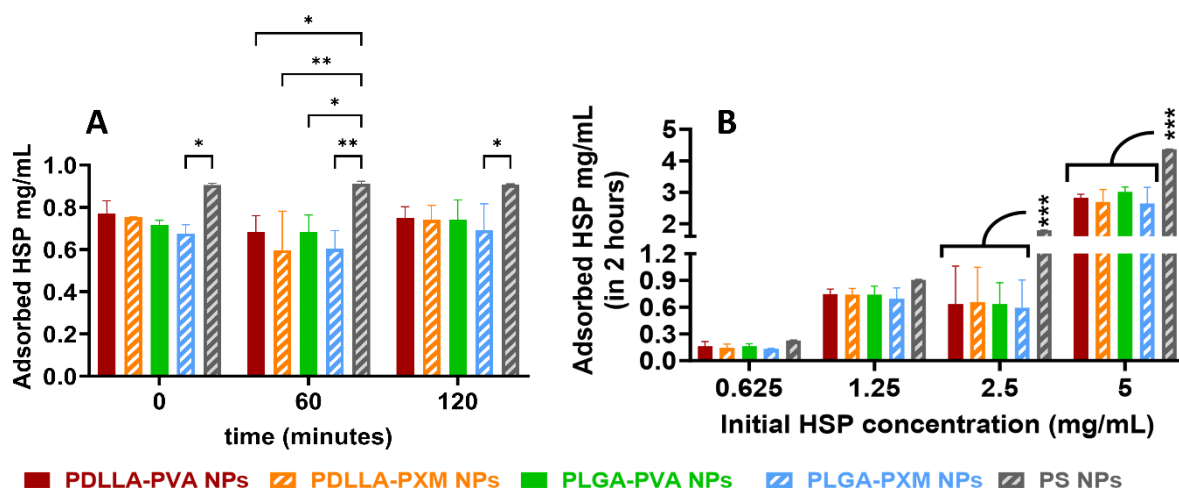


**Figure 2.15 HSP adsorption onto NPs.** (A) Quantification of the HSP adsorbed on P-NPs 0, 60, and 120 min after NPs were exposed to HSP (1.25 mg/mL) at 37°C, (B) Impact of concentration (0.625-5 mg/mL) on HSP adsorption after 2h at 37°C. Data is presented as mean±SD (n=3), \*p<0.05, \*\*p<0.01 \*\*\*p<0.001, two-way ANOVA, Tukey post-hoc test).

As it was suggested before, differences in the composition of the protein containing media used in the test could explain these results (191). HSP is composed of different kinds of proteins and adsorption to NP surfaces may be faster for proteins with more exposed binding sites or flexible conformations. Additionally, each kind of protein may exhibit varied electrostatic interactions, hydrophobic interactions, and ligand-receptor binding which cause difference on binding onto NPs. PS NPs were used as a control only in the HSP study. As expected, HSP adsorption on PS NPs was higher compared to polyester NPs, though this difference was statistically significant only at 60 min (**Figure 2.15-A**). No differences were seen between all tested polyester NPs for BSA adsorption (**Figure 2.14-A**). However, initial HSP adsorption appeared higher for PDLLA vs. PLGA NPs and for PVA vs. PXM, though these were not statistically significant. As time progressed, those differences disappeared.

The concentration-dependence of BSA and HSP adsorption on polyester NPs was evaluated (**Figure 2.14-B** and **figure 2.15-B**). The results confirmed that adsorption increased as a

function of protein concentration in both cases. At higher BSA concentrations, the binding sites on the NPs were more exposed, resulting in higher adsorption rates. Although it remains a challenge to differentiate NPs based on adsorption characteristics, a significant difference was observed for PS NPs. At concentrations of 2.5 mg/mL and 5 mg/mL, PS NPs showed significantly higher adsorption of HSP (**Figure 2.15-B**). So, the higher hydrophobicity of PS NPs was confirmed by all methods used here.

According to the results obtained here, stabiliser coating had no impact on protein adsorption which prevents a comparison of the NPs' hydrophobicity. However, stability studies in BSA solution (37°C, 30 min) (**Figure 2.12**) and 10% FBS containing cell culture media (37°C, 1<sup>st</sup> day) suggested that the stabiliser had some impact. These differences may be due to differences in timing and sensitivity of the method and may depend on how strongly proteins are adsorbed on NP surface. Overall, HIC and SAT appeared better at discriminating between NPs of varying hydrophobicity, compared to protein adsorption.

In this chapter, the surface charge and hydrophilicity of the PDLLA and PLGA NPs prepared with two different stabilisers (PVA and PXM) were found to be different due to the difference in coating. Even though, the different coatings did not create a significant difference in the protein adsorption, it is decided to test these NPs on cellular uptake. Thus, it will be tested whether the choice of stabiliser makes a difference in the uptake of NPs by the liver cells.

## 2.5 CONCLUSION

The nanoprecipitation method was preferred over the ESE method because of its simplicity and efficiency. Once the nanoprecipitation method was optimised, spherical 140-200 nm NPs were prepared with low PDI (<0.2) using 1% polyester (PDLLA or PLGA) and 1% stabiliser (PVA or PXM). Characterisation of the NPs highlighted differences depending on both coating and

core composition. Core composition mostly affected stabiliser adsorption, though small differences were also seen in surface hydrophobicity. More noticeable differences were seen between the two stabilisers in terms of zeta potential and surface hydrophobicity, though these did not negatively impact stability or affect protein adsorption.

# Chapter 3: MONOCULTURE STUDIES OF POLYESTER NANOPARTICLES

## 3.1 INTRODUCTION

Assessing the safety of NPs is crucial in establishing suitable *in vitro* working conditions (193, 194). Equally, knowledge of the biological interactions between NPs and cells is important for predicting and understanding the biological fate of NPs, including their biodistribution (195, 196). By elucidating these interactions, this research contributes to a better understanding of how polyester NPs interact with liver cells.

Thus, polyester NPs with different surface properties, prepared in the previous section, were tested in selected liver-associated cells in this chapter. For this purpose, 4 different cells were used: HEP-G2 hepatoma cell line to represent hepatocytes, HMEC-1 endothelial cells to represent LSEC cells, DTHP-1 macrophages to represent KCs and THP-1 cells to represent monocytes. Firstly, none of the NPs expected to be toxic or inflammatory to the cells because they are made from biocompatible materials. It is expected to observe difference on internalisation rate of NPs with different hydrophobicity by macrophages and monocytes. Due to their opsonisation properties, hydrophobic materials tend to be highly internalised by phagocytic cells. Meanwhile, HEP-G2 uptake may change according to NPs surface charge because it known that hepatocytes favour positively charged NPs while LSECs expected to internalise negatively charged NPs (24).

### **3.2 AIM AND OBJECTIVES:**

After assessing the safety of the NPs, the aim was to compare the uptake behaviours in various liver cell lines and evaluate the potential impact of NP surface properties by comparing various stabilizers.

Objectives:

1. The toxicity of the stabilisers and NPs was investigated using thiazolyl blue tetrazolium bromide (MTT) and water-soluble tetrazolium (WST-8) viability tests.
2. Inflammation responses of DTHP-1 to NPs was tested by measuring the cytokine (TNF- $\alpha$ , IL-6, and IL-10) release in 24-h using an enzyme-linked immunosorbent assay (ELISA).
3. Nile red loaded polyester NPs uptake by HEP-G2 human liver cancer epithelial cells, HMEC-1 endothelial cells, THP-1 monocytes and DTHP-1 macrophages in 1-h was assessed using flow cytometry and a fluorescent microscope.

### 3.3 MATERIALS AND METHODS

#### 3.3.1 MATERIALS

Human liver cancer epithelial cell (HEP-G2; 104-114 passage numbers), monocytic leukaemia cell line (THP-1; 10-20 passage numbers), human microvascular endothelial cells (HMEC-1; 27-35 passage numbers), macrophage-like murine reticulum cell sarcoma (J774) were obtained from European Collection of Authenticated Cell Cultures (ECACC; Salisbury, UK).

WST-8 solution was purchased from AAT Bioquest (Strattech- Ely, UK).

4',6-diamidino-2-phenylindole (DAPI), Dimethyl sulfoxide (DMSO), ethylenediaminetetraacetic acid tetrasodium salt hydrate (EDTA), hydrocortisone, MEM non-essential amino acid solution (NEAA), Nile red, phorbol 12-myristate 13-acetate (PMA), Phosphate buffered saline tablet (PBS tablets), Poloxamer 407 (PXM), Poly(vinyl alcohol) (PVA), thiazolyl blue tetrazolium bromide (MTT), trypan blue solution, sodium azide ( $\text{NaN}_3$ ), Dulbecco's modified Eagle's Medium (DMEM), Dulbecco's Phosphate Buffered Saline (DPBS), heat-inactivated fetal bovine serum (FBS) were all purchased from Merck (Darmstadt, Germany). MCDB-131 medium, RPMI 1640 medium, L-Glutamine, Penicillin-Streptomycin 10,000 U/mL (PenStrep), recombinant human epidermal growth factor (Hu-EGF), 0.25% Trypsin-EDTA, human TNF- $\alpha$  ELISA kit, human IL-6 ELISA kit, human IL-10 ELISA kit, and lipopolysaccharide (LPS), polystyrene latex (PS) NPs (0.20 micron, 2.5 wt%) were bought from Thermo Fisher Scientific (Invitrogen; Loughborough, UK).

### 3.3.2 METHODS

#### *Preparation of cell cultures:*

##### J774 and HEP-G2 cell culture preparation:

Macrophage-like murine reticulum cell sarcoma (J774) cells and human hepatic cancer cells (HEP-G2) were cultured in DMEM supplemented with 10% (v/v) FBS and 1% (v/v) PenStrep. J774 were collected using a cell scraper when the 80-90% confluency was reached. HEP-G2 cells tend to grow in clusters. HEP-G2 were passaged in a 1:5 ratio, by dissociating them using 0.25% trypsin-EDTA, twice a week when 80-90% confluency was reached.

##### HMEC-1 cell culture preparation:

Human microvascular endothelial cells (HMEC-1) were cultured in an MCDB-131 medium supplemented with 10% (v/v) FBS, 1% (v/v) PenStrep, 10 ng/mL Hu-EGF, 1 µg/mL hydrocortisone, and 10 mM L-glutamine. The cells passaged in a 1:10 ratio, by dissociating them using 0.25% trypsin-EDTA, twice a week when 80-90% confluency was reached.

##### THP-1 and DTHP-1 cell culture preparation:

Monocytic leukaemia cell lines (THP-1) were cultured in RPMI 1640 media supplemented with 10 µM L-glutamine and 10 % FBS. These cells were kept between 200,000 and 800,000 cells/mL. Once the cell number reached 800,000 cell/mL, THP-1 were centrifuged, and the old media was replaced with fresh media discarding the excess cells to obtain a final concentration between 200,000-300,000 cell/mL. THP-1 cells were differentiated into macrophages (DTHP-1) by incubating cells with 100 nM phorbol 12-myristate 13-acetate (PMA) in RPMI media for 48 h. Then the PMA including media was removed and the attached cells were rested in the fresh RPMI media for 24 h before further experiments. All cells were incubated at 37°C in 5% CO<sub>2</sub> in a 90% humidified air environment.

### ***Viability studies:***

#### ***Stabilisers toxicity***

The toxicity of PVA and PXM was tested on J774 cells. 10,000 cells were seeded in a flat-bottomed 96-well plate and incubated overnight. Cells were exposed to various concentrations of the stabilisers (0-10 mg/mL in DMEM) for 24 h. The supernatant was removed, and the cells were washed three times with DPBS. MTT (100  $\mu$ L; 0.5 mg/mL in DMEM) was added to each well and incubated at 37 °C for 4h. The media was removed, and the formazan crystals were dissolved in DMSO (100  $\mu$ L). The absorbance ( $\lambda_{\text{max}}$ : 570 nm) was recorded on a Fluostar Omega plate reader (BMG Labtech, Aylesbury, UK). The experiment was performed in triplicate. DMSO (10% v/v in DPBS) was used as the positive control and, untreated cell culture served as negative control.

$$\text{Eq. 3.1} \quad \text{Cell viability}\% = \frac{(OD_{\text{treatment}} - OD_{\text{positive control}})}{(OD_{\text{untreated}} - OD_{\text{positive control}})} \times 100$$

Cell viability was determined using Eq 3.1., where OD refers to optical density.

#### ***Polyester NPs toxicity***

The toxicity of the polyester NPs was tested on J774, HEP-G2, HMEC-1, THP-1, and DTHP-1 cells. In all cases, 10,000 cells were seeded in a flat-bottomed 96-well plate and incubated for 24 h. Cells were treated with various concentrations of the polyester NPs, (0-8 mg/mL in media) for 24 h. 10% (v/v) DMSO was used as the positive control group. For THP-1, cells were incubated under shaking (200 rpm) for the duration of the experiment. Then, centrifuged (700 RCF, 5 min) using an Allegra 25R plate centrifuge (Beckman Coulter, Indianapolis, US). The supernatant was removed from each well, and the cells were washed three times with DPBS. Fresh cell culture media (90  $\mu$ l) containing WST-8 working solution (10 $\mu$ L) was added to each



well and the plates were returned to the incubator for 3 h. Absorption from each well was monitored using a Fluostar Omega plate reader at  $\lambda=460$  nm. Eq3.1 was used to calculate the viability %.

***Inflammatory response:***

10,000 DTHP-1 cells were seeded into a 96-well plate and incubated for 24 h at 37°C in 5% CO<sub>2</sub> in a 90% humidified air environment. The cells were exposed to of PLGA, PDLLA, and PS NPs (8 mg/mL in all cases). Lipopolysaccharide (LPS; 0.25 mg/mL) was used as the positive control. The cell culture medium was collected from each well and centrifuged at 300 RCF for 5 min to sediment the cell or cell debris. The supernatant was stored at -80°C until analysis.

The cell count was determined using trypan blue as a viability stain. IL-6, IL-10, and TNF- $\alpha$  were quantified by ELISA according to the supplier's instructions. For each cytokine, a standard curve was generated and used to determine cytokine concentration. The study investigated the linearity of the method over a concentration range of 0-500 pg/mL for TNF- $\alpha$ ; 0-100 pg/mL for IL-6; and 0-300 pg/mL for IL-10. The linear range was found to be between 0-250, 0-100, and 0-150 pg/mL for TNF- $\alpha$ , IL-6, and IL-10, respectively. The resulting equation and the regression coefficient ( $R^2$ ) were  $y= 0.0053x+0.1039$  ( $R^2=0.996$ ) for TNF- $\alpha$ ;  $y=0.005x+0.0337$  ( $R^2=0.999$ ) for IL-6; and  $y=0.0121x+0.3396$  ( $R^2=0.999$ ) for IL-10. LOD and LOQ were determined on the basis of signal-to-noise (S/N) ratios of 3 and 10. LOD calculation was explained before (Chapter 2). The LOD was calculated to be 42.66 pg/mL and the LOQ was determined to be 127.98 pg/mL for TNF- $\alpha$ . For IL-6, LOD=18.48 pg/mL, LOD=55.44 pg/mL. Finally for IL-10, LOD=4.36 pg/mL, and LOQ=13.09 pg/mL (**Table 3.1**).

**Table 3.1 Cytokine concentration calculation factors**

<b>Cytokine</b>	<b>Linear Range (pg/mL)</b>	<b>Equation</b>	<b>R<sup>2</sup></b>	<b>LOD (pg/mL)</b>	<b>LOQ (pg/mL)</b>
TNF- $\alpha$	0-250	$y = 0.0053x + 0.1039$	0.996	42.66	127.98
IL-6	0-100	$y = 0.005x + 0.0337$	0.999	18.48	55.44
IL-10	0-150	$y = 0.0121x + 0.3396$	0.999	4.36	13.09

Finally, cytokine concentration was normalised against the number of viable cells and presented as cytokine concentration per 10,000 cells (Eq. 3.2).

**Eq. 3.2** 
$$\text{Cytokine release} = \frac{\text{Cytokine concentration } (\frac{pg}{mL})}{[(\text{viable cell number})/10,000]}$$

#### *Uptake studies*

The uptake of Nile red-loaded polyester NPs (prepared as described in Chapter 2.3.2) by HEP-G2, HMEC-1, THP-1 and DTHP-1 was assessed by flow cytometry (CytoFLEX S, Beckman Coulter, Indianapolis, US), and fluorescent microscopy (Evos® FL, Thermo Fisher Scientific, Loughborough, UK).

#### *Flow Cytometry*

$3 \times 10^5$  HEP-G2 cells were seeded in a 6-well plate and incubated for 24 h at 37°C in an environment with 5% CO<sub>2</sub> and 90% humidity. Then, these cells were treated with 0.25 mg/ml of Nile red-loaded polyester NPs for 1 hour. 10% (v/v) DMSO was used as the positive control. After treatment, the cells were detached using 0.5% Trypsin-EDTA, and collected by centrifugation (300 g, 5 min). The cell pellet was then washed three times with DPBS. The cells were stained with DAPI for 20 min at room temperature then, rinsed with DPBS three times. The DAPI-stained cells were dispersed in 500  $\mu$ L of DPBS containing 1mM EDTA and 1% (v/v) FBS.

An uptake inhibition study was conducted by treating cells with 50 mM NaN<sub>3</sub> solution (in media) for one hour prior to NP treatment. Once cells were exposed to polyester NPs, the well plates were kept at 4°C for 1 hour (197). Then, the cells were handled and processed as described for flow cytometry analysis.

The same procedure (uptake and uptake inhibition) was used for HMEC-1 and DTHP-1 cells. For DTHP-1, cells were differentiated using PMA (100 nM) prior to incubation with NPs and inhibitors. A slightly different procedure was used for THP-1 cell suspension. After exposure to NPs, cells were collected by centrifugation (300 rpm, 5 min). THP-1 cells were then washed thrice using DPBS and dispersed in 500 µL DPBS (1 mM EDTA, 1% FBS) for both uptake and inhibition studies for flow cytometry analysis.

#### *Flow cytometry analysis*

Gating was applied to the forward (FSC) vs side scattering (SSC) plot to exclude debris and doublet cells. The cytoflex is equipped with excitation lasers of 405 nm for DAPI and 561 nm for Nile red, with corresponding emission filters of 450/45 and 585/42. Default voltages of the device for each channel were maintained. Automatic compensation was applied to analyses and 10,000 events (within the gating) per sample were recorded. Median fluorescence intensity (MFI) of Nile red was detected for each sample as a sign of NP uptake (Eq.3.3). MFI ratios were calculated for each polymer cores:

$$\text{Eq.3.3} \quad \textbf{MFI ratio} = \frac{\textbf{MFI PDLLA-PVA}}{\textbf{MFI PDLLA-PXM}} \quad \textbf{or} \quad \textbf{MFI ratio} = \frac{\textbf{MFI PLGA-PVA}}{\textbf{MFI PLGA-PXM}}$$

#### *Fluorescent microscopy*

3x10<sup>5</sup> HEP-G2 cells were seeded in a 6-well plate and incubated for 24 h. The cells were then treated with 0.25 mg/ml of polyester NPs loaded with Nile red for 1 hour. The wells were

washed three times with DPBS. Then, the cells were fixed (2% paraformaldehyde) for 20 min at 37°C. The cells were washed and stained with ReadyProbes™ cell viability imaging kit NucBlue® stain (Thermofisher, Loughborough, UK). The images were recorded using a fluorescence microscope (EVOS® FL, Invitrogen) with Texas red (Ex:585/29, Em: 628/32) and DAPI (Ex: 357, Em: 447/60) light cubes. The intensity and the brightness on the device were kept the same for each images. Finally, the images were processed using Image J (FIJI) software. The same method was used for HMEC-1 and DTHP-1 cells.

### ***Statistical analysis***

Replicate numbers for all experiments are stated below the results plots and data are expressed as mean  $\pm$  standard deviation (SD). Statistical analyses were selected based on the nature of the data and were performed using GraphPad Prism 10 (GraphPad Software, Inc., San Diego, CA) software with a 95% confidence interval. Statistical significance of differences was assessed using paired t-tests, one-way ANOVA with Tukey's or Dunnet's multiple comparison test, and two-way ANOVA with Tukey's multiple comparison test. For non-parametric data, the Kruskal-Wallis test coupled with Dunn's test was used.

## **3.4 RESULTS AND DISCUSSION**

### **3.4.1 Viability studies**

#### ***Stabiliser toxicity***

The toxicity of the stabilisers used in the preparation of the polyester NPs was assessed on J774. Using one cell line initially serves as a screening step. Since stabilisers showed low toxicity at expected concentration of residual stabilisers, repeating the cytotoxicity test on the other four cell lines could be resource waste. So, considering their phagocytic nature, the cytotoxicity was only tested on macrophage-like tumour cell line J774. This cell line is commonly used for preliminary cytotoxicity assessment and others have reported preferential accumulation of PVA

compared to non-phagocytotic cancer cells lines, including: mouse leukaemia (P388), mouse hepatoma (MH134-TC) and human histiocytic lymphoma (U937) (198).

A  $IC_{50}$  value of  $2.67 \pm 0.4$  mg/mL was obtained for PXM, while cell viability was maintained at ca. 75%, even at the higher PVA concentration tested (**Figure 3.1**). This difference in toxicity can be explained by the amphiphilic nature of PXM (199, 200), which has surfactant properties and is able to disrupt the cell membrane (201, 202).

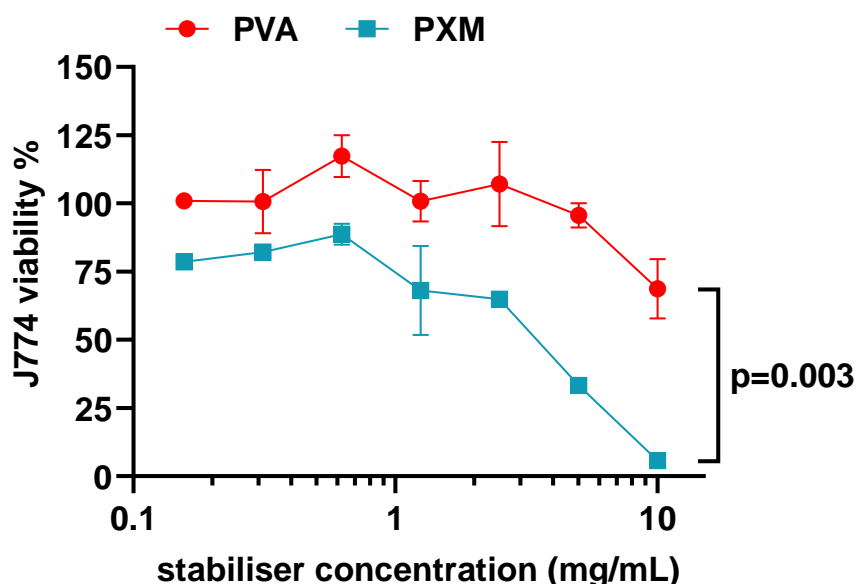


**Figure 3.1 Stabilisers toxicity.** The viability of J774 cells was assessed after exposure to PVA and PXM for 24 h. The results showed a significant difference in toxicity between PVA and PXM solution on J774 cells with the latter showing a higher toxicity. The  $IC_{50}$  value was  $39.9 \pm 16.6$  mg/mL for PVA and  $2.67 \pm 0.4$  mg/mL for PXM. Results are represented as mean  $\pm$  SD (n=3 independent experiments). Paired t-test (each concentration point was paired) (\*\* $p=0.003$ ).

The toxicity of the stabilisers used in the preparation of the polyester NPs was assessed on J774. Using one cell line initially serves as a screening step. Since stabilisers showed low toxicity at expected concentration of residual stabilisers, repeating the cytotoxicity test on the other four cell lines could be resource waste, however it can be conducted in the future to see the different

cell lines sensitivity. So, considering their phagocytic nature, the cytotoxicity was only tested on macrophage-like tumour cell line J774. This cell line is commonly used for preliminary cytotoxicity assessment and others have reported preferential accumulation of PVA compared to non-phagocytotic cancer cells lines, including: mouse leukaemia (P388), mouse hepatoma (MH134-TC) and human histiocytic lymphoma (U937) (198).

A  $IC_{50}$  value of  $2.67 \pm 0.4$  mg/mL was obtained for PXM, while cell viability was maintained at ca. 75%, even at the higher PVA concentration tested for 24 h (**Figure 3.1**). This difference in toxicity can be explained by the amphiphilic nature of PXM (199, 200), which has surfactant properties and is able to disrupt the cell membrane (201, 202), while PVA has -OH functional groups to create hydrogen bonds with water and avoids aggregation.

Grabowski *et al* (203) studied the 48-hour toxicity of various surface coating materials such as PVA and poloxamer 188 on DTHP-1 cells and pointed out that PVA was not toxic at 3.5 mg/mL, while poloxamer 188 showed a ca. 5% decrease in cell viability at 2 mg/mL. There is a small difference in molecular weight between PXM (12,600 Da) and Poloxamer 188 (8,400 Da) (204), which could affect uptake by cells (205). Lower MW polymers are prone to be taken up more easily and can create toxicity since they can reach toxic concentration more rapidly in the cells. Also, the two stabilisers differ in terms of their chemical composition with the length of the hydrophobic segment being twice as long in PXM [56 unit polypropylene oxide (PPO)] compared to Poloxamer 188 (27 unit PPO) (126), however it is known that the degradation products of the poloxamer are not toxic, so a significant difference between poloxamer 188 and PXM stabilised NPs is not expected. Quantification of residual stabilisers (**chapter 2.3.2**) showed the presence of approximately 0.2 to 0.4 mg/mL of free chains of PVA or PXM. Therefore, at the concentrations detected (0.2 mg/mL PVA, 0.4 mg/mL PXM), neither PVA nor PXM would be expected to induce toxicity.

### *Polyester NPs toxicity*

The 24-hour cytotoxicity of the polyester NPs was assessed on J774 cells using WST-8 solution which is based on the reduction of WST-8 tetrazolium salts by cellular dehydrogenases (206). The WST-8 test was used instead of the MTT because the washing steps resulted in loss of cells and false positive results. As WST-8 is a water-soluble tetrazolium salt, washing is not required. J774 cells were used initially to gain insight on how macrophages reacted to polyester NP's and help to decide on the working concentration range.

Most polyester NPs tested showed a similar pattern with cell viability decreasing to ca.10% after 24h when cells were treated with 8 mg/mL concentration (which is the maximum concentration for produced NPs in CCM). PDLLA-PXM NPs were the only exception for the viability decrease pattern. Similar to what was observed for PVA, J774 viability never dropped below 75%, even at the higher concentration tested (**Figure 3.1**). A noticeable difference in  $IC_{50}$  was observed for PDLLA NPs coated with PVA vs. PXM ( $3.5 \pm 1.3$  vs.  $37.6 \pm 20.7$  mg/mL). This was somewhat unexpected considering that PXM was more toxic on the J774 cells compared to PVA. Yet, this confirms that the association of stabilisers with NPs affects the toxicity of NPs. Interestingly, the opposite trend was seen for PLGA NPs, where PXM-coated particles were more toxic to cells ( $1.6 \pm 0.5$  mg/mL) than PVA-coated NPs ( $0.5 \pm 0.2$  mg/mL) and overall, more toxic than PDLLA NPs.

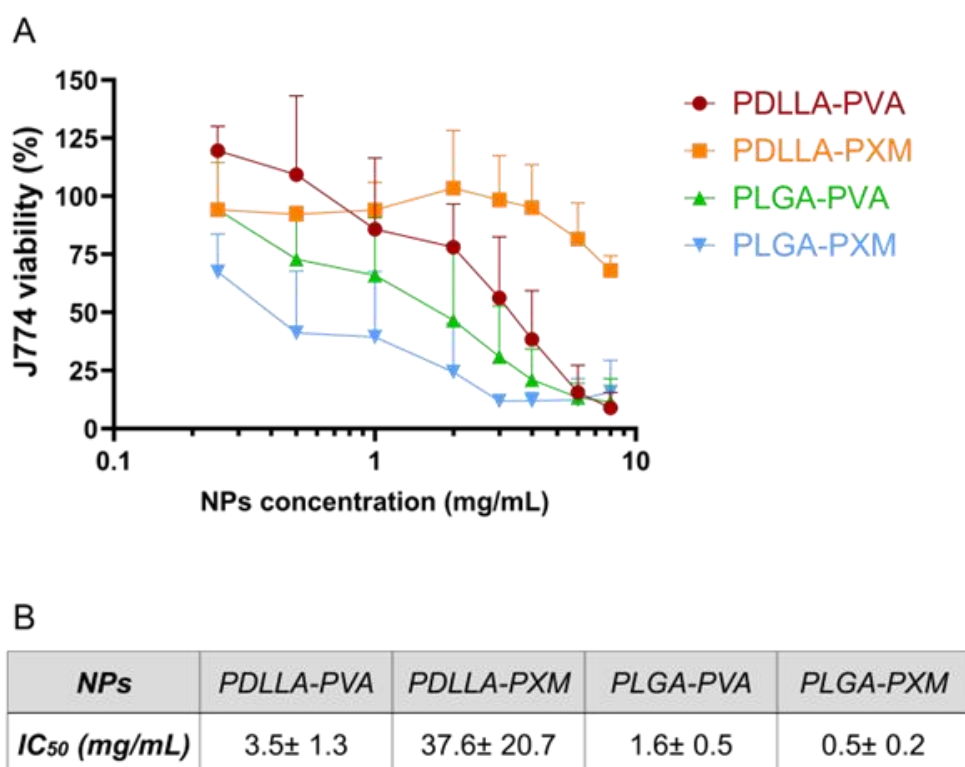


**Figure 3.2 Cytotoxicity of polyester NPs on J774 cells.** Cytotoxicity of polyester NPs on J774 cells. (A) The viability of J774 cells was assessed after exposure to PDLLA-PVA, PDLLA-PXM, PLGA-PVA, and PLGA-PXM NPs for 24 h. (B) IC<sub>50</sub> values of polyester NPs on J774 cells were calculated by GraphPad Prism 10.1.2 using dose-response-inhibition equation with 95% CI. Results are represented as mean± SD (n=3 independent experiments). (One-way ANOVA on IC<sub>50</sub> values PDLLA-PXM NPs showed significantly higher IC<sub>50</sub> value;  $p < 0.05$ )

In the previous chapter, a similar coating efficiency was achieved for both PXM- and PVA-coated NPs. However, the two stabilisers have very different properties and, likely, different arrangements on the surface of the NPs as seen from the surface hydrophobicity results. At this stage, no clear trend can be highlighted that explains the differences in toxicity observed for the different NPs in J774. Since these cells are murine in origin and considering that the choice of cell lines and models should be based on the target organism, human-derived cells were preferred for follow-up studies to obtain more relevant data, after studied on J774 murine cells for concentration screening.



The polyester NPs were tested at the same concentrations on HEP-G2, HMEC-1, THP-1, and DTHP-1 cells (**Figure 3.3**). No clear sign of toxicity was observed in HEP-G2 cells over the 24h period and at the range of concentrations tested (**Figure 3.3-A**); while in HMEC-1 a slight decrease (*ca.* 25%) in cell viability was seen at higher concentration (8 mg/mL), though viability remained above 75% (**Figure 3.3-B**). Some other studies have reported the toxicity of polyester NPs on endothelial cells; noticeably, the work of Alkholief *et al.*(207) suggested HEP-G2 cells lost nearly 50% viability after PLGA-PVA NPs treatment (1 mg/mL; 24h) which is not significantly different to the results obtained in our study, where the viability of HEP-G2 was  $87 \pm 23\%$  under similar conditions.

Conflicting results were obtained for THP-1 cells before and after differentiation to macrophages. Both PLGA NP formulations were toxic to THP-1 cells at concentrations above 3 mg/mL (**Figure 3.3-C**). The trend was not as clear for PDLLA, but the nature of the stabiliser did not seem to have an effect since PVA-coated NPs and PXM coated NPs did not follow the same trend on toxicity. In contrast to J774 cells, polyester NPs appeared to promote the growth of THP-1-derived macrophages (**Figure 3.3-D**), although there was some variability in the results obtained. Grabowski *et al.* (203) reported the viability of DTHP-1 cells treated with PLGA-PVA NPs (0.05-3.5 mg/mL) for 48 h (203). In that study, the cell viability decreased to 75% at 1 mg/mL NPs and to 50% at 3.5 mg/mL while viability was always over 75% in our study. The longer duration of treatment may explain the results, as twice as many cells underwent apoptosis after 48 hours compared to 24 hours (203).

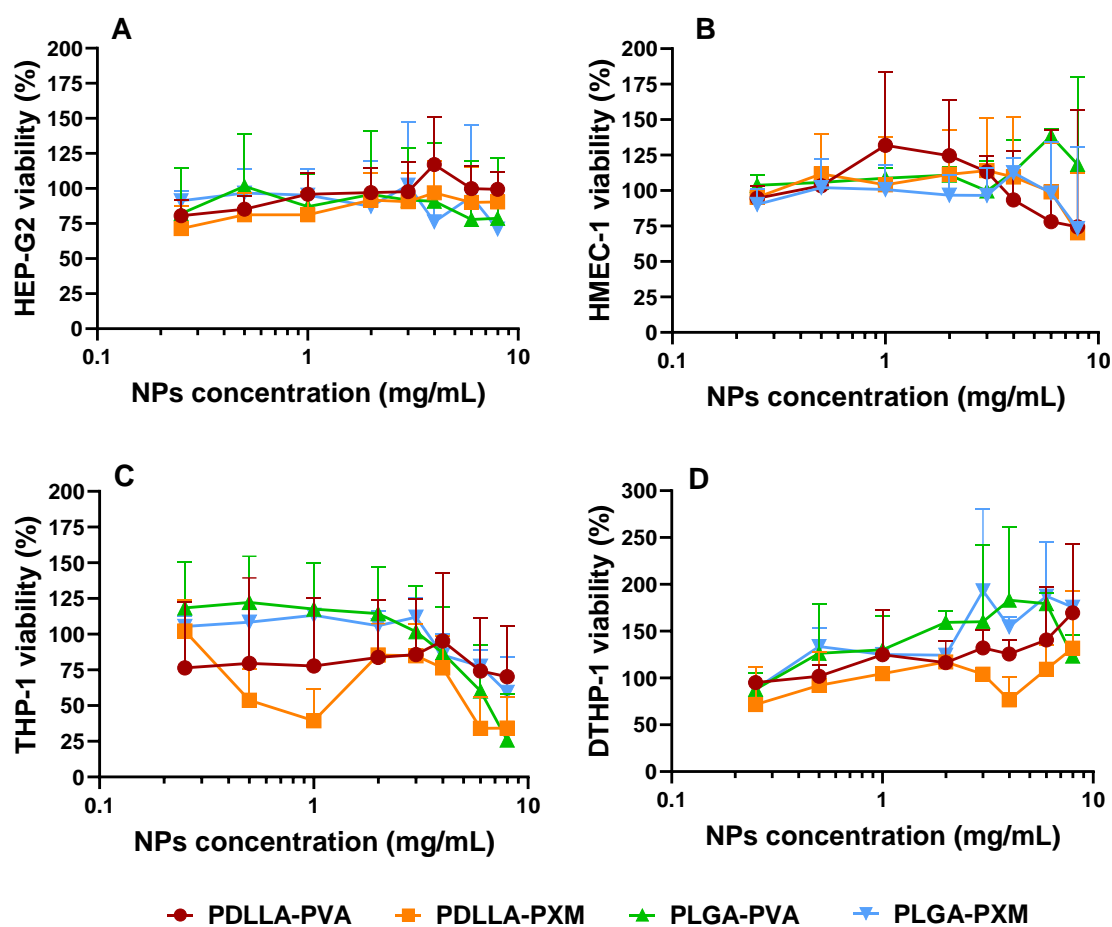


**Figure 3.3 Cytotoxicity of polyester NPs on human cell lines.** Cytotoxicity of polyester NPs on (A) HEP-G2, (B) HMEC-1, (C) THP-1, and (D) DTHP-1 cells. Cells were treated for 24h in all cases. Results are represented as mean  $\pm$  SD (n=3 independent replicates).

Even though, PVA is more common than PXM in the manufacture of polyester NPs, some information can still be found on PXM-coated NP toxicity, though not necessarily on the same cell lines. In the study of Frasco *et al.* (208) drug-free PLGA-PXM NPs (~200 nm; 16-160 ng/mL) were not significantly toxic to human pancreatic nestin-expressing cells following 48h exposure (208). Joseph *et al.* (209) stated that the number of metabolically active endothelial brain cells viability decreased 15% when treated with PLGA-PXM NPs (70 nm; 1mg/mL) for 4 h (209). Both studies were performed on endothelial-like cells and the test conditions were

clearly different than that of HMEC-1 cells in our study. Yet, findings seem to indicate relative safety of larger PLGA-PXM NPs over 24-48 h compared to smaller (<100 nm) NPs. Crucially, similar sized-NPs (150-200 nm) were very mildly toxic towards HEK-293 (human embryonic kidney cells) and L-929 (murine fibroblasts) cells with survival rate > 90% when treated with PDLLA-PXM NPs (~100 nm; 0.0001-1 mg/mL) for 72 h (210).

There are ample examples in the literature confirming that PVA-coated NPs do not exhibit cytotoxicity. Indeed, no loss of viability was seen for 200-nm PDLLA-PVA NPs tested on endothelial cells and Caco-2 cells at concentrations between 0.001 and 1 mg/mL (211, 212). Therefore, based on published findings, it can be assumed that PDLLA-PVA NPs will not affect cells when used at concentrations  $\leq 1$  mg/mL for 24 to 72 h. Our results suggest that PDLLA-PVA NPs could be safe even at concentrations up to 3 mg/mL, except on J774 murine cells, though there were times when toxicity was seen at a concentration of 1 mg/mL. The variability observed highlights the challenges associated with common cytotoxicity assays which measure metabolic activity, rather than cell death. Further studies should be performed using alternative methods to detect cell death as a mean to confirm our conclusions. Between the alternative methods trypan blue technique utilises hemocytometer and obtain a visual counting of the dead cells. Some fluorescent DNA binding dyes (propidium iodide, Hoechst, SYTOX green nucleic acid stain) can be also used for dead cell counting alongside of lactate dehydrogenase test. Additionally, toxicity will need to be evaluated in normal, non-cancerous cells to confirm biocompatibility.

### **3.4.2 Inflammatory potential**

Assessment of cytokine release contributes to biocompatibility studies by providing information on the pro-inflammatory potential of NPs (213). Here, an ELISA assay was used to estimate the levels of TNF- $\alpha$ , IL-6 and IL-10 released by 10,000 THP-1-derived macrophages

after 24 h of exposure to NPs. These cells were selected as a relevant phagocytotic cell model and tested after exposure to polyester and PS NPs. Since DTHP-1 macrophages can produce those cytokines, and TNF- $\alpha$  and IL-6 are primary pro-inflammatory cytokines that play a role in immunomodulation with IL-10, those three cytokines were tested on DTHP-1 cells.

Out of the cytokines tested, TNF- $\alpha$  is considered proinflammatory, IL-10 is anti-inflammatory and IL-6 can be either based on the signalling pathways involved and whether exposure is acute or chronic (214). Although NPs are not expected to activate the TLR, more hydrophobic nanomaterials may share characteristics with pathogen-associated or damage-associated molecular patterns (PAMPs and DAMPs) found in bacteria and lipoproteins amongst other sources. This resemblance could explain the pro-inflammatory potential observed with PS NPs seen in this study (**Figure 3.4**).

As expected, release of TNF- $\alpha$  was similar for DTHP-1 exposed to polyester NPs and untreated cells (only media treated cells or negative control). For PS NPs, there was an approximately 8-fold increase in TNF- $\alpha$  levels compared to the control group. However, this observed increase did not reach statistical significance in this study, while it is known that PS NPs induce the release of TNF- $\alpha$  by macrophages (215).

Exposure to PDLLA-PVA NPs induced IL-6 release compared to the untreated group (ca. 6-fold increase). In comparison, IL-6 levels were ~30 times higher for cells exposed to PS NPs, compared to both the media and polyester NP groups. Finally, exposure to NPs or LPS led to a decrease in IL-10 release compared to the negative control. Interestingly, IL-10 levels observed after exposure to PS NP ( $8.45 \pm 1.07$  pg/mL) were higher than those seen for polyester NPs (<1 pg/mL). This may be attributed to feedback between anti-inflammatory and pro-inflammatory cytokines (216). An increase in IL-10 leads to a decrease in TNF- $\alpha$  (214). And vice versa; IL-10 release can be inhibited by some pro-inflammatory cytokines such as IL-1 $\beta$  and TNF- $\alpha$ . This

is because these cytokines induce the release of IFN- $\gamma$  and Granulocyte-Macrophage Colony-Stimulating Factor (GM-CSF), and these cytokines inhibit the release of IL-10 (217). LPS also stimulates macrophages to release GM-CSF which lead to decrease in IL-10 release. Also, there is an autocrine inhibition of IL-10 receptor by IL-10 (218).

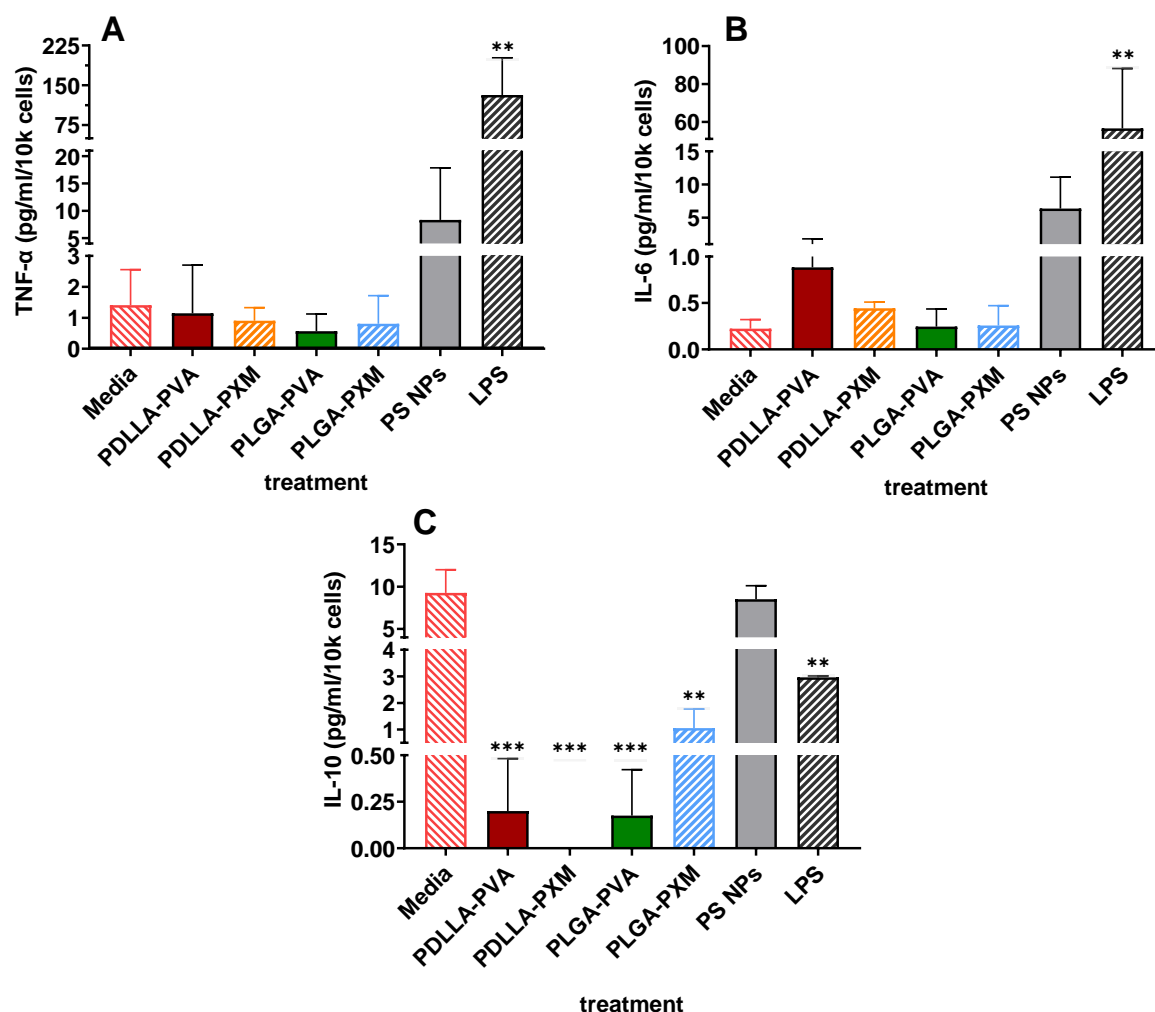


**Figure 3.4 Inflammatory potential of polyester NPs.** The release of three cytokines (A) TNF- $\alpha$ ; (B) IL-6 and (C) IL-10 was assessed on DTHP-1 cells exposed to 8mg/mL PDLLA-PVA, PDLLA-PXM, PLGA-PVA, and PLGA-PXM NPs for 24 h. PS NPs (8 mg/mL) and LPS (0.25 mg/mL) were included as positive controls. Results are presented as mean  $\pm$  SD of two independent biological replicate (n=2). One-way ANOVA, Dunnet post-hoc test compared to negative control (media) group (\* $p$ <0.05, \*\*  $p$ < 0.01, \*\*\* $p$ <0.001).

Indeed, it was suggested that TNF- $\alpha$  can trigger the release of anti-inflammatory cytokines such as IL-10 which agrees with our observations for PS NPs and LPS (218). The lower IL-10 levels

seen for polyester NPs suggest that a similar mechanism may be implicated, but involving pro-inflammatory cytokines which were not tested in this study, for example IL-1 $\beta$  or MCP-1 (219). Interestingly, the biggest decrease in IL-10 was seen for PDLLA-PXM which were the most hydrophilic NPs (HIC index 0.11), while PLGA-PXM had a lesser impact, despite an HIC index in a similar range. Currently, there is not enough data to establish a link between NP composition, surface properties and pro-inflammatory potential. However, the data available suggests this should be investigated further.

Few have tested the pro-inflammatory potential of polyester NPs at the concentration (8 mg/mL) used in this study. According to Grabowski *et al.* (203), PLGA NPs (200 nm, 1 mg/mL) coated with either PVA or Poloxamer 188 triggered the release of TNF- $\alpha$  and IL-6 from DTHP-1 cells, but this was not statistically different compared to the negative control (untreated cells). Their results also suggested that PVA-coated particles were more likely to trigger the release of TNF- $\alpha$ , while IL-6 release was preferentially associated with PXM-coated NPs. In an *in vivo* study, PDLLA-PVA NPs significantly increased the release of TNF- $\alpha$  (ca. 6 fold) and IL-6 (ca. 20 fold) compared to saline treatment in mice (220). Therefore, detailed *in vivo* experiments suggested to be performed before concluding that NPs are biocompatible, given that *in vitro* results may not reproduce *in vivo* behaviour.

### 3.4.3 Uptake studies

The uptake of PDLLA and PLGA NPs coated with either PVA or PXM was evaluated in HEP-G2, HMEC-1, DTHP-1 and THP-1 cells in the absence and presence of a broad-spectrum endocytosis inhibitor: NaN<sub>3</sub>, a metabolic inhibitor, reduces energy production in cells and, therefore, diminishes all energy-dependent transport mechanisms (213, 214). Here, the study with NaN<sub>3</sub> was performed to determine whether uptake of NPs is *via* energy-dependent endocytosis and differentiate between adsorption on the cell membrane and internalisation.

Uptake of all NPs was reduced after inhibition for HEP-G2 and HMEC-1 cells as assessed by both flow cytometry (**Figure 3.5-A, 3.6-A**) and fluorescence microscopy [**Figure S1-3, 3.5-B, 3.6-B**]. No clear difference in uptake was seen in HMEC-1 for PLGA-PXM NPs in the presence or absence of NaN<sub>3</sub>, when assessed by flow cytometry. The impact of inhibition on uptake by DTHP-1 cells seemed to depend on the method used. Indeed, a decrease in signal was seen for PDLLA-PVA, PDLLA-PXM, and PLGA-PXM NPs when uptake was studied by flow cytometry (**Figure 3.7-A**), but not by fluorescence microscopy (**Figure 3.7-B**). It should be noted that when the flow cytometry experiment was repeated, no difference was seen without and with NaN<sub>3</sub> which supported the fluorescence microscopy results (**Figure S4**). Similarly, uptake by THP-1 monocytes was not inhibited by NaN<sub>3</sub>, in some cases the fluorescence signal was higher in the presence of the inhibitor (**Figure 3.8**). Phagocytosis is an energy dependent mechanism. The lack of effect of NaN<sub>3</sub> may be due to the short treatment period (60 min) as it has been suggested that 3h may be needed for phagocytotic cells. Further investigation is needed to clarify this observation, including exploring different inhibition times and including additional controls. For the most part, coating did not seem to have a major impact on NPs uptake (**Figure 3.9**). For PDLLA NPs, where a difference was seen, uptake of PVA-coated NPs was slightly higher, apart for HEP-G2 cells. It should be noted that there was a difference in Nile red loading between the NPs used in the different assays. Indeed, for HMEC-1 and DTHP-1, the fluorescence of PDLLA-PVA NPs was 1.1-fold lower than for PDLLA-PXM NPs; while the PDLLA-PVA NPs used in tests with HEP-G2 and THP-1 were 1.1-times more fluorescent compared to their PXM-coated counterpart. Taking these differences into consideration would suggest that HMEC-1 and DTHP-1 internalised PDLLA-PVA NPs to a greater extent, while HEP-G2 and THP-1 preferentially took up PDLLA-PXM NPs, though these differences may not be statistically or clinically different.

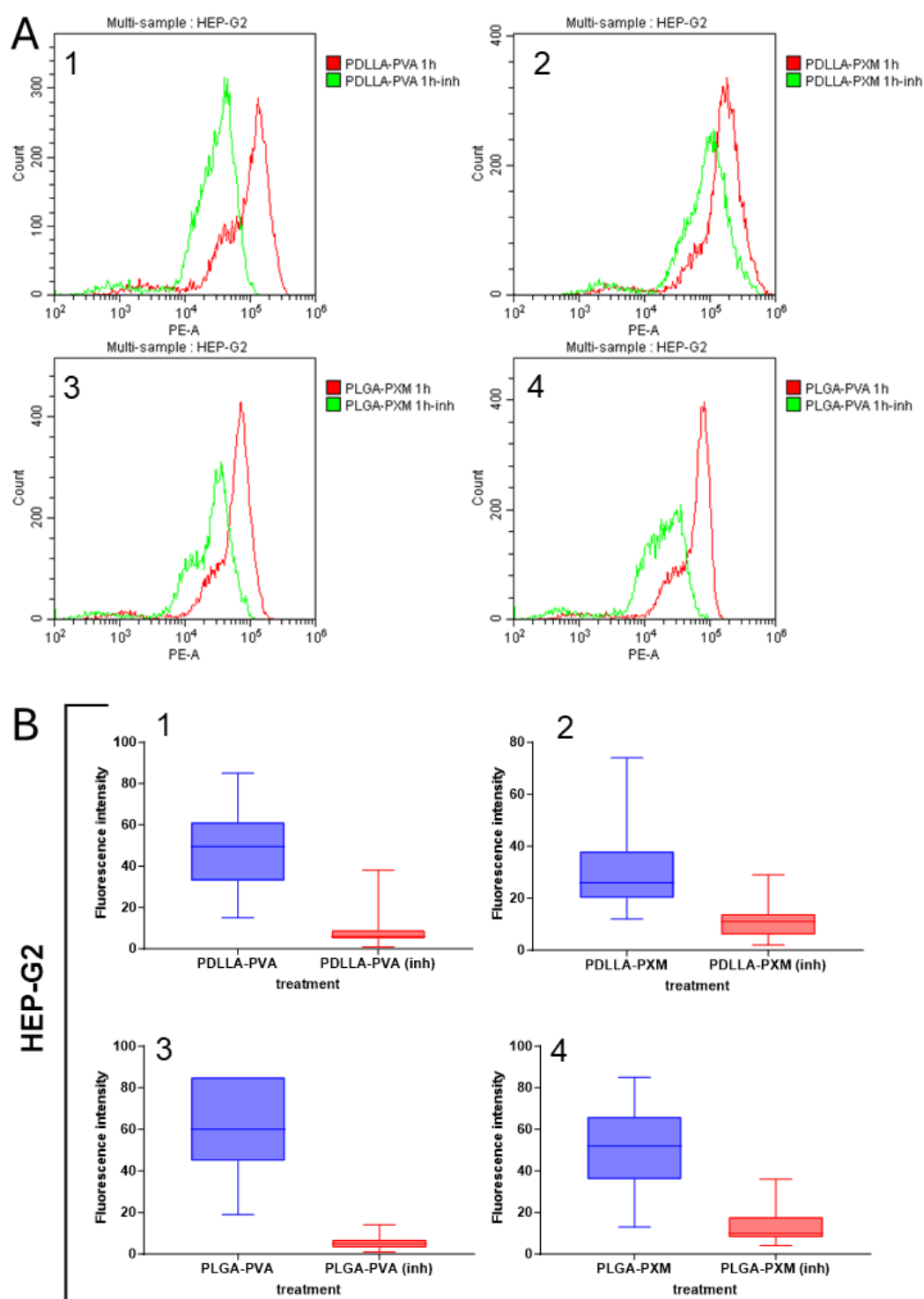


**Figure 3.5 Uptake on NPs by HEP-G2 cells.** Uptake of PDLLA and PLGA NPs was assessed in the absence and presence of sodium azide by (A) flow cytometry (cell number=50,000) and (B) fluorescent microscopy (cell number>50) after 1h. (1) PDLLA-PVA, (2) PDLLA-PXM, (3) PLGA-PVA, (4) PLGA-PXM. Addition of  $\text{NaN}_3$  decreased NP uptake by HEP-G2 cells.



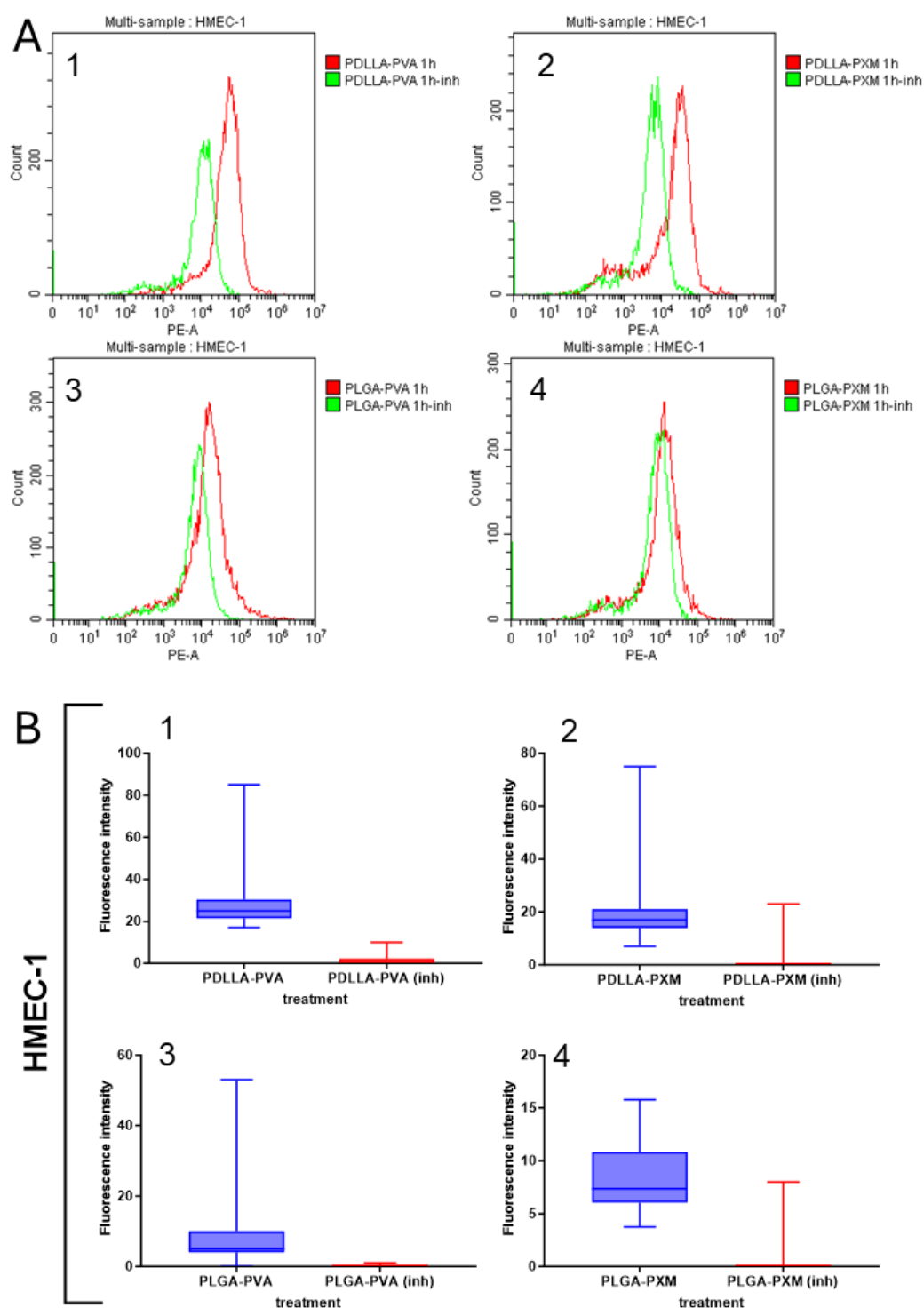


**Figure 3.6 Uptake on NPs by HMEC-1 cells.** Uptake of PDLLA and PLGA NPs was assessed in the absence and presence of sodium azide by (A) flow cytometry (cell number 50,000) and (B) fluorescent microscopy (cell number >50) after 1h. (1) PDLLA-PVA, (2) PDLLA-PXM, (3) PLGA-PVA, (4) PLGA-PXM. Addition of  $\text{NaN}_3$  decreased NP uptake by HMEC-1 cells.

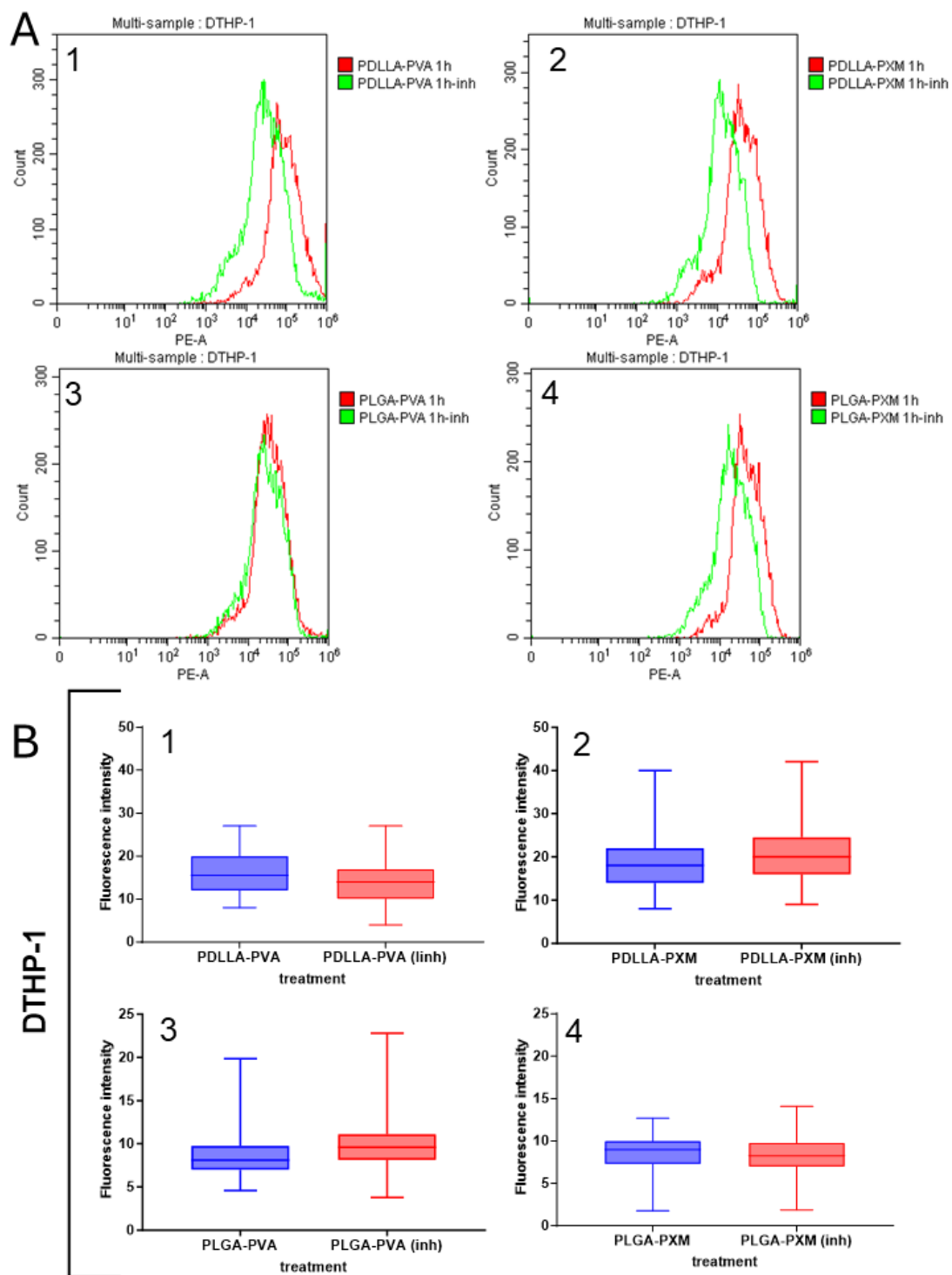


**Figure 3.7 Uptake on NPs by DTHP-1 cells.** Uptake of PDLLA and PLGA NPs was assessed in the absence and presence of sodium azide by (A) flow cytometry (cell number=50,000) and (B) fluorescent microscopy (cell number>50) after 1h. (1) PDLLA-PVA, (2) PDLLA-PXM, (3) PLGA-PVA, (4) PLGA-PXM. Addition of  $\text{NaN}_3$  decreased NP uptake by DTHP-1 cells according to flow cytometry but not fluorescence microscopy.

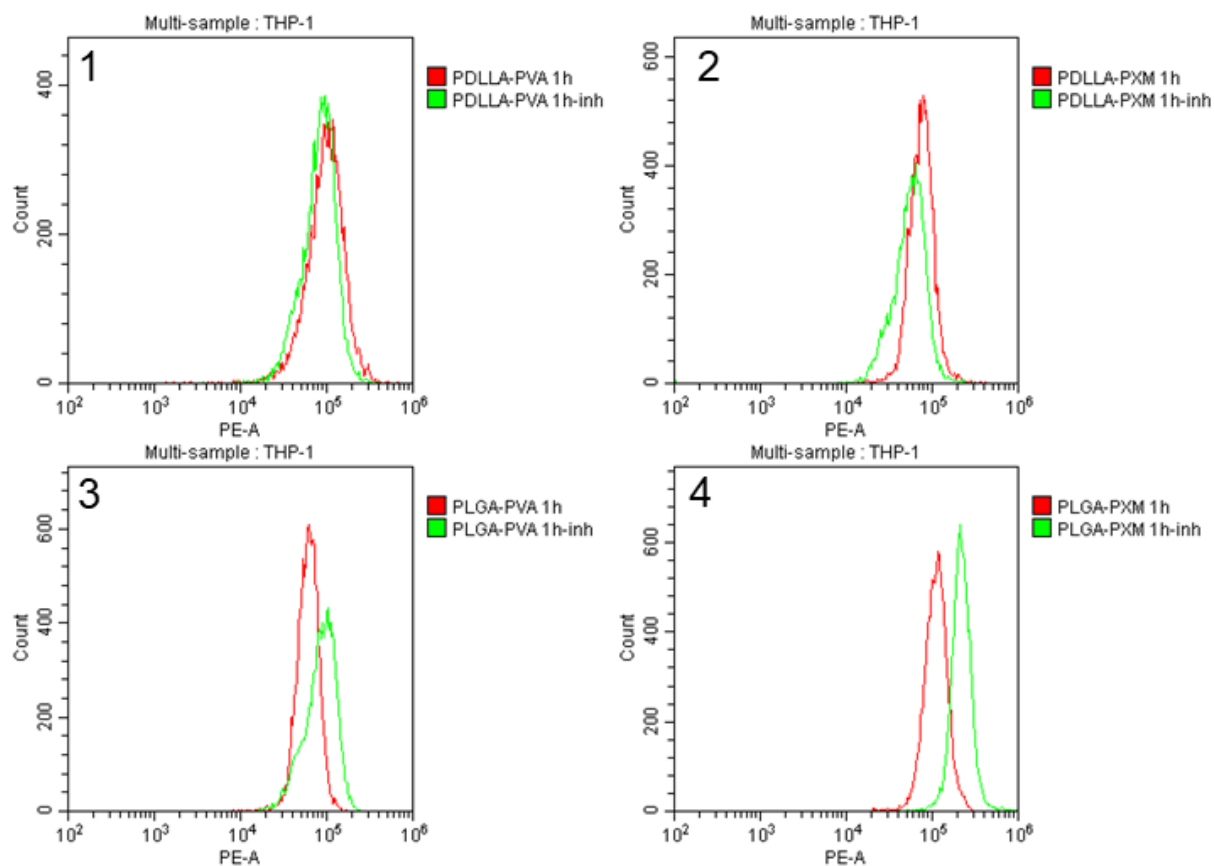


**Figure 3.8 Uptake on NPs by THP-1 cells.** Uptake of PDLLA and PLGA NPs was assessed in the absence and presence of sodium azide by flow cytometry (cell number=50,000) after 1h. (1) PDLLA-PVA, (2) PDLLA-PXM, (3) PLGA-PVA, (4) PLGA-PXM. Addition of  $\text{NaN}_3$  decreased NP uptake by THP-1 cells according to flow cytometry.

Direct comparison of the quantity of NPs internalised is not feasible due to variations in the fluorescence intensity for the different formulations and batches. An attempt was made to correct for variations in Nile red loading, but this proved challenging. Additionally, using SSC in flow cytometry cannot accurately measure polymer NP uptake as it does with metallic NPs (221). The lack of alteration to cell granularity in the presence of polyester nanomaterials may be due to their degradation in lysozymes (222). Still, flow cytometry can provide an initial indication of the impact of the coating on NP uptake.

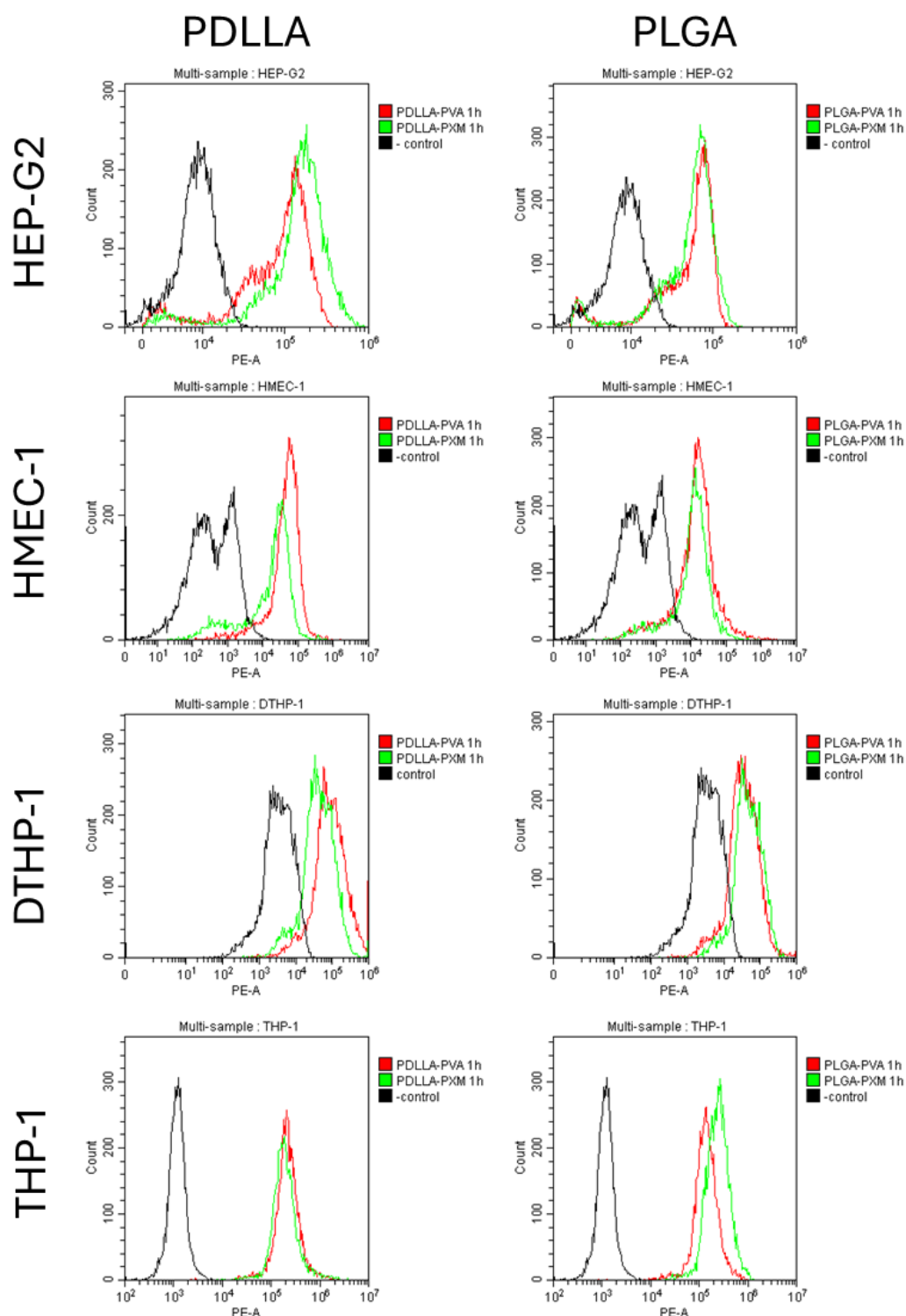


**Figure 3.9 Impact of NP coating on uptake.** The uptake of PVA- or PXM-coated PDLLA and PLGA NPs' studied by flow cytometry. Fluorescence intensity after exposure to NPs (0.25 mg/mL) for 1h was compared to untreated cells. There was no clear difference between PVA- and PXM-coated PLGA NPs, apart in THP-1 cells. For PDLLA NPs, only HEP-G2 seem to preferentially internalised PXM-coated PDLLA NPs over their PVA-coated counterpart.

To ease comparison, a PVA:PXM MFI ratio was calculated (**Figure 3.10**) which confirmed, to some extent, the observations from flow cytometry, apart for DTHP-1. In these cells PVA:PXM MFI ratio of  $1.9 \pm 0.1$  which is higher than the difference in fluorescence intensity detected between NPs. However, the error was larger for the ratios obtained for HMEC-1 (PVA:PXM MFI ratio  $1.4 \pm 0.5$ ) and THP-1 (PVA:PXM MFI ratio  $1.6 \pm 0.6$ ) and therefore, additional studies are needed to confirm the true impact of coating on PDLLA NP uptake in these cells.

For PLGA NPs, flow cytometry studies revealed no clear difference between PVA- and PXM-coated NPs, apart for THP-1 cells which appeared to preferentially internalise PLGA-PXM NPs (**Figure 3.9**). In contrast, the PVA:PXM MFI ratios calculated all suggest that PLGA-PXM NPs were taken up more by all cells, apart for HMEC-1 (**Figure 3.10**). In this case, the fluorescence intensity of PLGA-PVA NPs was 1.4-times weaker vs. PLGA-PXM NPs in all assays which mostly accounts for the differences in MFI ratios observed.

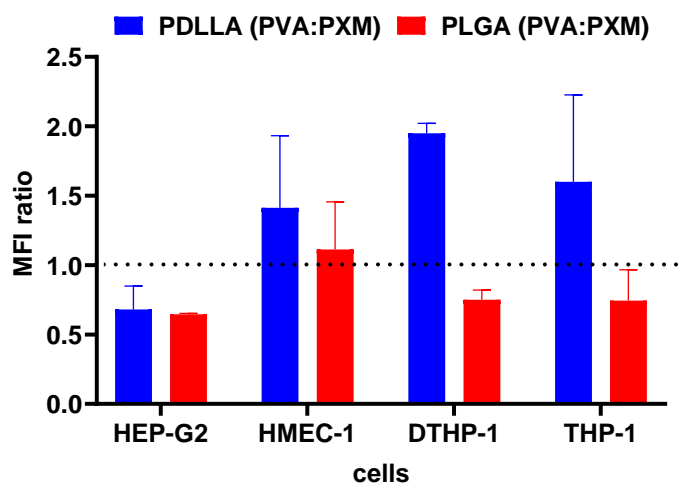


**Figure 3.10 PVA:PXM MFI ratio for NPs.** PVA:PXM MFI ratios for PDLLA and PLGA NPs determined from flow cytometry data. HEP-G2 appeared to preferentially internalise PXM-coated NPs; HMEC-1 internalised PVA-coated NPs. For PDLLA NPs, DTHP-1 and THP-1 took up PVA-coated particles over PXM-coated ones, but the opposite was seen for PLGA NPs.

Overall, the type of coating used had limited impact on PLGA NPs uptake, despite some differences in surface hydrophobicity (**Figure 3.10**). Hydrophobicity has been shown to

enhance cellular uptake. For example, PEGylation led to a decrease in the uptake of PDLA NPs by HeLa and J774 cells (223-226) because the coating lessened the particle-cell interaction (226). Considering that PXM is a triblock of PEG, modification with PXM was expected to decrease uptake, but this was not always the case here. According to both SAT and HIC results, PVA-coated NPs were more hydrophobic than PXM-coated NPs (**Chapter 2, Figure 2.13**). However, there was no difference in protein adsorption (**Chapter 2, Figure 2.14-2.15**) which may indicate that all NPs presented a similar level of protein corona to cells. However, it should be noted that only the concentration of the proteins had been measured, the difference in adsorbed protein type onto NPs may still have significant biological behaviour and cellular interactions.

In this study, it was found that the uptake of NPs by cells can vary depending on surface properties and that different cell lines may show different uptake preferences for NPs. HEP-G2 tend to internalise nearly neutral NPs (PXM coated) while others preferred more hydrophobic NPs (PVA- coated). However, the reliability of these results obtained by flow cytometry is limited by the variations in intensity between NPs. Instead, radiolabelling can be utilised by using radioactive isotopes to label NPs and measuring the radioactivity with the concern of the safety of the handling of the radioactive materials (227). Mass spectroscopy could also be used as a sensitive uptake measurement method which detects only ionised NPs, so it is not suitable for polyester NPs unless they have a ionisable part (228). TEM is a method to count the NPs in the cell. Tough, it is very time consuming it may provide absolute results (229).

Still, the results helped to improve our understanding of nanomaterial-cell dynamics and provide valuable insights into the design of tailored NPs for biomedical applications.

### **3.5 CONCLUSION**

Polyesters used to prepare NPs can be considered biocompatible at concentrations up to 1-3 mg/mL. Pro- or anti-inflammatory cytokine release was not significantly induced by the polyester NPs, indicating their safety, even at high concentrations. A single clear trend could not be identified from the results of uptake studies. HEP-G2 generally appear to internalise PXM-NPs to a greater extent, while for other cells, uptake seems to be affected by the nature of the NP core. In the future, carefully-designed studies will be required to fully understand the impact of surface properties on uptake, using more relevant cell models.

# **Chapter 4: ACTIVE TARGETED PLGA NANOPARTICLES ON LIVER COCULTURE SYSTEM**

## **4.1 INTRODUCTION**

The liver tissue consists of different types of cells, with KCs being the residential macrophages and the most abundant macrophage population in the body (**Figure 4.1**). It is well-known that the opsonisation of NPs and capture by KC leads to the accumulation in the liver often seen with passively-targeted nanomedicines (230-232). Preferential accumulation in KC has been exploited for sustained delivery of liposomes or inorganic NPs as leishmaniacides, against liver inflammation, to control macrophage phenotype or increase on tumoricidal activity (40). However, if hepatocytes, rather than KC are the target, a more effective approach will be needed. Although it is stated that liver tumour tissues can be targeted to some extent by passive targeting, active targeting methods are used to increase the efficiency and specificity of NPs accumulation. In this chapter, the interaction of actively-targeted NPs with different cells found in and around the liver will be investigated.

Different strategies can be used to actively target hepatocytes, but the potential challenges and limitations of these strategies need to be understood better. In receptor-mediated active targeting, ligands must be specific for hepatocytes and avoid uptake by endothelial cells or capture by KC.



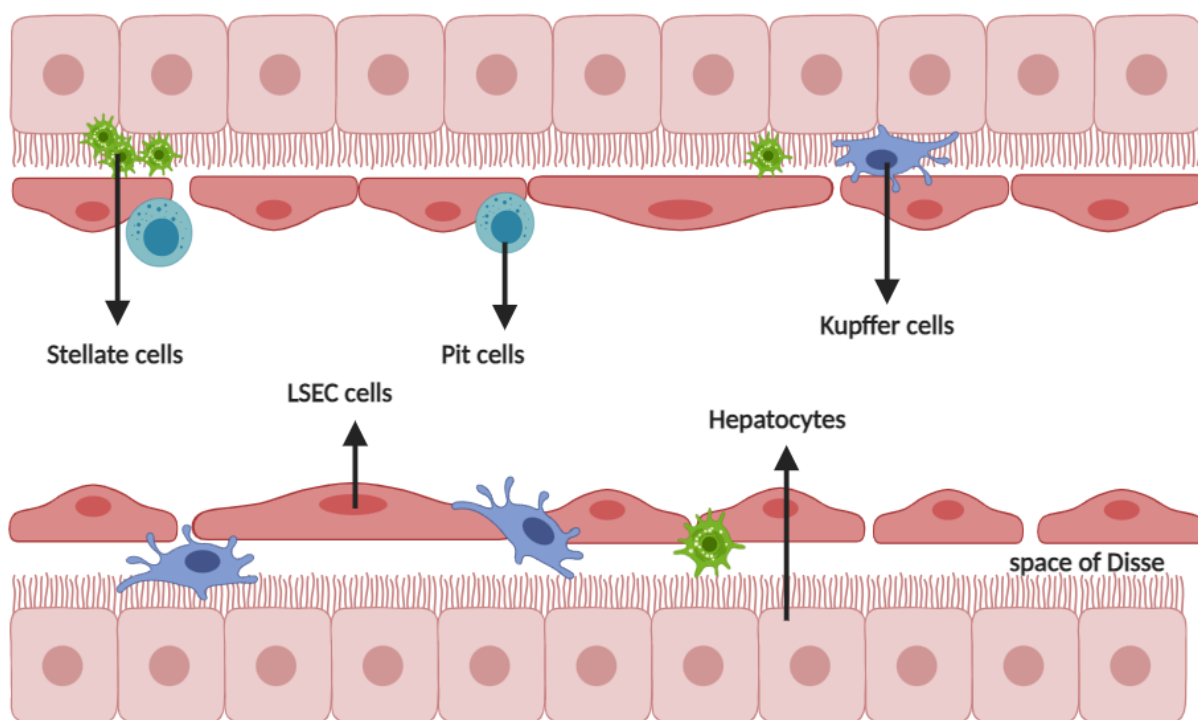


**Figure 4.1. Hepatic sinusoid structure.** Hepatocytes are walled by liver sinusoidal endothelial cells (LSECs), with the space of Disse between them. Kupffer cells are found either in the sinusoidal lumen or in the space of Disse together with hepatic stellate cells. Pit cells are located on the LSECs facing the sinusoidal lumen. (Created with BioRender.com)

Hepatocytes express ASGP-R which recognise glycoproteins with exposed galactose residues following sialic acid removal (i.e. asialoglycoproteins) (233). LCF, biocompatible molecule and GRAS (234) iron-binding glycoprotein, is a natural ligand of the ASGP-R, and can aid in the uptake of targeted NPs (235-238). In this study, LCF as the active targeting ligand to HEP-G2. Since HEP-G2 express ASGP-R, it is expected to direct LCF-coated NPs selectively to hepatocytes, avoiding macrophages (239-241).

Modification of NPs was achieved by simply mixing LCF, which is cationic, with the negatively-charged NPs (242). Therefore, PLGA-PVA NPs were selected instead of PLGA-PXM NPs to maximise interaction with LCF. LCF-target NPs were characterised and tested in

an experimental co-culture model, mimicking the cellular barriers NPs will encounter following i.v. administration.

It is expected that LCF-coated PLGA-PVA NPs will be selectively targeted and taken up by HEP-G2 hepatocytes expressing ASGP-R, thereby increasing delivery efficiency and specificity to hepatocytes while avoiding uptake by macrophages.

## **4.2 AIM AND OBJECTIVES:**

The main aim is to assess uptake of LCF-targeted PLGA NP in an *in vitro* co-culture model mimicking the liver, compared to passively-targeted NPs.

Objectives:

1. LCF-PLGA NPs were prepared and then characterised using DLS for size, size distribution and zeta potential.
2. LCF density on PLGA NPs was determined using a BCA kit and surface hydrophobicity was assessed by SAT.
3. Selective uptake of LCF-coated NPs by ASGP receptors of HEP-G2 was tested in media inhibited by GAL or LCF.
4. The uptake of the NPs in co-culture systems was assessed using flow cytometry.

The results of these experiments are designed to provide a baseline understanding of the ease of preparing the LCF-coated polyester NPs and their efficiency in targeting HEP-G2 cells.

## 4.3 MATERIALS AND METHODS

### 4.3.1 MATERIALS

Human liver cancer epithelial cell (HEP-G2), monocytic leukaemia cell line (THP-1), and human microvascular endothelial cells (HMEC-1) were obtained from the European collection of authenticated cell cultures (ECACC; Salisbury, UK).

Dulbecco's modified Eagle's medium (DMEM), Dulbecco's phosphate buffered saline (DPBS), and fetal bovine serum (FBS), 4',6-diamidino-2-phenylindole (DAPI), dimethyl sulfoxide (DMSO), amine-modified polystyrene (fluorescent orange latex beads, 100 nm mean particle size, F-PS NPs), ethylenediaminetetraacetic acid tetrasodium salt hydrate (EDTA), D(+) galactose (GAL), lactoferrin human (recombinant, expressed in rice, iron saturated, LCF), poly(lactide-co-glycolide) fluorescein (lactide: glycolide 50:50, MW: 10,000-20,000, FITC-PLGA), hydrocortisone, phorbol 12-myristate 13-acetate (PMA), poly(vinyl alcohol) (PVA) were purchased from Merck (Darmstadt, Germany).

MCDB-131 medium, RPMI 1640 medium, L-Glutamine, penicillin-streptomycin (PenStrep), and recombinant human epidermal growth factor (Hu-EGF) Pierce™, bicinchoninic acid assay (BCA protein assay kit) and ethanol absolute ( $\geq 99.0\%$  purity) was purchased from Thermo Fisher Scientific (Loughborough, Leicestershire, UK). 0.4  $\mu\text{m}$  pore-sized polycarbonate membraned translucent inserts purchased from Corning (Greiner bio-one, Kremsmünster, Austria).

Ultrapure water with a resistivity of 18.2 M $\Omega$ .cm is used for all experiments. All the solvents were of analytical grade and used without further purification.

### 4.3.2 METHODS

#### *Preparation of LCF decorated PLGA-PVA NPs*

##### *FITC-PLGA-PVA NPs preparation*

FITC-PLGA was dissolved in acetone (1 mg/mL; 10 mL) and added dropwise to 40 mL of a 1% PVA solution in water at a 1 mL/min rate, under stirring. Acetone was evaporated at room temperature, under a fume cupboard for 4 h. The FITC-PLGA-PVA NP suspension was centrifuged at 50,000 RCF for 40 min at 15 °C. Collected NPs were sonicated, washed three times with DPBS, and dispersed in DPBS for further characterisation.

##### *LCF coating on PLGA-PVA NPs*

LCF attachment onto PLGA NPs was conducted as previously reported, with slight modifications (243). For LCF coating, LCF was dissolved (5 mg/mL; 1 mL) and mixed with FITC-PLGA-PVA NPs (5 mg/mL; 1 mL) in HEPES buffer to achieve a final concentration of 10 mM. This mixture was gently shaken at 500 rpm at 30-35°C for overnight. The LCF-PLGA-PVA NP suspension was centrifuged at 50,000 RCF for 40 min at room temperature. Collected NPs were sonicated in a sonic bath, washed two times with 10 mL DPBS, and dispersed in 2 mL DPBS for further characterisation.

#### *Characterisation of the LCF-coated NPs*

##### *Particle size and zeta potential analysis*

Particle size and zeta potential analysis were performed on LCF-PLGA-PVA NPs as described before in the **chapter 2-section 2.3.2**.

##### *LCF quantification on LCF-PLGA-PVA NPs*

LCF levels on NP surfaces were measured with a BCA kit. A standard curve was used for quantification of unknown samples; equation:  $y=0.424x+0.155$ , R-square value: 0.993; linear range: 0 to 2.5 mg/mL. The LOD was 0.05 mg/mL and the LOQ was 0.15 mg/mL, based on signal-to-noise S/N ratios of 3 LOD and 10 LOQ.

#### Hydrophobicity of LCF-PLGA-PVA NPs

SAT was applied as described before in the **chapter 2-section 2.3.2**.

#### *Co-culture uptake assay*

##### LCF and GAL competitive binding

HEP-G2 cells were seeded in a 12-well plate (100,000 cells/well) and incubated for 24 h in serum-free media. Cells were treated with free LCF (1 mL; 1mg/mL in DMEM) or free GAL (1 mL; 5 mg/mL in DMEM) before returning the cell to the incubator for 30 min. LCF-PLGA-PVA NPs (0.2 mL; ~1.2 mg/mL) were added to the wells, without removing the natural ligands, and incubated for an additional hour. The cell culture media containing the NPs was discarded, cells were washed three times with DPBS, and collected as described previously for flow cytometry analysis in the **chapter 3- section 3.3.2**.

##### Insert permeability for NPs

Diffusion of PLGA NPs through the polycarbonate membrane insert was tested to ensure the membrane itself is not a barrier. To this end, the well (1 mL) and insert (0.5 mL) were filled with PBS (with 10% FBS) and incubated at 37°C. NPs (100 µL) were added to the apical side of the insert. Samples were taken from the well every 30 min for two hours. The initial and final fluorescence signal of the NPs was tested at the start and end of the experiment. The fluorescence of the samples was measured using Fluostar Omega plate reader (BMG Labtech, Aylesbury, UK; 485/520 nm).

##### Preparation of the transwell plate

The basolateral side of the inserts (24 mm; translucent polycarbonate membrane; 0.4 µm pore size) was seeded with 30,000 THP-1 cells. These cells were incubated in RPMI, containing 100 nM PMA media for 48 h at 37°C and 5% CO<sub>2</sub>. After differentiation, the inserts were placed in the wells of a 6-well plate containing 1 mL of MCDB-131 media. The apical side of the insert was seeded with 100,000 HMEC-1 cells in 0.5 mL MCDB-131 media. On a separate plate,

300,000 HEP-G2 cells were seeded directly in the well of the 6-well plate and left to incubate for 24 h in DMEM. Finally, the insert with DTHP-1 and HMEC-1 was transferred to the wells containing HEP-G2 and the media was replaced with MCDB-131 media (**Figure 4.2**). Assays were started shortly after this last step.

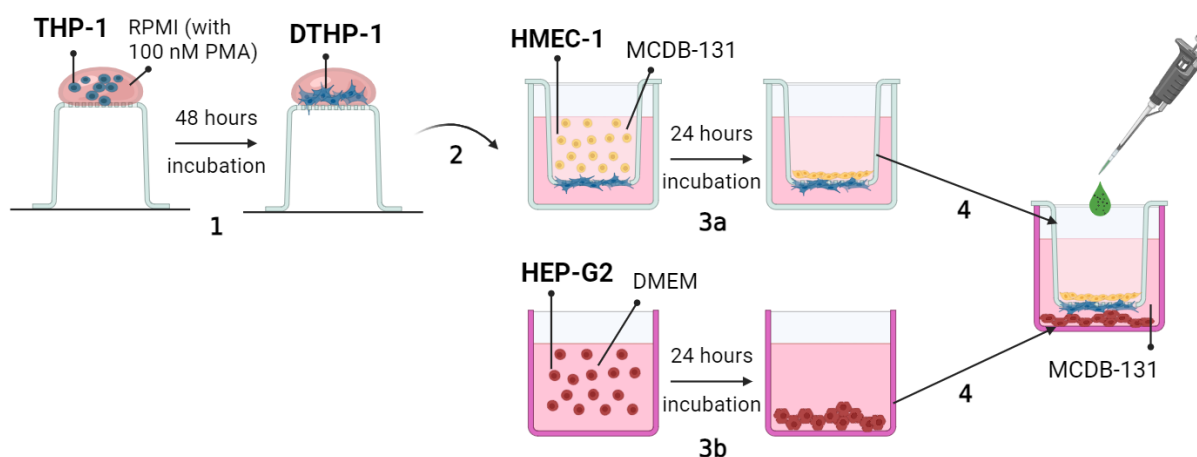


**Figure 4.2 Preparation of co-cultures.** (1) THP-1 cells were seeded on the basolateral side of the insert and differentiated to DTHP-1. (2) HMEC-1 cells were then seeded in the apical side of the insert (3a), while HEP-G2 cells were seeded directly into the well, and then incubated for 24 h (3b). (4) The insert was then placed into the well for the transport and uptake experiments. (Created with BioRender.com)

#### Cellular uptake of NPs

Co-cultures of liver cells were treated with NPs (LCF-PLGA-PVA NPs, PLGA-PVA NPs; all 1 mg/mL). NPs were added to the apical side of the insert and incubated with the cells for 2h. All the media was discarded, all cells were washed three times with DPBS and collected using a scraper into 1% FBS and 1 mM EDTA-supplemented DPBS for flow cytometry analysis. The settings of the flow cytometer were the same as the uptake analysis previously described in the **chapter 3-section 3.3.2**.

## 4.4 RESULTS AND DISCUSSION

### 4.4.1 Characterisation of the LCF-coated NPs

The diameter, size distribution and zeta potential of the NPs were measured by DLS at room temperature. The particle size of the PLGA NPs and LCF-PLGA NPs were both around 200 nm with low PDI ( $<0.2$ ) and zeta potentials around -12 mV (**Table 4.1**).

**Table 4.1. Impact of active targeting on NPs properties. (n=3, mean $\pm$  SD)**

	PLGA-PVA NPS	LCF-PLGA-PVA NPS
<b>Zeta potential (mV)</b>	-11 $\pm$ 8	-13 $\pm$ 4
<b>Size (nm)</b>	201 $\pm$ 24	206 $\pm$ 33
<b>PDI</b>	0.19 $\pm$ 0.04	0.12 $\pm$ 0.07
<b>LCF concentration (mg/mL)</b>	-	0.58 $\pm$ 0.3

Here, PVA was preferred as the stabiliser since PLGA-PVA NPs have a stronger anionic surface charge than PXM- coated NPs. PDLLA could not be used in this instance due to lack of availability at the time of the experiments. Given the cationic charge of LCF, electrostatic interaction enabled the binding of LCF to anionic PLGA-PVA NPs.

Modification of PLGA-PVA NPs led to a minimal change of NP properties (**Table 4.1**). Previous reports on LCF-targeted polyester NPs suggested that modification was accompanied by an increase in particle size of ca. 20-50 nm, depending on yield (243, 244). Since LCF itself has a molecular weight ca. 80 kDa (~3 nm) (245), it was expected that diameter would increase by up to 60 nm as this change is often used to confirm successful modification (246). However, some reports exist where particle size remained the same before and after modification with LCF, supporting what was observed here (247).

Similarly, limited impact on zeta potential was seen. LCF has a cationic charge at pH<8-8.5 (248), therefore one could expect LCF-coated NPs to have a much higher zeta potential

compared to uncoated NPs (243, 249). Others have reported similar results where modification of PLGA-PVA NPs with LCF led to a marginal change in zeta potential (-27 vs -23 mV before and after coating, LCF onto PLGA-PVA NPs) or no change at all (247). A more noticeable change (from -41 to -31 mV) was reported by Wei *et al.* but this was for PEGylated liposomes after LCF coating (250). This suggests that the effect of LCF on zeta potential may depend on the type of NP and the specific surface properties of the coating. The smaller change in zeta potential for PLGA-PVA NPs could be due to the inherent properties of the polymer matrix or the interaction between LCF and PVA, whereas the larger change observed for PEGylated liposomes could be due to the different surface chemistry and hydrophilicity introduced by PEGylation.

Here, a protein assay was used to confirm successful modification with LCF, since no change in size or charge was observed. After modification, the concentration of LCF was found to be  $0.58 \pm 0.3$  mg per mL of NPs. Similarly Li *et al.* (251) reported the detection of  $0.6 \pm 0.1$   $\mu\text{g}/\text{mg}$  of LCF coating on NPs using microBCA method. In their case, an increase of 14 nm in size and 10 mV in zeta potential were observed, and PLGA-PEG NPs were used.

The hydrophobicity of the LCF-PLGA-PVA NPs was compared with PLGA-PVA NPs using SAT. Neither of the NPs showed a significant increase in their size between 0 and 2 M of NaCl solution. Above this concentration, PLGA-PVA NPs started to aggregate with particle size growing by ca. 3-fold. LCF-modified NPs resisted the change in ionic strength and size hovered around 300 nm, corresponding to a 1.5-fold increase. At the highest concentration of NaCl tested (5 M), the results were less consistent, with different batches showing a size increase ranging from 0.5 to 3-fold. This variability suggests lower stability under those conditions (**Figure 4.3**).



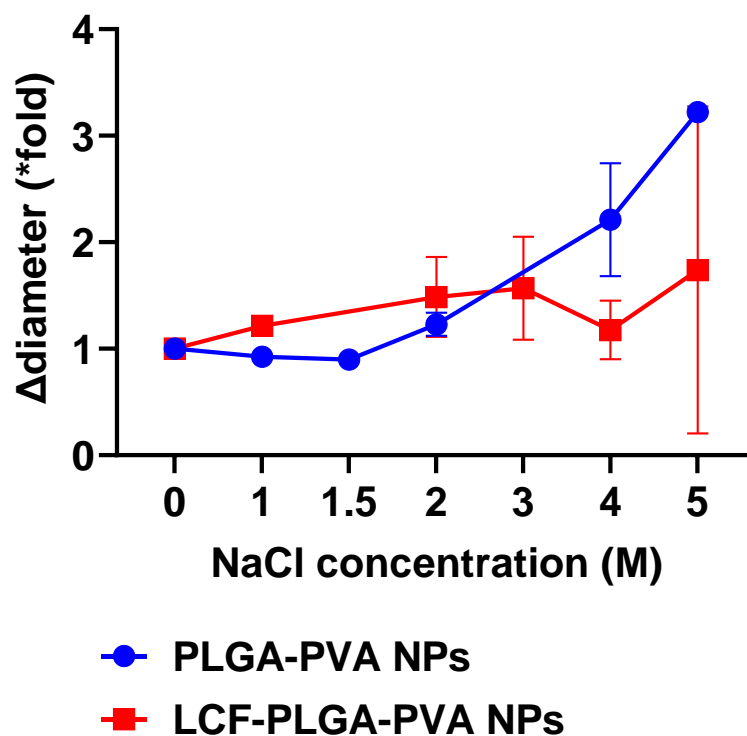


**Figure 4.3 SAT of passively- and actively-targeted NPs.** Aggregation of PLGA-PVA and LCF-PLGA-PVA NPs in  $\text{NaCl}_{\text{aq}}$  on increasing concentration of NaCl at  $37^\circ\text{C}$  tested using DLS by measuring increase in size (\*fold=final d.nm/initial d.nm). LCF-PLGA NPs were more hydrophilic than PLGA-NPs. Results are presented as the mean  $\pm$  SD (n=3 independent experiments).

Nevertheless, the SAT results suggest that LCF increased the hydrophilic character of the NPs, or at least, prevented their aggregation, which is expected following protein adsorption (252).

The study did not evaluate the storage stability of the LCF-coated NPs, or in the cell culture conditions. Also, the serum stability of the LCF coating on the PLGA-PVA NPs did not studies. Given the possibility of the LCF coating being replaced by serum proteins, analysis of the protein corona may benefit from techniques such as Western blot analysis or mass spectrometry.

#### 4.4.2 Co-culture uptake assay

Polyester NPs were found to be non-toxic at the concentration used in monoculture studies (chapter 3- section 3.4.1). Based on the literature, the LCF coating is not expected to negatively affect toxicity (234). For example, LCF NPs (~300 nm; 1 mg/mL) were found to be safe to use

on melanoma cells (B16F10) (253); while HEP-G2 could be treated for 48 h with low concentrations of LCF-targeted liposomes [(Soybean phosphatidylcholine:cholesterol, 3:2),(160 nm, 200 µg/mL)] without visible signs of toxicity (250). Safety towards mouse brain endothelial cells was also demonstrated for LCF-PLGA NPs at concentrations ranging from 0.03 to 3 mg/mL (244). All these results strongly suggest that LCF-coated NPs should be safe to test in the co-culture model.

### ***LCF and GAL competitive binding***

In receptor-mediated endocytosis, ligands on the surface of NPs are recognised by specific receptors on the cells and rapid NP uptake occurs. HEP-G2 cells are known to express a high number of ASGP-R (254, 255) whose ligands are LCF (28, 255) or GAL(24, 254). Therefore, the receptor-mediated uptake of LCF-PLGA-PVA NPs by HEP-G2 was tested in the presence of natural ASGP-R ligands (247).

Uptake of LCF-coated NPs resulted in a ~8-fold increase in fluorescence signal compared to untreated group. Addition of LCF or GAL decrease the fluorescence of HEP-G2 cells, suggesting a decrease in NP uptake (**Figure 4.4-A**). This suggest that the ASGP-R is at least partially responsible for the uptake of LCF-targeted NPs. Uptake of non-targeted NPs was not affected by the GAL or LCF inhibition and was, on average, lower than for LCF-targeted NPs (**Figure 4.4-B**). Similar results have been reported by Saraswat *et al.* (256) where uptake of GAL-targeted liposomes by HEP-G2 cells decreased by ca. 50% after cells were exposed to free GAL (250 mM) for 30 min. Wei *et al.* (250) showed that the internalisation of LCF-coated PEGylated liposome NPs decreased after treatment with the free ligand. It should be noted that serum-free conditions are required for this assay to be successful to avoid binding of the free LCF to serum proteins in the cell culture medium. Therefore, the behaviour of LCF-coated NPs characteristics remains unknown under *in-vivo* conditions. However, these experiments

indirectly confirmed the presence of ASGP-R on HEP-G2 cells, and it was observed that LCF could enhance the internalisation of LCF-PLGA-PVA by these cells.

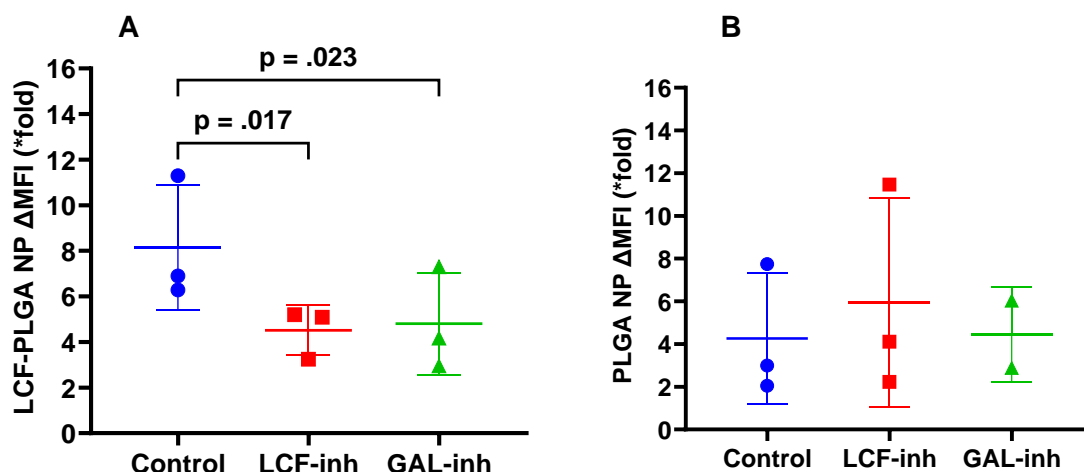


**Figure 4.4 Uptake of coated and uncoated PLGA NPs in receptor inhibition condition.** The uptake of (A) LCF-PLGA-PVA NPs and (B) PLGA-PVA NPs tested using flow cytometry after exposure to LCF or GAL for 1h. \*fold= MFI treated/MFI untreated. The uptake of LCF-PLGA-PVA NPs by HEP-G2 was significantly inhibited by free LCF or GAL. Results are presented as the mean  $\pm$  SD (n=3). One-way ANOVA, Dunnet's post-hoc test, \*p<0.05.

#### *Uptake of LCF-coated NPs*

The core experiment for this chapter involves a co-culture system of DTHP-1 macrophages, HMEC-1 endothelial cells and HEP-G2 hepatocytes, partly mimicking the complexity of the liver and the barriers NPs would have to cross after i.v. administration. By using this model and analysing uptake by flow cytometry, we aim to validate the potential of LCF-PLGA NPs to be selectively internalised by HEP-G2 while avoiding DTHP-1 uptake.

#### Insert permeability:

Firstly, a quick experiment was performed to confirm that NPs could diffuse across the insert membrane. Diffusion of NPs was assessed in two ways (**Figure 4.5**). First the fluorescence intensity for the NPs dispersions (apical side) was measured initially (**Figure 4.5; i-0**) and after

2h (**Figure 4.5; i-120**); in this time, mean intensity decreased by 30% (from ~100,000 to ~70,000). Second, the appearance of fluorescence in the receiving media was measured over time by sampling the media in the well. As shown in **Figure 4.5**, the signal increased rapidly in the first 30 min (intensity ca. 20,000) then more gradually to reach ca. 40,000 after 120 min.

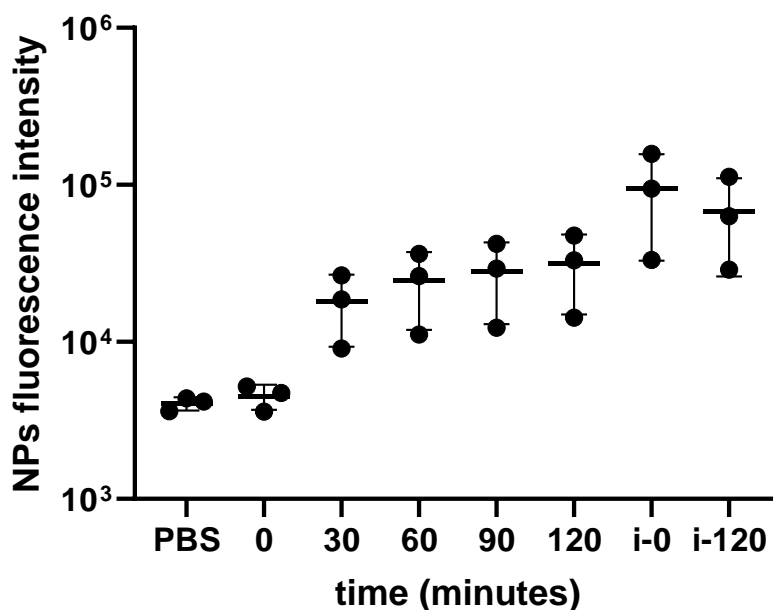


**Figure 4.5 Kinetics of PLGA-PVA NP diffusion through the naked insert.** The fluorescence intensity of the FITC-PLGA-PVA NPs in the insert (i-0; 0 min and i-120; 120 min), and in the well (0-120 min). NPs through the insert were fast for the first 30 min, with a slight increase by 120 min. Results are presented as the mean ± SD (n=3).

This simple experiment confirmed that the NPs do not aggregate in the serum at 37°C to an extent that would prevent their diffusion through the insert.

#### Cellular uptake of NPs:

Having demonstrated that the uptake of LCF-coated NPs by HEP-G2 was mediated by ASGPR, we investigated the effect of LCF coating on NP uptake by HEP-G2, HMEC-1 and DTHP-1 cells. Studies of the uptake of PLGA-PVA NPs by individual cell lines had already been reported in **chapter 3 -section 3.4.3**. Here, the uptake of LCF-coated and plain NPs by cells

was evaluated in a co-culture system as a preliminary step to evaluation of more complex systems, such as organoids or liver tissue.

HEP-G2 cells showed significantly higher internalisation of LCF-PLGA NPs compared to PLGA NPs. Despite the higher uptake of LCF-PLGA NPs, both types of NPs showed a broad uptake pattern by HMEC-1 cells. In contrast, DTHP-1 macrophages showed no difference in uptake between PLGA and LCF-PLGA NPs (**Figure 4.6**). A much stronger fluorescence signal was measured for HMEC-1 cells, though this may be due to these being the first cells NPs face. Still, the observed difference between unmodified and LCF-targeted NPs is promising, especially as LCF-modification did not seem to affect the capture by macrophages of PLGA-PVA NPs.

*In vitro* studies are usually focussed on single cell lines. However, the interaction of NPs with cells is directly related to their localisation in the organism (33). Co-culture studies can be considered as a useful first step in this regard. Co-cultures can be used to mimic the different cellular barriers NPs will face when leaving the systemic circulation to accumulate in the liver. Although interesting, this model would require optimisation to better simulate *in vivo* conditions. For example, the experiment was performed with gentle stirring. This does not reflect the effect of blood flow, which may reduce the contact time with HMEC-1. Furthermore, monocytes and circulating phagocytes were not included in this study. It is also challenging to mimic or characterise the unique fenestra structure of endothelial cells. Further studies should be conducted on organoids or organ-on-a-chip for more realistic uptake results that can simulate *in vivo* conditions.

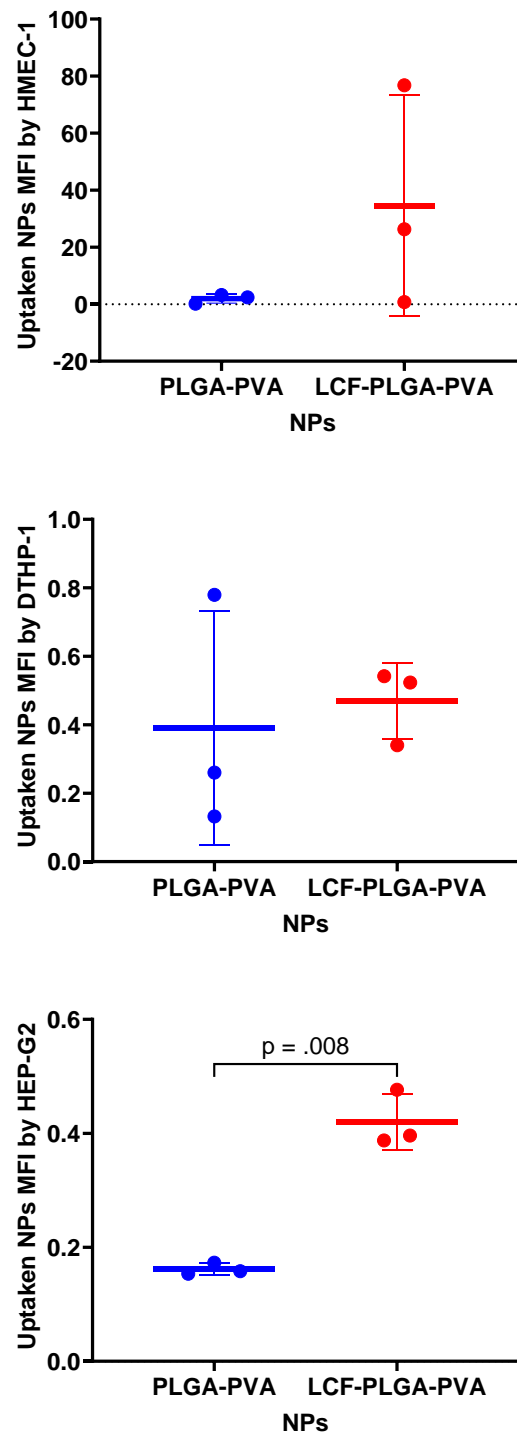


**Figure 4.6 The uptake of LCF-PLGA NPs and PLGA NPs.** Uptake of PLGA-PVA NPs and LCF-PLGA-PVA NPs tested in a transwell co-culture model after 2h using flow cytometry. LCF-PLGA NPs were internalised significantly more than PLGA NPs by HEP-G2 cells. Results are presented as the mean $\pm$  SD (n=3). (Paired t-test, \*\*p<0.01).

Although not tested here, others have reported that LCF-PLGA NPs with a diameter 90-200 nm accumulated preferentially in the liver and/or spleen, *in vivo* (243, 247). However, these studies did not show biodistribution between different hepatic cells and provided no data on uptake by macrophages or endothelial cell lines. However, targeting NPs to the correct cell type is important in liver diseases such as liver fibrosis, HCC and viral hepatitis. In their *in vivo* liver biodistribution studies, Park *et al.* (257) reported that the vast majority of PLGA NPs were taken up by LSECs (21%), followed by KCs (15%) and hepatocytes (4.2%). Even after KC number was reduced using clodronate liposomes, LSEC cells took up the most NPs (20.5%) and there was no change in uptake by hepatocytes (4%). These results suggest that, in the liver, which has a multilayered cell organisation, avoiding KC alone may not be enough to target hepatocytes. It has already been suggested that the high exocytosis ability of KC can be exploited to create a NP reservoir within the liver. Another approach could be to reduce the uptake of NPs by LSEC, which may be beneficial for targeting in general, not just for the liver. In our study, endothelial cells also showed affinity for the ASGP-R ligand, LCF. More studies should be conducted on the uptake behaviour of LSEC cells to confirm whether receptor-mediated endocytosis is involved, or a different mechanism is at play; for example, LCF or GAL inhibition in HMEC-1 cells could be tested.

## 4.5 CONCLUSION

LCF-PLGA NPs were successfully prepared with a ligand density of 0.58 mg/mL. The LCF coating gave the NPs a more hydrophilic character. When tested in a liver co-culture system, LCF-targeted NPs were preferentially internalised by HEP-G2 hepatocytes compared to non-targeted NPs. However, targeting also seemed to increase interaction with endothelial cells in this model, which warrants further investigation.

# **Chapter 5: BSA NANOPARTICLES**

## **OPTIMISATION AND**

## **MONOCULTURE STUDIES**

### **5.1 INTRODUCTION**

This chapter will present preliminary results obtained from the assessment of BSA NPs. BSA was chosen as a model protein for basic comparison with polyester NPs.

The first part of this chapter focuses on the optimisation, preparation and characterisation of BSA NPs using two different methods: thermal denaturation and desolvation techniques. The main aims are to ensure that the method is reproducible and to achieve the desired size range of 150-200 nm. The latter part of the chapter focuses on the safety assessment and cellular uptake of BSA NP, similar to the experiments performed on polyester NPs and presented in **chapters 2-4** (195, 196).

It is hypothesized that the thermal denaturation and desolvation techniques will produce stable BSA NPs within the desired size range of 150-200 nm, with high reproducibility. BSA NPs will exhibit low short-term toxicity on various liver-associated cell lines when assessed using the WST-8 viability test, indicating their biocompatibility. It is expected that the exposure to BSA NPs will not induce significant inflammatory responses in DTHP-1 cells. Nile red-loaded BSA NPs are more likely to be internalised by THP-1 and DTHP-1 cells because they are macrophage-like cells, although GAL or LCF attached to BSA NPs may alter the uptake behaviour and HEP-G2 cells may eventually take up more NPs than macrophages. However, GAL and LCF binding studies could not be completed for this thesis.



## 5.2 AIM AND OBJECTIVES:

The main aims are to manufacture and characterise 150-200 nm BSA NPs and assess their interaction with various cell lines associated with the liver.

Objectives:

1. Identify a suitable and reproducible method for the manufacture of BSA NPs.
2. Study particle size and morphology by DLS and TEM.
3. Assess the stability of the NPs under the following conditions: water (4°C), PBS at room temperature and cell culture medium (DMEM; 37°C).
4. Assess surface hydrophobicity by hydrophobic interaction chromatography (HIC), salt aggregation test (SAT).
5. Study the short-term toxicity of BSA NPs on various cells using the WST-8 viability test
6. Assess the inflammatory responses of DTHP-1 to BSA NPs by measuring cytokine (TNF- $\alpha$ , IL-6, and IL-10) release using an enzyme-linked immunosorbent assay (ELISA).
7. Fluorescently label BSA NPs with Nile red and study their uptake by HEP-G2, HMEC-1, THP-1 and DTHP-1 by flow cytometry.

## 5.3 MATERIALS AND METHODS

### 5.3.1 MATERIALS

Human liver cancer epithelial cell (HEP-G2), monocytic leukaemia cell line (THP-1), human microvascular endothelial cells (HMEC-1), macrophage-like murine reticulum cell sarcoma (J774) were obtained from European Collection of Authenticated Cell Cultures (ECACC; Salisbury, UK).

4',6-diamidino-2-phenylindole (DAPI), BSA lyophilised powder, Dulbecco's modified Eagle's medium (DMEM), Dulbecco's phosphate buffered saline (DPBS), dimethyl sulfoxide (DMSO), fetal bovine serum (FBS) ethylenediaminetetraacetic acid tetrasodium salt hydrate (EDTA), hydrocortisone, 2-(N-Morpholino) ethane sulfonic acid (MES solution), Nile red (F-NR), phorbol 12-myristate 13-acetate (PMA), phosphate buffered saline tablet (PBS tablets), thiazolyl blue tetrazolium bromide (MTT), trypan blue solution, sodium azide ( $\text{NaN}_3$ ), and sodium chloride (NaCl), sodium hydroxide (NaOH) flakes were purchased from Merck (Darmstadt, Germany).

MCDB-131 medium, RPMI 1640 medium, L-Glutamine, Penicillin-Streptomycin (PenStrep), recombinant human epidermal growth factor (Hu-EGF), 0.5% Trypsin-EDTA, citric acid, dimethyl sulfoxide (DMSO), ethanol absolute ( $\geq 99.0\%$  purity), and Triton X-100 were purchased from Thermo Fisher Scientific (Loughborough, Leicestershire, UK).

Ultrapure water is used for all experiments. All the solvents were of analytical grade and used without further purification.

### 5.3.2 METHODS

#### *Preparation of BSA NPs*

##### *Protein denaturation*

A modified thermal denaturation method was used to prepare BSA NPs (98). Stock BSA solution were prepared in MES (50 mM, pH 5) at different BSA concentrations; 2,3, and 5 mg/mL. All solutions were filtered through a 0.22 µm cellulose filter and stirred in a water bath at 750 rpm until their temperature reached 65 °C. At this point, the BSA solutions were heated for an additional 90 seconds to allow sampling for size assessment. Each sample was immediately cooled on ice, before the NPs were washed and collected by centrifugation (9500 RCF, 30 min).

##### *Modified desolvation*

100 mg BSA was dissolved in deionised water (25 mg/mL; 4 mL) under gentle stirring. The pH of the solution was adjusted to 7.5-8 with NaOH (0.5 mM) and the solution was filtered through a 0.4 µm cellulose filter. 16 mL of ethanol (without or with 0.1 mg/mL Nile red) was added dropwise to the BSA solution at a rate of 1 mL/min, under stirring (258); this was followed by citric acid (0.1-1% w/v, 0.1 mL) which was added at the same rate. The resulting solution was covered and left stirring at room temperature overnight. Finally, 15 mL deionised water was added to the BSA NP suspension, before centrifugation (45,000 RCF, 30 min). The pellet containing the NPs was sonicated at 10 amp, 2 min, room temperature), washed three times with DPBS, and dispersed in 5 mL DPBS for further characterisation.

#### *Characterisation of BSA NPs*

##### *The size and zeta potential of the NPs*

Particle size and zeta potential analysis were repeated for BSA NPs as described before in the **chapter 2 -section 2.3.2.**

### *Transmission Electron Microscopy (TEM)*

The TEM analysis and image processing were conducted as described in **chapter 2-section 2.3.2.**

### ***Colloidal stability testing***

Particle size and distribution (PDI) were measured at regular intervals over a 30-day period. NP dispersions in DPBS were stored at 4°C, and room temperature. The size was measured at t=0 then on days 1, 2, 4, 7, 10, 14, 20, and 30. The stability of the NPs under cell culture conditions was also assessed for dispersions prepared in DMEM containing 10% FBS stored at 37°C.

### ***Hydrophobicity of the NPs***

The surface hydrophobicity of the particles was studied by HIC and the SAT.

SAT and HIC analysis were conducted as described in the **chapter 2- section 2.3.2.**

### ***Monoculture studies with BSA NPs***

Cell culture preparation, the toxicity of the BSA NPs, cytokine release rates, inflammation response were assessed as described in the methods in the **chapter 3-section 3.3.2.** The uptake of Nile red-loaded BSA NPs (0.25 mg/mL) by HEP-G2, HMEC-1, THP-1 and DTHP-1 cells within one hour was also assessed by flow cytometry, according to the methodology described in **chapter 3-section 3.3.2.**

## 5.4 RESULTS AND DISCUSSION

### 5.4.1 Preparation techniques of BSA NPs

BSA NPs were initially prepared using a protein denaturation protocol (98, 259). This method is based on the thermal denaturation of albumin proteins at temperatures above 65°C. Heat-induced protein-protein interactions are thought to initiate the assembly of BSA into NPs through the formation of disulfide bonds though other forces including hydrophobic interactions, electrostatic interactions, hydrogen bonding, and disulfide-sulfhydryl interchange interactions also play a role (98, 260). Although less common for the manufacture of BSA NPs, this technique has the advantage of being solvent-free, which could make it more easily scalable.

Here, the impact of volume and concentration was quickly studied: three initial BSA concentrations (2,3, and 5 mg/mL) and two different volumes (10 and 25 mL) were tested. Particle size was assessed at specified time intervals during the assembly process to determine how quickly aggregation took place; once BSA NPs size reached beyond the desired size (150-200 nm), sampling was stopped. This brief kinetic study confirmed that increasing the BSA concentration resulted in faster aggregation rates. Indeed, at the lowest concentration (2 mg/mL) tested, BSA NPs took 70 seconds in to form, while evidence of aggregation was seen within 60 and 50 seconds when BSA concentration was increased to 3 and 5 mg/mL, respectively (**Table 5.1**). This was expected as there is an increased possibility of protein collision at higher concentration (261).

Concentration also affected the extent of aggregation. As shown in **Table 5.1**, when working with a 5 mg/mL solution, the size of the NPs increases rapidly from <15 nm to >365 nm in 10 seconds. A similar trend was observed when the concentration was adjusted to 3 mg/mL BSA, but to a lesser extent, as the size increased only ca. 11-fold from 21 nm to 226 nm in the same

time. In contrast, at the lowest concentration tested, double the time was needed (20 seconds) to achieve a 28-fold increase in particle size from 10 nm to 267 nm.

**Table 5.1 Kinetics of formation for BSA NPs prepared by by the denaturation technique (n=1)**

BSA concentration	50 mg:25 mL 2 mg/mL		30 mg:10 mL 3 mg/mL		50 mg:10 mL 5 mg/mL	
Time (second)	d.nm	Pdl	d.nm	Pdl	d.nm	Pdl
30	-	-	-	-	12	0.3
40	-	-	-	-	13	0.4
50	-	-	20	0.6	366	0.3
60	10	0.4	226	0.3	1425	0.8
70	79	0.6	738	0.2	-	-
80	267	0.5	-	-	-	-
90	2732	0.4	-	-	-	-

Contradictory results on the impact of concentration have been reported. Galisteo-Gonzales *et al.* (262) showed that increasing BSA concentration from 12 to 100 mg/mL led to an increase in NP size (75 nm to 135 nm) and decrease in Pdl. However, Rahimnejad *et al.* (263) observed a decrease in diameter (204 to 146 nm) when concentration was changed from 5 to 30 mg/mL. The opposite results in the studies can be explained by differences in experimental conditions, including pH, temperature, initial BSA concentration, or solvent use. In our study, the concentrations tested were lower than the most concentrations reported in the literature and this likely created different physicochemical conditions for NP nuclei creation and agglomeration. This might also explain why it was possible to partially assess the kinetics of NP formation. As,

Qi *et al.* (260) also experienced increasing BSA concentration (0.5-5 mg/mL) resulted with increased NP size and PDI (131-226 nm; 0.12-0.24 PDI).

Additionally, increased incubation time of the BSA led to increased protein-protein interaction and created larger NPs by the time, similar to work of Zhou *et al.* (264) which showed thicker BSA film formation on graphene by heat denaturation (80°C). It explains the increasing NP diameter with increasing incubation duration at 65°C.

Overall, the results of this initial test revealed that controlling over size and size distribution when using this method might be difficult, due to the quick aggregation process. Here, a diameter ca. 150-200 nm was targeted, but was not achieved although previous studies succeeded in obtaining 143 nm (98) and 167-226 nm (260) BSA NPs. This suggest that experimental conditions must be closely monitored and optimised. Therefore, the decision was made to focus on the desolvation technique, which has become the preferred method for the preparation of BSA NPs (265).

The desolvation method is based on triggering the association of hydrophilic BSA by adding a poor solvent (often ethanol) at a constant rate and volume (266). This method often requires crosslinkers, *e.g.* glutaraldehyde, to stabilise the BSA NPs through the formation of covalent bonds between individual proteins (258, 267). Even though it was suggested that glutaraldehyde was not toxic at concentrations used in NPs manufacture, the risk of interaction with physiological peptides and proteins cannot be completely discarded, therefore safer alternatives are needed (268, 269).

With the restricted use of glutaraldehyde because of its toxicity, an alternative crosslinker was sought. Here, citric acid was chosen as the preferred cross-linking agent due to its biocompatibility and GRAS status (270). In this case, crosslinking is thought to result from the

formation of covalent bonds between the carboxylic acids of citric acid and amine groups of BSA, though interaction with OH functions on the protein can also be involved.

Various concentrations of citric acid (0 to 1%) were tested during the optimisation steps (**Figure 5.1**). The size of the BSA NPs increased slightly from 160 nm to 200 nm with increasing concentrations of citric acid while neither the Pdl (< 0.15) nor the zeta potential (~-15 mV) were affected.

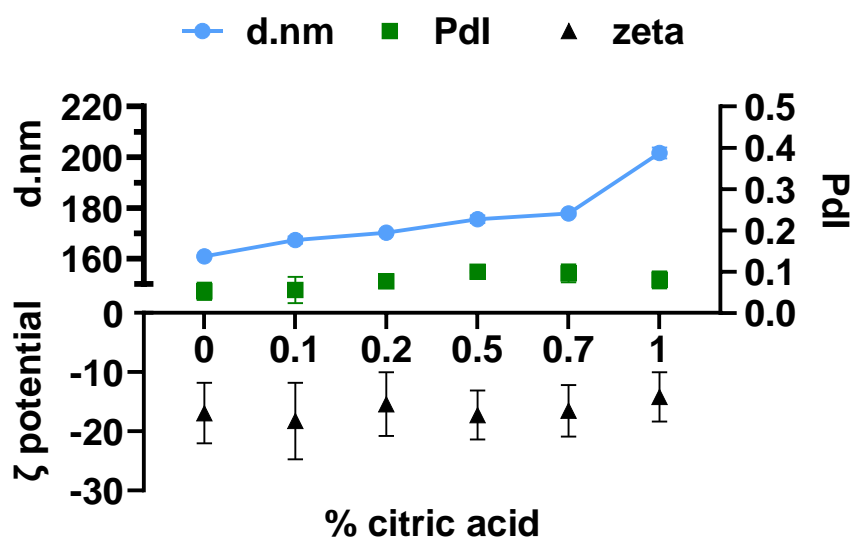


**Figure 5.1 Impact of citric acid concentration on BSA NPs properties.** BSA NPs were prepared by the desolvation technique, using citric acid as the crosslinker. The effect of citric acid concentration (0 to 1%) on particle diameter, polydispersity and zeta potential was tested. No impact was seen on Pdl or zeta potential, but diameter increased slightly with crosslinker concentration. Results are presented as the mean  $\pm$  SD of three technical replicates (n=1).

This preliminary study seems to confirm that desolvation could allow better control over the size and polydispersity of BSA NPs. This method was therefore selected for all further studies as NPs within the desired size could be obtained; 0.1% was selected as an adequate citric acid concentration as the higher concentration of the citric acid did not have a profound influence on the size of the NPs. However, stability differences between the BSA NPs stabilised with different concentrations of citric acid could be studied in the future.



## 5.4.2 Characterisation of BSA NPs

### *Particle size and zeta potential*

The results obtained during optimisation were successfully reproduced, confirming the robustness of the method (**Figure 5.2**). The sizes measured by DLS and TEM (**Figure 5.3**) were similar at  $162\pm15$  nm (PdI:  $0.07\pm0.01$ ) and  $163\pm36$  nm, respectively. TEM also confirmed that BSA NPs were spherical (**Figure 5.3-A**). The NPs had a negative zeta potential of  $-23\pm6$  mV as expected for BSA at pH 7.4.

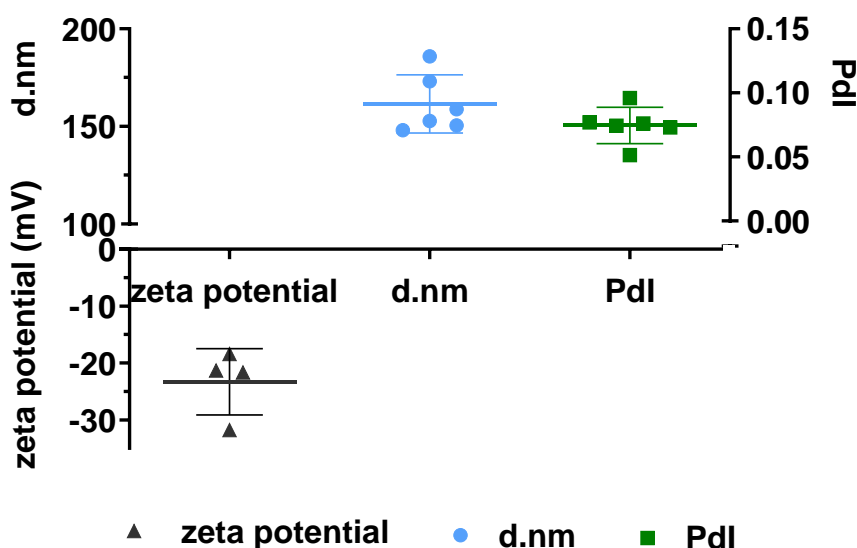


**Figure 5.2 Characterisation of BSA NPs.** NPs were prepared using the desolvation technique in the presence of 0.1% citric acid as a crosslinker. 150-200 nm BSA NPs obtained with low dispersity ( $<0.1$  PdI) and a negative zeta potential ( $-23$  mV). Results are presented as the mean $\pm$ SD; each data symbol represents a unique experiment as replicates.

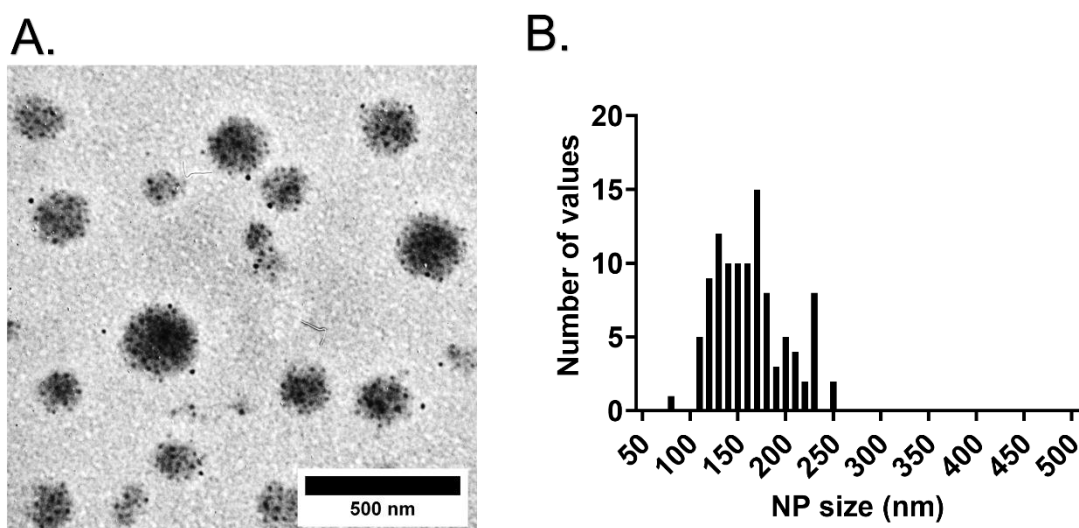


**Figure 5.3 TEM analysis of BSA NPs.** (A) TEM imaging and (B) particle size distribution of BSA NPs. Particles were spherical with a diameter of  $163 \pm 36$  nm sized (NPs were measured by ImageJ software, event number = 104). A representative image out of three images from one batch is shown.

#### 5.4.3 Colloidal stability

Colloidal stability of the BSA NPs was assessed over 30 days at different temperatures and dispersing media: 4°C in deionised water, room temperature in PBS, and 37°C in serum-containing cell culture media.

BSA NPs exhibited sustained stability, maintaining a constant size at 4°C in deionised water. At RT (in PBS), fluctuations in PdI were evident from day 4, though the size appeared to increase only from day 30. In cell culture media at 37°C, the particles were stable at least 20 days (**Figure 5.4**). Between day 20 and day 30, the PdI increased dramatically, though the size stayed roughly the same, suggesting that the NPs will remain stable when used in *in vitro* studies. Overall, the results suggest that BSA NPs should be stored in water in the fridge and can be kept at that temperature for 1 month.

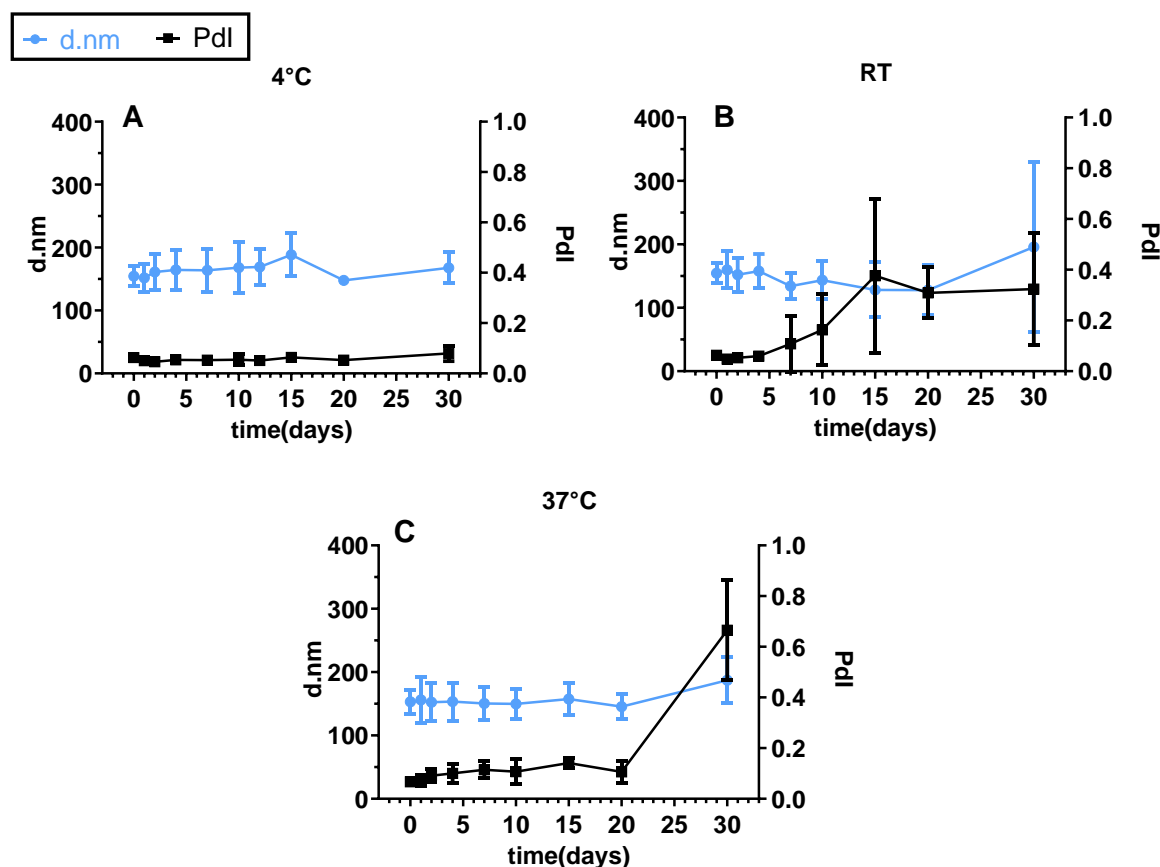


**Figure 5.4 Colloidal stability of BSA NPs.** Particle size and polydispersity were studied (A) In water at 4°C (B) in PBS at room temperature, and (C) in complete cell culture media at 37°C. NPs were stable for at least a month at 4°C, and for 20 days at 37°C and less than 10 days at room temperature in PBS. Results are presented as mean $\pm$ SD (n=3 independent experiments).

The presence of salts and temperature seem to affect stability and this needs to be considered when making large batches of the NPs. Since citric acid crosslinking is not common in BSA NP stabilisation, there is limited information on their stability in the literature. NPs (162 nm, -34 mV) prepared using glutaraldehyde as a crosslinker showed similar stability when stored at 4°C (271). A different study showed that the size of the BSA NPs (~160 nm, -31mV) started to fluctuate after 2 days in PBS at RT (272), which is earlier than was observed here, but confirms poor stability under these conditions. The impact of drug loading was not studied here, but

previous reports suggest that prolonged stability under physiologically relevant conditions could be maintained, even in the presence of a drug. Indeed, celastrol loaded BSA NPs (118 nm, -2.5 mV; 2% glutaraldehyde) were stable for 3 months at 37°C in PBS and in PBS+10% FBS media (273). It is unclear where the drug or crosslinker contributed to the increased stability observed. In any case, these particles were more stable than the BSA NPs prepared here, using citric acid. Further studies will be required to understanding what could have led to these differences in stability. Additionally, comparing glutaraldehyde and citric acid stabilisation should be tested.

#### 5.4.4 Hydrophobicity of the BSA NPs

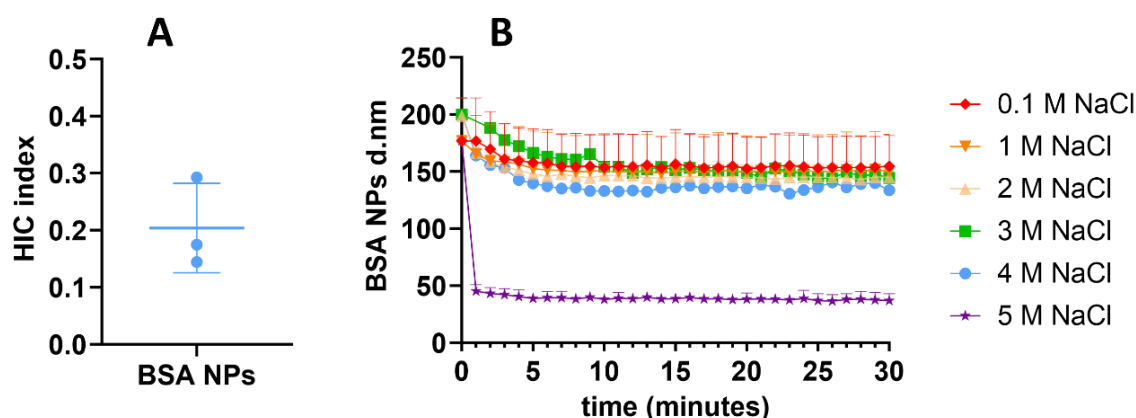


**Figure 5.5 Hydrophobicity assessment of BSA NPs.** (A) HIC index (B) Aggregation of BSA NPs in NaCl solutions of increasing concentration at 37°C. Both tests suggest that BSA NPs are hydrophilic. Results are presented as the mean $\pm$  SD (n=3 independent experiment).

HIC and SAT were used to assess the surface hydrophobicity of BSA NPs. As expected, both tests indicated that BSA NPs were hydrophilic, with a low HIC index of  $0.2 \pm 0.1$  and lack of aggregation in concentrated NaCl solutions (**Figure 5.5**). When tested in NaCl<sub>aq</sub> at concentrations 0.1-4 M, BSA NPs maintained a size between 150 and 200 nm with a tendency for diameter to decrease with time. At the highest concentration, NPs appeared to de-aggregate. This may be explained by a disruption of the electrostatic interactions or hydrogen bonding

responsible for NP formation (274); yet, some interactions may remain, which explains the incomplete dissociation on the BSA NPs (275, 276). It is also possible, that NaCl competitively bond to water molecules around the NPs causing them to shrink. Notably, the BSA NPs did not show aggregation in 0.1 M NaCl solution which is close to isotonic conditions (0.15 M).

#### **5.4.5 Monoculture studies with BSA NPs**

##### ***Viability studies***

It is known that BSA is biodegradable and non-toxic *in vivo* (267). It is broadly expected, that these features will be maintained after NPs assembly (277). However, the crosslinkers used may affect the compatibility of BSA NPs, though maybe less so for citric acid. In order to confirm safety, BSA NPs were tested on a variety of cells. While BSA NPs showed no toxic effect against DTHP-1 and THP-1, a gradual decrease in viability was observed at concentrations above 3 mg/ml in HMEC-1 and 2 mg/ml in HEP-G2 cells (**Figure 5.6**). The IC<sub>50</sub> values of BSA NPs on HEP-G2 and HMEC-1 were 8.3 and 27.1 mg/mL, respectively, emphasising the cell-specific responses to BSA NPs probably because of the material burden in the HEP-G2 and HMEC-1 cells in contrast to phagocytic cells such as THP-1 and DTHP-1 cell lines which are capable of high exocytosis capacity. Lankoff *et al.* (278) suggested that THP-1 and DTHP-1 cells may be naturally more resistant to NPs exposure because of their high endocytic and exocytic capacity, which allows them to quickly discharge NPs before they accumulate and cause toxicity.

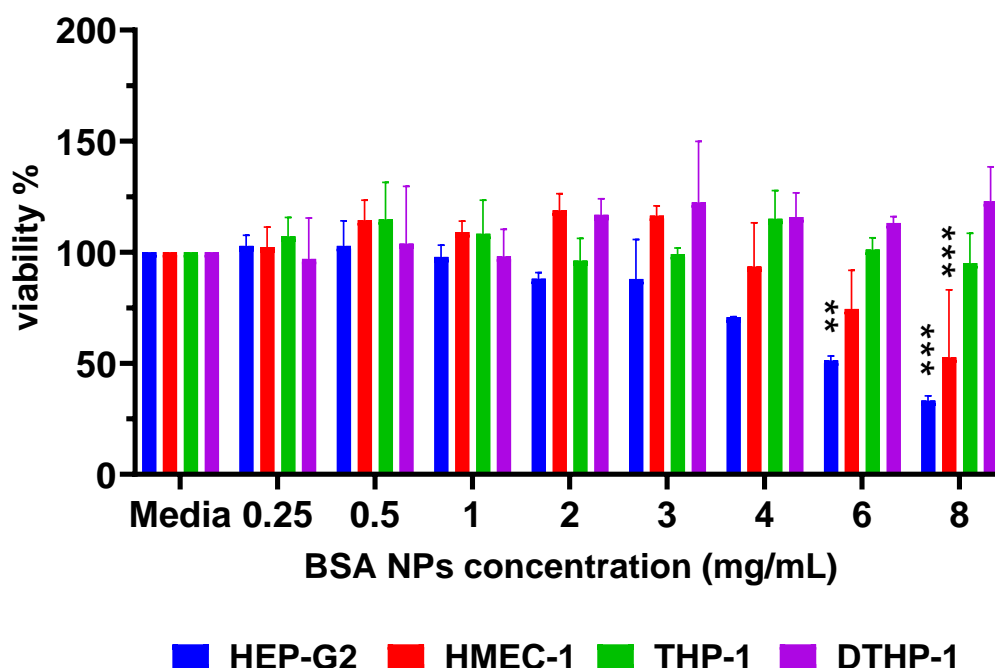


**Figure 5.6 Cytotoxicity of BSA NPs.** The viability of HEP-G2, HMEC-1, THP-1, and DTHP-1 cells was assessed after exposure to BSA NPs for 24 h. DTHP-1 and THP-1 viability remained above 80% at all concentrations tested. However, HMEC-1 and HEP-G2 viability dropped below 80% at concentrations >3-4 mg/mL. Results are presented as mean $\pm$  SD (n=3 independent experiments). Two-way ANOVA, Dunnet correction for multiple comparison, 8 mg/mL viability were compared to control group. \*\*p<0.01, \*\*\*p<0.001

Although exact comparison may be difficult since studies tend to assess drug-loaded particles, there is some evidence of the safety of BSA NPs in the literature. Iodinated BSA NPs (96 nm) did not show cytotoxicity towards RAW264.7 macrophages or endothelial cells (HUVEC) after 24h when tested at concentrations between 0-0.5 mg/mL (279). Jose *et al.* (280) showed that glutaraldehyde crosslinked 0.1 mg/mL BSA NPs (97-120 nm, 32mV) decreased the viability of MiaPaCa-2 human pancreatic cancer cells to 50% after 48 h. The reason of the toxicity might be high cationic charge on the NPs. Since NPs in our study have negative surface charge, cytotoxicity at lower concentration was not observed on HEP-G2 cancer cells. The toxicity of polyester NPs (**chapter 3-section 3.4.1**) on HEP-G2 and HMEC-1 was not observed on tested

concentrations, while BSA NPs showed toxicity at 6-8 mg/mL on the same cells. Both polyester NPs and BSA NPs were not toxic on THP-1 and DTHP-1 cells.

### ***Inflammation studies***

Understanding the pro-inflammatory potential of NPs is crucial for their safe and effective use in various biomedical applications. Here, the impact of BSA NPs on cytokine release was assessed using the same protocol as for polyester NPs: tests were performed on DTHP-1 macrophages as effectors of inflammation and levels of TNF- $\alpha$ , IL-6 and IL-10 were measured. BSA NPs did not exhibit a significant difference compared to the negative control (media). As expected, LPS (0.25  $\mu$ g/mL) triggered the release of TNF- $\alpha$ , IL-6 and IL-10 compared to the media (**Figure 5.7**). The results suggest that BSA NPs have limited impact on cytokine release and are neither pro- nor anti-inflammatory towards DTHP-1 macrophages under the experimental conditions tested here. These results confirm what was observed in the cytotoxicity test and suggest that BSA NPs are biocompatible and safe.

These results were as expected and reflect previous reports indicating that BSA NPs (4.3 mg/mL; 108 nm, -17.5 mV) did not induce TNF- $\alpha$  or IL-6 release on J774 macrophages (281). However, additional studies will be required on alternative non-cancerous cell models. Indeed, Schildberger *et al.* (282) demonstrated that TNF- $\alpha$ , IL-6, and IL-10 levels were consistently lower in DTHP-1 cells compared to PBMC (peripheral blood mononuclear cells) or monocytes treated with LPS. Nevertheless, these BSA NPs are considered safe enough to study on DTHP-1 cells; while for other cells, the findings can guide the selection of appropriate concentrations and experimental conditions for further studies.

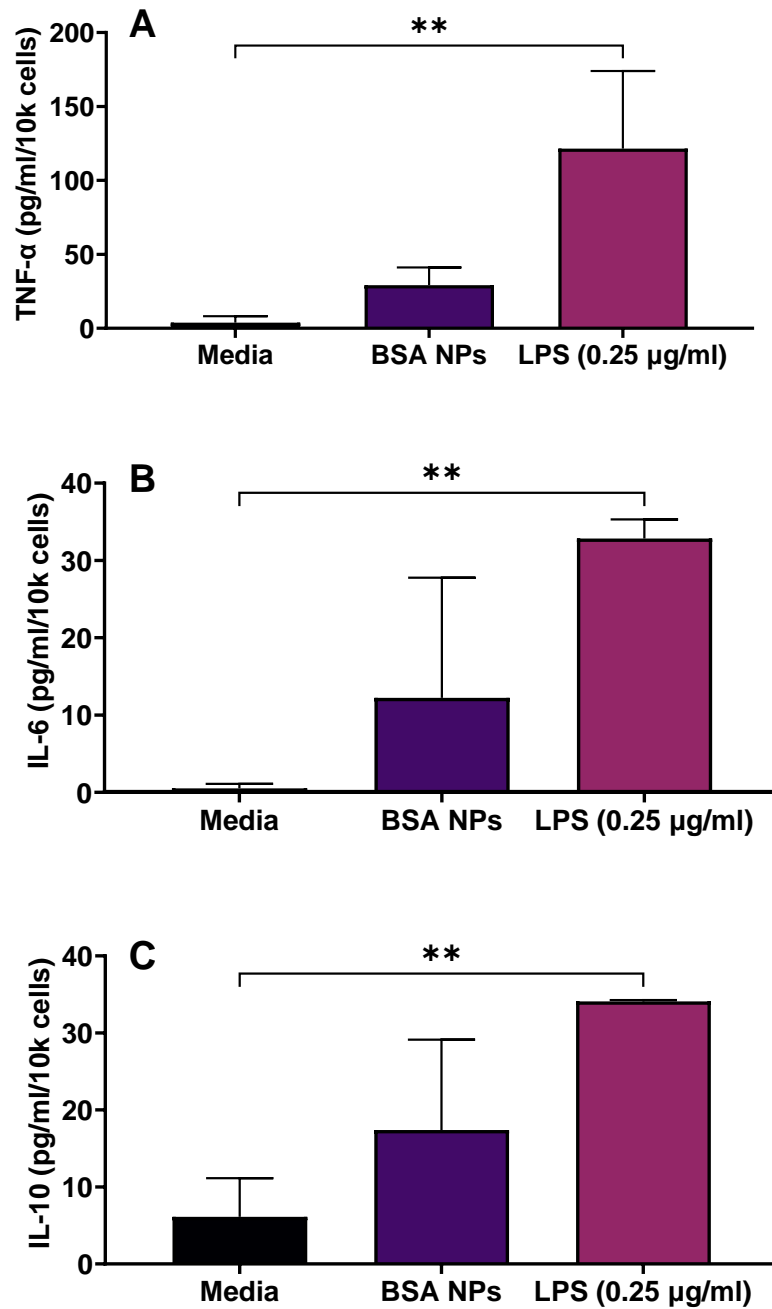


**Figure 5.7 Impact of BSA NPs on cytokine release.** The release of three cytokines (A) TNF- $\alpha$ ; (B) IL-6 and (C) IL-10 was assessed on DTHP-1 cells exposed to BSA NPs (8 mg/mL) for 24 h. BSA NPs (8 mg/mL) did not induce a significant inflammatory response on DTHP-1 cells. Results are presented as mean  $\pm$  SD (n=3). One-way ANOVA, Dunnet post-hoc test (\*\*  $p < 0.01$ ).



### *Uptake studies*

The uptake of BSA NPs by various liver cell lines, including HEP-G2 hepatocytes, HMEC-1 endothelial cells, THP-1 monocytes and DTHP-1 macrophages, was investigated by flow cytometry.

All cells showed an increased fluorescence intensity after exposure to BSA NPs (0.25 mg/mL). However, THP-1 monocytes, and DTHP-1 macrophages exhibited a higher uptake of BSA NPs compared to the other cell lines tested (**Figure 5.8**). This higher uptake could be related to the specific nature and functional characteristics of THP-1 and DTHP-1. Monocytes, as precursors of macrophages, are known for their active phagocytic behaviour, allowing efficient internalisation of particles. In contrast, HEP-G2 and HMEC-1, although involved in liver functions, may have different uptake mechanisms or a lower tendency to internalise NPs. Interestingly, Ahmed *et al.* (283) claimed that NPs with BSA corona were taken-up less by HEP-G2 cells because of their weaker capacity for endocytosis, which supports the results observed here.

It is important to remember that drugs delivered by NPs targeted to the liver tissue will encounter endothelial cells and must access hepatocytes without being captured by circulating monocytes or by KCs. Therefore, targeting methods that allow BSA NP to avoid capture and increases their uptake by hepatocytes may be required. In the literature, targeting using lactose has been reported to improve receptor-mediated uptake by the liver *in vivo*. A competitive assay with free galactose confirmed that the ASGP receptor contributed to the uptake (284).

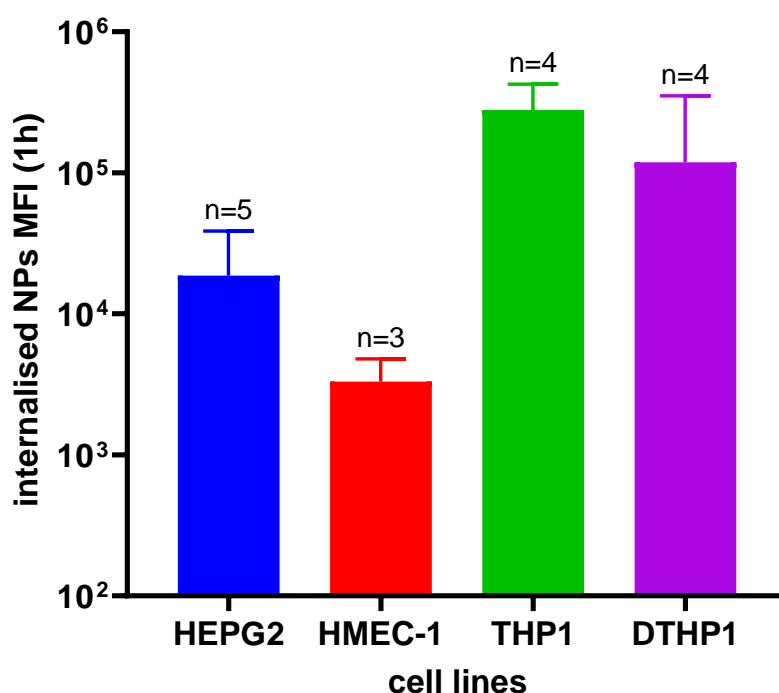


**Figure 5.8 Cellular uptake of BSA NPs.** Mean fluorescence intensity (MFI) of BSA NPs (0.25 mg/mL) taken-up by HEP-G2, HMEC-1, THP-1 and DTHP-1 cells in 1h. THP-1 and DTHP-1 cells internalised more BSA NPs than HEP-G2 and HMEC-1. Results are presented as mean±SD (n=3-5 independent experiments) (One-way ANOVA, Tukey multiple comparison test).

## 5.5 CONCLUSION

A desolvation method with citric acid as the crosslinker was preferred because of the reproducibility over the thermal denaturation method. Anionic BSA NPs were produced within the targeted size range (150-200 nm). Characterisation studies showed that NPs were hydrophilic and stable in 4°C storage conditions for a month, and stable in cell culture conditions at least for 21 days. The particles were not toxic towards THP-1 and DTHP-1 and did not trigger cytokine release. However, IC<sub>50</sub> values of 8 and 27 mg/mL, were obtained in HEP-G2 and HMEC-1, respectively. Finally, uptake was cell-dependent with phagocyte taking up more NPs compared to other cells. These results suggest that citric acid may be a suitable

alternative to glutaraldehyde as a crosslinker, although further studies are required to complete the assessment of BSA NPs for targeted delivery to hepatocytes.

# Chapter 6: CONCLUSION AND FUTURE WORK

## 6.1 CONCLUSION

In this work, NPs were prepared by nanoprecipitation. This method was preferred due to its simplicity and ability to generate NPs with the correct properties. Although three types of polyester and five stabilisers were used initially, the decision was made to focus the work on two polyesters (PDLLA and PLGA) since they produced the NPs with desired size and two stabilisers (PVA and PXM) as generated NPs with different surface characteristics.

All preparations were characterised extensively, including to detect differences in surface hydrophobicity. All NPs were of similar size (150-200 nm) and narrowly distributed. The surface charge was stabiliser- dependent, with PVA NPs found to be more anionic compared PXM-coated NPs; this was likely caused by differences in coating thickness and arrangement on the surface of the NPs. Two different surface hydrophobicity conducted on these particles revealed that PXM-coated NPs were more hydrophilic than PVA-coated NPs, but this did not affect stability or protein adsorption.

*In vitro* experiments were performed to assess NPs toxicity, pro-inflammatory potential and uptake. Here, cells were selected from hepatoma cells, endothelial cells, monocytes and macrophages to mimic liver cell types to understand better the interaction between passively-targeted NPs and the different cells found in the liver. None of the NPs appeared to be cytotoxic at concentration up to 3 mg/mL. In the pro-inflammatory assay, polyester NPs did not induce the release of TNF- $\alpha$ , IL-6, IL-10, contrarily to PS NPs and LPS, which were used as a control. Overall, no clear impact of the stabiliser was found, though further studies are needed to fully explain all the results obtained.

Uptake of Nile red-loaded NPs was studied using either flow cytometry or fluorescence microscopy. Treatment of the cells with a broad-spectrum inhibitor confirmed that NPs were internalised through an energy-dependent process, although 1 h was not enough to prevent phagocytosis. An attempt was made to assess the impact of the stabiliser on cellular uptake. A clear trend was not always easy to define and differences in Nile red-loading complicated analysis. Overall, it was observed that NPs were more likely to be internalised by hepatoma cells were more hydrophilic and less anionic, but no clear difference was seen in uptake by endothelial, monocyte and macrophage cells.

With the aim of enhancing internalisation by hepatocyte cells, LCF-coated PLGA NPs targeted to ASGP receptors were prepared. Protein concentration tests confirmed successful modification with LCF, which is thought to occur through electrostatic interactions. To assess the uptake of these actively targeted NPs, a co-culture system was established. In these studies, uptake of actively targeted NPs by hepatoma cells was significantly higher compared to passively targeted NPs. Additionally, no significant difference in internalisation was observed in macrophages and an increase in uptake was observed in endothelial cells. The latter finding may be explained by endothelial cells being the first cells encountered by NPs in the co-culture system or suggest that these cells can bind LCF. Further studies are needed to explore this in more depth.

The final phase of this work focused on a different type of NP. Albumin NPs were prepared using a desolvation method with citric acid as a cross-linking agent. Hydrophilic, anionic BSA NPs could be obtained which showed good stability, lasting one month at 4°C and at least 21 days under cell culture conditions. The BSA NPs were non-toxic and cell-dependent uptake was observed, with higher uptake by THP-1 and DTHP-1. From these studies, citric acid emerged as a potential alternative cross-linking agent that warrants further investigation.

## 6.2 FUTURE WORKS

The work performed during this PhD brought up interesting results, but also new routes of investigation. Choices had to be made early in the work, taking into consideration time constraints and disruption caused by the COVID-19 pandemic.

The work performed on polyester NPs could easily be extended to include other polymers and stabilisers. In the short term, PVA or PXM coated PLGA NPs can be compared to Span 80 stabilised PLGA NPs, as Span 80 forms a more hydrophobic interface (285) on the NPs. Later, the preparation of chitosan stabilised NPs will provide information for positively charged polyester NPs (286). In addition, the hydrophobicity of the prepared NPs should be tested in cell culture media and in serum conditions to test the effect of the protein corona of the NPs on their hydrophobicity and subsequently on their cellular uptake.

It will be necessary to repeat the uptake studies, taking steps to ensure that differences in fluorescence are taken into consideration for a more reliable interpretation of the results. Differing from fluorescent dye loading, radiolabelling of NPs can be used for more sensitive data of internalised polyester NPs. Radiolabelling data can be supported by TEM imaging of the cells by counting internalised NPs, so that the amount of NPs adsorbed to the surface or internalised can be differentiated.

In this study, it was shown that HMEC-1 endothelial cells showed tendency to uptake LCF-coated PLGA NPs. Interaction between NPs and endothelial cells should be probed further. The probability of having receptors for ligands similar to ASGP-R ligands for endothelial cells should be investigated. As a first step, the GAL or LCF inhibition uptake test for endothelial cells can be utilised. For the more specific following test, the PCR technique can be used with the ASGP-R specific primers (287). For more reliable data, it is preferable to perform all cell tests on primary liver cells.

Colloidal stability and LCF attachment stability of the LCF-PLGA NPs should be tested in storing and serum conditions. More importantly, more work should be done to develop in vitro models that are representative of physiological environment. Here, this could also include performing experiments under flow conditions to mimic the NPs in a blood stream and restricting their contact time with the endothelial cells. Microfluidic devices such as organ-on-a-chip models, and a plate-scale perfusion systems (288) could be optimised to mimic the flow and pressure on the cells would provide more information. Subsequently, ex vivo or in vivo testing should be performed in the future.

## Chapter 7: REFERENCES

1. Britannica. Liver. In: Britannica Teoe, editor. Encyclopedia Britannica 2023.
2. Drake RLPF, Vogl AWPf, Mitchell AWMMBBSFF. Abdomen. Fourth Edition ed 2020. p. 249-412.e8.
3. Katavic V, Jens Waschke, Tobias M. Bockers, Friedrich Paulsen (editors): Sobotta Anatomy Textbook  
English edition with Latin nomenclature. Croatian medical journal. 2019;60(6):574.
4. Sargent S. Liver diseases : an essential guide for nurses and health care professionals / edited by Suzanne Sargent: Chichester, U.K.  
Ames, Iowa : Wiley-Blackwell, 2009.; 2009.
5. Paulsen F, Böckers TM, Waschke J, Winkler S, Dalkowski K, Mair J, et al. Sobotta anatomy textbook: English edition with Latin nomenclature. Elsevier Health Sciences; 2018.
6. Rhyu J, Yu R. Newly discovered endocrine functions of the liver. World J Hepatol. 2021;13(11):1611-28.
7. Stillman AE. Jaundice. In: Walker HK, Hall WD, Hurst JW, editors. Clinical Methods: The History, Physical, and Laboratory Examinations. Boston: Butterworths  
Copyright © 1990, Butterworth Publishers, a division of Reed Publishing.; 1990.
8. Joseph A, Samant H. Jaundice. StatPearls. Treasure Island (FL) ineligible companies. Disclosure: Hrishikesh Samant declares no relevant financial relationships with ineligible companies.: StatPearls Publishing  
Copyright © 2023, StatPearls Publishing LLC.; 2023.
9. Selzner M, Clavien P-A. Fatty Liver in Liver Transplantation and Surgery. Seminars in Liver Disease. 2001;21(01):105-14.
10. Odenwald MA, Paul S. Viral hepatitis: Past, present, and future. World J Gastroenterol. 2022;28(14):1405-29.
11. Aydin MM, Akcali KC. Liver fibrosis. The Turkish Journal of Gastroenterology. 2018;29(1):14-21.
12. Bataller R, Brenner DA. Liver fibrosis. Journal of Clinical Investigation. 2005;115(2):209-18.
13. Marengo A, Rosso C, Bugianesi E. Liver Cancer: Connections with Obesity, Fatty Liver, and Cirrhosis. Annual Review of Medicine. 2016;67(1):103-17.
14. Sung H, Ferlay J, Siegel RL, Laversanne M, Soerjomataram I, Jemal A, et al. Global Cancer Statistics 2020: GLOBOCAN Estimates of Incidence and Mortality Worldwide for 36 Cancers in 185 Countries. CA Cancer J Clin. 2021;71(3):209-49.
15. Devarbhavi H, Asrani SK, Arab JP, Nartey YA, Pose E, Kamath PS. Global burden of liver disease: 2023 update. Journal of Hepatology. 2023;79(2):516-37.
16. Llovet JM, Kelley RK, Villanueva A, Singal AG, Pikarsky E, Roayaie S, et al. Hepatocellular carcinoma. Nature Reviews Disease Primers. 2021;7(1):1-28.
17. Balogh J, Victor D, Asham EH, Burroughs SG, Boktour M, Saharia A, et al. Hepatocellular carcinoma: a review. Journal of Hepatocellular Carcinoma. 2016;Volume 3:41-53.



18. Ehrlich A, Duche D, Ouedraogo G, Nahmias Y. Challenges and Opportunities in the Design of Liver-on-Chip Microdevices. *Annual Review of Biomedical Engineering*. 2019;21:219-39.
19. Seo W. Hepatic non-parenchymal cells: Master regulators of alcoholic liver disease? 2016;22(4):1348.
20. Cullen JM, Stalker MJ. Chapter 2 - Liver and Biliary System. Sixth Edition ed: Elsevier Ltd; 2016. p. 258-352.e1.
21. Vainio S, Bykov I, Hermansson M, Jokitalo E, Somerharju P, Ikonen E. Defective insulin receptor activation and altered lipid rafts in Niemann–Pick type C disease hepatocytes. *Biochemical Journal*. 2005;391(3):465-72.
22. Trueba M, Rodriguez P, Vallejo AI, Marino A, Sancho MJ, Macarulla JM. Binding of progesterone to specific sites in isolated hepatic cells and purified plasma membrane fraction. *Exp Clin Endocrinol*. 1990;95(2):169-80.
23. Perez JH, Wight DG, Wyatt JI, Van Schaik M, Mullock BM, Luzio JP. The polymeric immunoglobulin A receptor is present on hepatocytes in human liver. *Immunology*. 1989;68(4):474-8.
24. Wang H, Thorling CA, Liang X, Bridle KR, Grice JE, Zhu Y, et al. Diagnostic imaging and therapeutic application of nanoparticles targeting the liver. *Journal of Materials Chemistry B*. 2015;3(6):939-58.
25. Shah MR, Imran M, Ullah S. Chapter 4 - Ligand-functionalized nanocarrier-based active drugs targeting for liver cancer therapy. In: Shah MR, Imran M, Ullah S, editors. *Nanocarriers for Cancer Diagnosis and Targeted Chemotherapy*: Elsevier; 2019. p. 79-106.
26. Out R, Kruijt JK, Rensen PCN, Hildebrand RB, Vos Pd, Eck MV, et al. Scavenger Receptor BI Plays a Role in Facilitating Chylomicron Metabolism. *Journal of Biological Chemistry*. 2004;18401-6.
27. Devi SS. Structure and Function of Hepatic Parenchymal Cells\*. 2010. p. 11-30.
28. Xu Y, Guo X, Tu L, Zou Q, Li Q, Tang C, et al. Lactoferrin-modified PEGylated liposomes loaded with doxorubicin for targeting delivery to&nbsp;hepatocellular carcinoma. *International Journal of Nanomedicine*. 2015:5123.
29. Twisk J, Gillian-Daniel DL, Tebon A, Wang L, Barrett PHR, Attie AD. The Role of the LDL Receptor in Apolipoprotein B Secretion. *Journal of Clinical Investigation*. 2000.
30. Roth EM, Davidson MH. PCSK9 Inhibitors: Mechanism of Action, Efficacy, and Safety. *Rev Cardiovasc Med*. 2018;19(S1):31-46.
31. Pandey E, Nour AS, Harris EN. Prominent Receptors of Liver Sinusoidal Endothelial Cells in Liver Homeostasis and Disease. *Frontiers in Physiology*. 2020;11.
32. Wisse E, De Zanger RB, Charels K, Van Der Smissen P, McCuskey RS. The liver sieve: considerations concerning the structure and function of endothelial fenestrae, the sinusoidal wall and the space of Disse. *Hepatology*. 1985;5(4):683-92.
33. Zhang Y-N, Poon W, Tavares AJ, McGilvray ID, Chan WCW. Nanoparticle–liver interactions: Cellular uptake and hepatobiliary elimination. *Journal of Controlled Release*. 2016;240:332-48.
34. Øie CI, Appa RS, Hilden I, Petersen HH, Gruhler A, Smedsrød B, et al. Rat liver sinusoidal endothelial cells (LSECs) express functional low density lipoprotein receptor-related protein-1 (LRP-1). *Journal of Hepatology*. 2011;55(6):1346-52.

35. Bouwens L, Bleser P, Vanderkerken K, Geerts B, Wisse E. Liver Cell Heterogeneity: Functions of Non-Parenchymal Cells. *Enzyme*. 1992;46:155-68.
36. Ganesan LP, Kim J, Wu Y, Mohanty S, Phillips GS, Birmingham DJ, et al. FcγRIIb on liver sinusoidal endothelium clears small immune complexes. *J Immunol*. 2012;189(10):4981-8.
37. Bilzer M, Gerbes AL. Kupffer Cells. In: Dufour J-F, Clavien P-A, Trautwein C, Graf R, editors. *Signaling Pathways in Liver Diseases*. Berlin, Heidelberg: Springer Berlin Heidelberg; 2005. p. 45-52.
38. Dixon LJ, Barnes M, Tang H, Pritchard MT, Nagy LE. Kupffer cells in the liver. *Compr Physiol*. 2013;3(2):785-97.
39. Fisher JE, McKenzie TJ, Lillegard JB, Yu Y, Juskewitch JE, Nedredal GI, et al. Role of Kupffer cells and toll-like receptor 4 in acetaminophen-induced acute liver failure. *Journal of Surgical Research*. 2013;180(1):147-55.
40. Colino CI, Lanao JM, Gutierrez-Millan C. Targeting of Hepatic Macrophages by Therapeutic Nanoparticles. *Frontiers in Immunology*. 2020;11.
41. Nakatani K, Kaneda K, Seki S, Nakajima Y. Pit cells as liver-associated natural killer cells: morphology and function: Official Journal of the Clinical Electron Microscopy Society of Japan. *Medical Electron Microscopy*. 2004;37(1):29-36.
42. Luo DZ, Vermijlen D, Ahishali B, Triantis V, Plakoutsi G, Braet F, et al. On the cell biology of pit cells, the liver-specific NK cells. *World J Gastroenterol*. 2000;6(1):1-11.
43. Nakatani K, Kaneda K, Seki S, Nakajima Y. Pit cells as liver-associated natural killer cells: morphology and function. *Medical Electron Microscopy*. 2004;37(1):29-36.
44. Friedman SL. Hepatic stellate cells: protean, multifunctional, and enigmatic cells of the liver. *Physiol Rev*. 2008;88(1):125-72.
45. Qian Y, Han J, Zhou L, Yu Q, Xu J, Jin Z, et al. Inhibition of Epidermal Growth Factor Receptor (EGFR) Reduces Lipopolysaccharide (LPS)-Induced Activation and Inflammatory Cytokines in Hepatic Stellate Cells In Vitro. *Med Sci Monit*. 2018;24:5533-41.
46. Paris JL, Vallet-Regí M. Chapter 1 - Nanostructures for imaging, medical diagnostics and therapy. In: Barhoum A, Hamdy Makhoul AS, editors. *Fundamentals of Nanoparticles*: Elsevier; 2018. p. 1-28.
47. Navya P, Daima HK. Rational engineering of physicochemical properties of nanomaterials for biomedical applications with nanotoxicological perspectives. *Nano Convergence*. 2016;3:1-14.
48. Bilensoy E. Nanopartiküller. A Zırh-Gürsoy içinde, *Nanofarmasötikler ve Uygulamaları*. 2014:23-37.
49. Duan Y, Sun X, Gong T, Wang Q, Zhang Z. Preparation of DHAQ-loaded mPEG-PLGA-mPEG nanoparticles and evaluation of drug release behaviors in vitro/in vivo. *Journal of Materials Science: Materials in Medicine*. 2006;17:509-16.
50. Arnida M, Ray A, Peterson C, Ghandehari H. Geometry and surface characteristics of gold nanoparticles influence their biodistribution and uptake by macrophages. *European Journal of Pharmaceutics and Biopharmaceutics*. 2011;77(3):417-23.
51. Sonavane G, Tomoda K, Makino K. Biodistribution of colloidal gold nanoparticles after intravenous administration: effect of particle size. *Colloids and Surfaces B: Biointerfaces*. 2008;66(2):274-80.

52. De Jong WH, Hagens WI, Krystek P, Burger MC, Sips AJ, Geertsma RE. Particle size-dependent organ distribution of gold nanoparticles after intravenous administration. *Biomaterials*. 2008;29(12):1912-9.
53. Hoshyar N, Gray S, Han H, Bao G. The effect of nanoparticle size on in vivo pharmacokinetics and cellular interaction. *Nanomedicine*. 2016;11(6):673-92.
54. Guterres SS, Alves MP, Pohlmann AR. Polymeric nanoparticles, nanospheres and nanocapsules, for cutaneous applications. *Drug Target Insights*. 2007;2:147-57.
55. Quintanar-Guerrero D, Allémann E, Doelker E, Fessi H. Preparation and characterization of nanocapsules from preformed polymers by a new process based on emulsification-diffusion technique. *Pharm Res*. 1998;15(7):1056-62.
56. Romero G, Moya SE. Chapter 4 - Synthesis of Organic Nanoparticles. In: de la Fuente JM, Grazu V, editors. *Frontiers of Nanoscience*. 4: Elsevier; 2012. p. 115-41.
57. Hong S, Choi DW, Kim HN, Park CG, Lee W, Park HH. Protein-Based Nanoparticles as Drug Delivery Systems. *Pharmaceutics*. 2020;12(7):604.
58. Mittal P, Saharan A, Verma R, Altalbawy FMA, Alfaidi MA, Batiha GE, et al. Dendrimers: A New Race of Pharmaceutical Nanocarriers. *Biomed Res Int*. 2021;2021:8844030.
59. García-Pinel B, Porras-Alcalá C, Ortega-Rodríguez A, Sarabia F, Prados J, Melguizo C, et al. Lipid-Based Nanoparticles: Application and Recent Advances in Cancer Treatment. *Nanomaterials (Basel)*. 2019;9(4):638.
60. Aguilar Z. Types of Nanomaterials and Corresponding Methods of Synthesis. United States: United States: Elsevier; 2012. p. 55-111.
61. Pandey P, Dahiya M. A brief review on inorganic nanoparticles. *J Crit Rev*. 2016;3(3):18-26.
62. Mitragotri S, Stayton P. Organic nanoparticles for drug delivery and imaging. *Mrs Bulletin*. 2014;39(3):219-23.
63. Vinod T, Jelinek R. Inorganic nanoparticles in cosmetics. *Nanocosmetics: from ideas to products*. 2019:29-46.
64. Zhao J, Weng G, Li J, Zhu J, Zhao J. Polyester-based nanoparticles for nucleic acid delivery. *Materials Science and Engineering: C*. 2018;92:983-94.
65. Rao JP, Geckeler KE. Polymer nanoparticles: Preparation techniques and size-control parameters. *Progress in Polymer Science*. 2011;36(7):887-913.
66. Huang RS, Kistner EO, Bleibel WK, Shukla SJ, Dolan ME. Effect of population and gender on chemotherapeutic agent-induced cytotoxicity. *Molecular Cancer Therapeutics*. 2007;6(1):31-6.
67. Niza E, Ocaña A, Castro-Osma JA, Bravo I, Alonso-Moreno C. Polyester Polymeric Nanoparticles as Platforms in the Development of Novel Nanomedicines for Cancer Treatment. *Cancers (Basel)*. 2021;13(14):3387.
68. Allémann E, Gurny R, Doelker E. Drug-loaded nanoparticles : preparation methods and drug targeting issues. *European Journal of Pharmaceutics and Biopharmaceutics*. 1993;39:173-91.
69. Zambaux MF, Bonneaux F, Gref R, Maincent P, Dellacherie E, Alonso MJ, et al. Influence of experimental parameters on the characteristics of poly(lactic acid) nanoparticles prepared by a double emulsion method. *Journal of Controlled Release*. 1998;50(1):31-40.

70. Smruthi MR, Nallamuthu I, Anand T. A comparative study of optimized naringenin nanoformulations using nano-carriers (PLA/PVA and zein/pectin) for improvement of bioavailability. *Food Chemistry*. 2022;369:130950.
71. Kızılbey K. Optimization of Rutin-Loaded PLGA Nanoparticles Synthesized by Single-Emulsion Solvent Evaporation Method. *ACS Omega*. 2019;4(1):555-62.
72. Sakhi M, Khan A, Khan I, Ahmad Khan S, Irum Khan S, Ali Khattak M, et al. Effect of polymeric stabilizers on the size and stability of PLGA paclitaxel nanoparticles. *Saudi Pharmaceutical Journal*. 2023;31(9):101697.
73. Fessi H, Puisieux F, Devissaguet JP, Ammoury N, Benita S. Nanocapsule formation by interfacial polymer deposition following solvent displacement. *International Journal of Pharmaceutics*. 1989;55(1):R1-R4.
74. Astete CE, Sabliov CM. Synthesis and characterization of PLGA nanoparticles. *Journal of Biomaterials Science, Polymer Edition*. 2006;17(3):247-89.
75. Wang Y, Li P, Truong-Dinh Tran T, Zhang J, Kong L. Manufacturing Techniques and Surface Engineering of Polymer Based Nanoparticles for Targeted Drug Delivery to Cancer. *Nanomaterials*. 2016;6(2):26.
76. ÇOMOĞLU T. An overview of polymeric particulate drug delivery system formulations. *Journal of Faculty of Pharmacy of Ankara University*. 2010;39(4):343-68.
77. DERMAN S, KIZILBEY K, AKDESTE ZM. Polymeric nanoparticles. *Sigma Journal of Engineering and Natural Sciences*. 2013;31(1):107-20.
78. Yıldız A, Kara AA, Acartürk F. Peptide-protein based nanofibers in pharmaceutical and biomedical applications. *International Journal of Biological Macromolecules*. 2020;148:1084-97.
79. Rezaei L, Safavi MS, Shojaosadati SA. Protein Nanocarriers for Targeted Drug Delivery. Elsevier; 2019. p. 199-218.
80. Cucinotto I, Fiorillo L, Gualtieri S, Arbitrio M, Ciliberto D, Staropoli N, et al. Nanoparticle Albumin Bound Paclitaxel in the Treatment of Human Cancer: Nanodelivery Reaches Prime-Time? *Journal of Drug Delivery*. 2013;2013:1-10.
81. Desai N. Nanoparticle albumin-bound paclitaxel (Abraxane®). *Albumin in Medicine*: Springer; 2016. p. 101-19.
82. Jain A, Singh SK, Arya SK, Kundu SC, Kapoor S. Protein Nanoparticles: Promising Platforms for Drug Delivery Applications. *ACS Biomaterials Science & Engineering*. 2018;4(12):3939-61.
83. Verma ML, Dhanya BS, Sukriti, Rani V, Thakur M, Jeslin J, et al. Carbohydrate and protein based biopolymeric nanoparticles: Current status and biotechnological applications. *International Journal of Biological Macromolecules*. 2020;154:390-412.
84. Wu P, Liu Q, Wang Q, Qian H, Yu L, Liu B, et al. Novel silk fibroin nanoparticles incorporated silk fibroin hydrogel for inhibition of cancer stem cells and tumor growth. *International Journal of Nanomedicine*. 2018;Volume 13:5405-18.
85. Zhang Y-Q, Shen W-D, Xiang R-L, Zhuge L-J, Gao W-J, Wang W-B. Formation of silk fibroin nanoparticles in water-miscible organic solvent and their characterization. *Journal of Nanoparticle Research*. 2007;9(5):885-900.
86. Gilissen LJ, van der Meer IM, Smulders MJ. Reducing the incidence of allergy and intolerance to cereals. *Journal of Cereal Science*. 2014;59(3):337-53.
87. Reddy N, Yang Y. Potential of plant proteins for medical applications. *Trends in Biotechnology*. 2011;29(10):490-8.

88. Peng YY, Glattauer V, Ramshaw JA, Werkmeister JA. Evaluation of the immunogenicity and cell compatibility of avian collagen for biomedical applications. *J Biomed Mater Res A*. 2010;93(4):1235-44.
89. Luo X, Al-Antaki AHM, Harvey DP, Ruan Y, He S, Zhang W, et al. Vortex Fluidic Mediated Synthesis of Macroporous Bovine Serum Albumin-Based Microspheres. *Acs Applied Materials & Interfaces*. 2018;10(32):27224-32.
90. Khramtsov P, Калашникова ТА, Бочкова МС, Кропанева М, Тимганова ВП, Zamorina SA, et al. Measuring the Concentration of Protein Nanoparticles Synthesized by Desolvation Method: Comparison of Bradford Assay, BCA Assay, Hydrolysis/Uv Spectroscopy and Gravimetric Analysis. 2020.
91. Maghsoudi A, Shojaosadati SA, Vasheghani-Farahani E. 5-Fluorouracil-Loaded BSA Nanoparticles: Formulation Optimization and in Vitro Release Study. *Aaps Pharmscitech*. 2008;9(4):1092-6.
92. Su C, Ji Y, Liu S, Gao S, Cao S, Xu X, et al. Fluorescence-Labeled Abamectin Nanopesticide for Comprehensive Control of Pinewood Nematode and *Monochamus Alternatus* Hope. *Acs Sustainable Chemistry & Engineering*. 2020;8(44):16555-64.
93. Huang Y, Hu L, Huang S, Xu W, Wan J, Wang D, et al. Curcumin-Loaded Galactosylated BSA Nanoparticles as Targeted Drug Delivery Carriers Inhibit Hepatocellular Carcinoma Cell Proliferation and Migration. *International Journal of Nanomedicine*. 2018;Volume 13:8309-23.
94. Bin C, Wu C, Zhuo RX, Cheng SX. A Self-Assembled Albumin Based Multiple Drug Delivery Nanosystem to Overcome Multidrug Resistance. *RSC Advances*. 2015;5(9):6807-14.
95. Lohcharoenkal W, Wang L, Chen YC, Rojanasakul Y. Protein Nanoparticles as Drug Delivery Carriers for Cancer Therapy. *BioMed Res Int*. 2014;2014:180549.
96. Tarhini M, Benlyamani I, Hamdani S, Agusti G, Fessi H, Greige-Gerges H, et al. Protein-Based Nanoparticle Preparation via Nanoprecipitation Method. *Materials*. 2018;11(3):394.
97. Meng R, Zhu H, Wang Z, Hao S, Wang B. Preparation of Drug-Loaded Albumin Nanoparticles and Its Application in Cancer Therapy. *Journal of Nanomaterials*. 2022;2022:1-12.
98. Lu Y-L, Ma Y-B, Feng C, Zhu D-L, Liu J, Chen L, et al. Co-delivery of Cyclophamide and Doxorubicin Mediated by Bovine Serum Albumin Nanoparticles Reverses Doxorubicin Resistance in Breast Cancer by Down-regulating P-glycoprotein Expression. *Journal of Cancer*. 2019;10(10):2357-68.
99. Fang J, Nakamura H, Maeda H. The EPR effect: Unique features of tumor blood vessels for drug delivery, factors involved, and limitations and augmentation of the effect. *Advanced Drug Delivery Reviews*. 2011;63(3):136-51.
100. Kang H, Rho S, Stiles WR, Hu S, Baek Y, Hwang DW, et al. Size-Dependent EPR Effect of Polymeric Nanoparticles on Tumor Targeting. *Advanced Healthcare Materials*. 2020;9(1):1901223.
101. Almazroo OA, Miah MK, Venkataramanan R. Drug Metabolism in the Liver. *Clinics in Liver Disease*. 2017;21(1):1-20.
102. Longmire M, Choyke PL, Kobayashi H. Clearance properties of nano-sized particles and molecules as imaging agents: considerations and caveats. *Nanomedicine*. 2008;3(5):703-17.

103. Yuan D, He H, Wu Y, Fan J, Cao Y. Physiologically Based Pharmacokinetic Modeling of Nanoparticles. *Journal of Pharmaceutical Sciences*. 2019;108(1):58-72.
104. Zhao Y, Wang Y, Ran F, Cui Y, Liu C, Zhao Q, et al. A comparison between sphere and rod nanoparticles regarding their in vivo biological behavior and pharmacokinetics. *Scientific Reports*. 2017;7(1).
105. Arami H, Khandhar A, Liggitt D, Krishnan KM. In vivo delivery, pharmacokinetics, biodistribution and toxicity of iron oxide nanoparticles. *Chemical Society Reviews*. 2015;44(23):8576-607.
106. Pozzi D, Colapicchioni V, Caracciolo G, Piovesana S, Capriotti AL, Palchetti S, et al. Effect of polyethyleneglycol (PEG) chain length on the bio-nano-interactions between PEGylated lipid nanoparticles and biological fluids: from nanostructure to uptake in cancer cells. *Nanoscale*. 2014;6(5):2782.
107. Fujiura K, Naito M, Tanaka Y, Tanaka M, Nakanishi Y, Ejima H, et al. Development of Stealth Nanoparticles Coated With Poly(2-methoxyethyl Vinyl Ether) as an Alternative to Poly(ethylene Glycol). *Journal of Applied Polymer Science*. 2023;141(11).
108. Perry JL, Reuter K, Kai MP, Herlihy KP, Jones S, Luft JC, et al. PEGylated PRINT Nanoparticles: The Impact of PEG Density on Protein Binding, Macrophage Association, Biodistribution, and Pharmacokinetics. *Nano Letters*. 2012;12(10):5304-10.
109. Cho K, Wang X, Nie S, Chen ZG, Shin DM. Therapeutic Nanoparticles for Drug Delivery in Cancer. *Clinical Cancer Research*. 2008;1310-6.
110. Yoon M-S. Nanotechnology-Based Targeting of mTOR Signaling in Cancer. *International Journal of Nanomedicine*. 2020:5767–81.
111. Steichen SD, Caldorera-Moore M, Peppas NA. A Review of Current Nanoparticle and Targeting Moieties for the Delivery of Cancer Therapeutics. *European Journal of Pharmaceutical Sciences*. 2013(48(3)):416-27.
112. Rasal A, Reddy ND. Chapter 14 - Nano-pharmacokinetics preclinical to clinical translation. In: Thorat ND, Kumar N, editors. *Nano-Pharmacokinetics and Theranostics*: Academic Press; 2021. p. 273-88.
113. Rotem R, Prosperi D, Colombo M. Chapter 10 - Targeted delivery of nanoparticles. In: Parak WJ, Feliu N, editors. *Frontiers of Nanoscience*. 16: Elsevier; 2020. p. 253-64.
114. Bilzer M, Roggel F, Gerbes AL. Role of Kupffer cells in host defense and liver disease. *Liver International*. 2006;26(10):1175-86.
115. Xiao K, Li Y, Luo J, Lee JS, Xiao W, Gonik AM, et al. The effect of surface charge on in vivo biodistribution of PEG-oligocholeic acid based micellar nanoparticles. *Biomaterials*. 2011;32(13):3435-46.
116. Poisson J, Lemoine S, Boulanger C, Durand F, Moreau R, Valla D, et al. Liver sinusoidal endothelial cells: Physiology and role in liver diseases. *Journal of Hepatology*. 2017;66(1):212-27.
117. Bartneck M, Warzecha KT, Tacke F. Therapeutic targeting of liver inflammation and fibrosis by nanomedicine. *Hepatobiliary Surg Nutr*. 2014;3(6):364-76.
118. Ishibashi H, Nakamura M, Komori A, Migita K, Shimoda S. Liver architecture, cell function, and disease. *Seminars in Immunopathology*. 2009;31(3):399-409.

119. Beljaars L, Olinga P, Molema G, De Bleser P, Geerts A, Groothuis GMM, et al. Characteristics of the hepatic stellate cell-selective carrier mannose 6-phosphate modified albumin (M6P28-HSA). *Liver International*. 2001;21(5):320-8.
120. Beljaars L, Molema G, Weert B, Bonnema H, Olinga P, Groothuis GM, et al. Albumin modified with mannose 6-phosphate: A potential carrier for selective delivery of antifibrotic drugs to rat and human hepatic stellate cells. *Hepatology*. 1999;29(5):1486-93.
121. Li Y, Pu S, Liu Q, Li R, Zhang J, Wu T, et al. An integrin-based nanoparticle that targets activated hepatic stellate cells and alleviates liver fibrosis. *Journal of Controlled Release*. 2019;303:77-90.
122. El-Nabarawi MA, Nafady MM, El-Menshawe SF, Elkarmalawy MH, Teaima MH. Liver Targeting of Daclatasvir via Tailoring Sterically Stabilized Bilosomes: Fabrication, Comparative in Vitro/in Vivo Appraisal and Biodistribution Studies. *International Journal of Nanomedicine*. 2021;Volume 16:6413-26.
123. Biessen EAL, Beuting DM, Vietsch H, Bijsterbosch MK, Van Berkel TJC. Specific targeting of the antiviral drug 5-Iodo 2'-deoxyuridine to the parenchymal liver cell using lactosylated poly-L-lysine. *Journal of Hepatology*. 1994;21(5):806-15.
124. Guan X, Gao M, Xu H, Zhang C, Liu H, Lv L, et al. Quercetin-loaded poly (lactic-co-glycolic acid)-d- $\alpha$ -tocopheryl polyethylene glycol 1000 succinate nanoparticles for the targeted treatment of liver cancer. 2016:1-12.
125. El-Naggar ME, Al-Joufi F, Anwar M, Attia MF, El-Bana MA. Curcumin-loaded PLA-PEG copolymer nanoparticles for treatment of liver inflammation in streptozotocin-induced diabetic rats. *Colloids and Surfaces B: Biointerfaces*. 2019;177:389-98.
126. Mao Y, Thompson MJ, Wang Q, Tsai EW. Quantitation of poloxamers in pharmaceutical formulations using size exclusion chromatography and colorimetric methods. *Journal of Pharmaceutical and Biomedical Analysis*. 2004;35(5):1127-42.
127. Harshe SN, Mandloi VS, Sharma GK. Colorimetric Method of Estimation of Polyvinyl Alcohol in Mixtures with Starch, Dextrin, Carboxy Methyl Cellulose and Gum. *Starch - Stärke*. 1983;35(1):18-22.
128. Schindelin J, Arganda-Carreras I, Frise E, Kaynig V, Longair M, Pietzsch T, et al. Fiji: an open-source platform for biological-image analysis. *Nature Methods*. 2012;9(7):676-82.
129. Crandon LE, Boenisch KM, Harper BJ, Harper SL. Adaptive methodology to determine hydrophobicity of nanomaterials in situ. *PLOS ONE*. 2020;15(6):e0233844.
130. Jones MC, Jones SA, Riffo-Vasquez Y, Spina D, Hoffman E, Morgan A, et al. Quantitative assessment of nanoparticle surface hydrophobicity and its influence on pulmonary biocompatibility. *J Control Release*. 2014;183:94-104.
131. Dailey LA, Hernández-Prieto R, Casas-Ferreira AM, Jones M-C, Riffo-Vasquez Y, Rodríguez-Gonzalo E, et al. Adenosine monophosphate is elevated in the bronchoalveolar lavage fluid of mice with acute respiratory toxicity induced by nanoparticles with high surface hydrophobicity. *Nanotoxicology*. 2015;9(1):106-15.
132. Tobío M, Gref R, Sánchez A, Langer R, Alonso MJ. Stealth PLA-PEG Nanoparticles as Protein Carriers for Nasal Administration. *Pharmaceutical Research*. 1998;15(2):270-5.

133. Rozgonyi F, Szitha KR, Ljungh Å, Baloda SB, Hjertén S, Wadström T. Improvement of the Salt Aggregation Test to Study Bacterial Cell-Surface Hydrophobicity. *Fems Microbiology Letters*. 1985;30(1-2):131–8.
134. Smith PK, Krohn RI, Hermanson GT, Mallia AK, Gartner FH, Provenzano MD, et al. Measurement of protein using bicinchoninic acid. *Anal Biochem*. 1985;150(1):76-85.
135. Alfonsi K, Colberg J, Dunn PJ, Fevig T, Jennings S, Johnson TA, et al. Green chemistry tools to influence a medicinal chemistry and research chemistry based organisation. *Green Chem*. 2008;10(1):31-6.
136. EngineeringToolBox. Vapor Pressure common Liquids 2006 [Available from: [https://www.engineeringtoolbox.com/vapor-pressure-d\\_312.html](https://www.engineeringtoolbox.com/vapor-pressure-d_312.html)].
137. Database I. Impurities guideline for residual solvents Q3C(R6) 2016 [updated 20.10.2016. Available from: [https://database.ich.org/sites/default/files/Q3C-R6\\_Guideline\\_ErrorCorrection\\_2019\\_0410\\_0.pdf](https://database.ich.org/sites/default/files/Q3C-R6_Guideline_ErrorCorrection_2019_0410_0.pdf)]
138. García Ibarra V, Sendón R, Rodríguez-Bernaldo de Quirós A. Chapter 29 - Antimicrobial Food Packaging Based on Biodegradable Materials. In: Barros-Velázquez J, editor. *Antimicrobial Food Packaging*. San Diego: Academic Press; 2016. p. 363-84.
139. Arakawa CK, DeForest CA. Chapter 19 - Polymer Design and Development. In: Vishwakarma A, Karp JM, editors. *Biology and Engineering of Stem Cell Niches*. Boston: Academic Press; 2017. p. 295-314.
140. Casalini T, Rossi F, Castrovinci A, Perale G. A Perspective on Polylactic Acid-Based Polymers Use for Nanoparticles Synthesis and Applications. *Frontiers in Bioengineering and Biotechnology*. 2019;7:259.
141. Makadia HK, Siegel SJ. Poly Lactic-co-Glycolic Acid (PLGA) as Biodegradable Controlled Drug Delivery Carrier. *Polymers (Basel)*. 2011;3(3):1377-97.
142. Singh R, kumar N, Mehrotra T, Bisaria K, Sinha S. Chapter 9 - Environmental hazards and biodegradation of plastic waste: challenges and future prospects. In: Saxena G, Kumar V, Shah MP, editors. *Bioremediation for Environmental Sustainability*: Elsevier; 2021. p. 193-214.
143. Thomas D, Zhuravlev E, Wurm A, Schick C, Cebe P. Fundamental thermal properties of polyvinyl alcohol by fast scanning calorimetry. *Polymer*. 2018;137:145-55.
144. Zhang H, Wang Z, Liu O. Simultaneous determination of kolliphor HS15 and miglyol 812 in microemulsion formulation by ultra-high performance liquid chromatography coupled with nano quantity analyte detector. *Journal of Pharmaceutical Analysis*. 2016;6(1):11-7.
145. Shirwaiker RA, Purser MF, Wusk RA. 6 - Scaffolding hydrogels for rapid prototyping based tissue engineering. In: Narayan R, editor. *Rapid Prototyping of Biomaterials*: Woodhead Publishing; 2014. p. 176-200.
146. Awasthi R, Manchanda S, Das P, Velu V, Malipeddi H, Pabreja K, et al. 9 - Poly(vinylpyrrolidone). In: Parambath A, editor. *Engineering of Biomaterials for Drug Delivery Systems*: Woodhead Publishing; 2018. p. 255-72.
147. Gatica N, Soto L, Moraga C, Vergara L. BLENDS OF POLY(N-VINYL-2-PYRROLIDONE) AND DIHYDRIC PHENOLS: THERMAL AND INFRARED SPECTROSCOPIC STUDIES. PART IV. *Journal of the Chilean Chemical Society*. 2013;58(4):2048-52.



148. McKean L. Chapter11 - The effect of heat aging on the properties of sustainable polymers. In: McKean L, editor. *The Effect of Long Term Thermal Exposure on Plastics and Elastomers (Second Edition)*: William Andrew Publishing; 2021. p. 313-32.
149. Zhang Z, Wang X, Zhu R, Wang Y, Li B, Ma Y, et al. Synthesis and characterization of serial random and block-copolymers based on lactide and glycolide. *Polymer Science Series B*. 2016;58(6):720-9.
150. Fakhari A, Corcoran ML, Schwarz A. Thermogelling Properties of Purified Poloxamer 407. *Heliyon*. 2017;3(8):e00390.
151. Iqbal M, Valour J-P, Fessi H, Elaissari A. Preparation of biodegradable PCL particles via double emulsion evaporation method using ultrasound technique. *Colloid and Polymer Science*. 2015;293(3):861-73.
152. Barba AA, Dalmoro A, D'Amore M, Vascello C, Lamberti G. Biocompatible nano-micro-particles by solvent evaporation from multiple emulsions technique. *Journal of Materials Science*. 2014;49(14):5160-70.
153. Das PP, Huda MK, Saikia PJ, Baruah SD. Study of the formation of biodegradable polycaprolactone particles using solvent evaporation method. *Journal of Macromolecular Science, Part A*. 2019;56(1):69-75.
154. Abamor ES, Tosyali OA, Bagirova M, Allahverdiyev A. Nigella sativa oil entrapped polycaprolactone nanoparticles for leishmaniasis treatment. *IET Nanobiotechnology*. 2018;12(8):1018-26.
155. Sathyamoorthy N, Magharla D, Chintamaneni P, Vankayalu S. Optimization of paclitaxel loaded poly ( $\epsilon$ -caprolactone) nanoparticles using Box Behnken design. *Beni-Suef University Journal of Basic and Applied Sciences*. 2017;6(4):362-73.
156. Ueda M, Kreuter J. Optimization of the preparation of loperamide-loaded poly (L-lactide) nanoparticles by high pressure emulsification-solvent evaporation. *Journal of Microencapsulation*. 1997;14(5):593-605.
157. Wei Y, Wang Y, Wang L, Hao D, Ma G. Fabrication strategy for amphiphilic microcapsules with narrow size distribution by premix membrane emulsification. *Colloids and Surfaces B: Biointerfaces*. 2011;87(2):399-408.
158. Wei Y, Wang Y, Zhang H, Zhou W, Ma G. A novel strategy for the preparation of porous microspheres and its application in peptide drug loading. *Journal of Colloid and Interface Science*. 2016;478:46-53.
159. Sonia TA, Sharma CP. 6 - Polymers in oral insulin delivery. In: Sonia TA, Sharma CP, editors. *Oral Delivery of Insulin*: Woodhead Publishing; 2014. p. 257-310.
160. Lemoine D, Francois C, Kedzierewicz F, Preat V, Hoffman M, Maincent P. Stability study of nanoparticles of poly( $\epsilon$ -caprolactone), poly(d,l-lactide) and poly(d,l-lactide-co-glycolide). *Biomaterials*. 1996;17(22):2191-7.
161. Ding AG, Schwendeman SP. Acidic microclimate pH distribution in PLGA microspheres monitored by confocal laser scanning microscopy. *Pharm Res*. 2008;25(9):2041-52.
162. Ekinci M, Yeğen G, Aksu B, İlem-Özdemir D. Preparation and Evaluation of Poly(lactic acid)/Poly(vinyl alcohol) Nanoparticles Using the Quality by Design Approach. *ACS Omega*. 2022;7(38):33793-807.
163. Desgouilles S, Vauthier C, Bazile D, Vacus J, Grossiord JL, Veillard, et al. The Design of Nanoparticles Obtained by Solvent Evaporation: a Comprehensive Study. *Langmuir*. 2003;19(22):9504-10.

164. Isojima T, Suh SK, Sande JBV, Hatton TA. Controlled Assembly of Nanoparticle Structures: Spherical and Toroidal Superlattices and Nanoparticle-Coated Polymeric Beads. *Langmuir*. 2009;25(14):8292-8.
165. Leroy P, Tournassat C, Bizi M. Influence of Surface Conductivity on the Apparent Zeta Potential of TiO<sub>2</sub> Nanoparticles. *Journal of Colloid and Interface Science*. 2011;356(2):442-53.
166. Aminu N, Audu MM. Chapter 3 - Polycaprolactone-based nanoparticles for advanced therapeutic applications. In: Hasnain MS, Nayak AK, Aminabhavi TM, editors. *Polymeric Nanosystems*: Academic Press; 2023. p. 37-84.
167. Jain RA. The manufacturing techniques of various drug loaded biodegradable poly(lactide-co-glycolide) (PLGA) devices. *Biomaterials*. 2000;21(23):2475-90.
168. Nawaz T, Iqbal M, Khan BA, Nawaz A, Hussain T, Hosny KM, et al. Development and Optimization of Acriflavine-Loaded Polycaprolactone Nanoparticles Using Box–Behnken Design for Burn Wound Healing Applications. *Polymers*. 2021;14(1):101.
169. Jeong Y-I, Kim D-G, Jang M-K, Nah J-W, Kim Y-B. All-trans retinoic acid release from surfactant-free nanoparticles of poly(DL-lactide-co-glycolide). *Macromolecular Research*. 2008;16(8):717-24.
170. Sah E, Sah H. Recent Trends in Preparation of Poly(lactide-co-glycolide) Nanoparticles by Mixing Polymeric Organic Solution with Antisolvent. *Journal of Nanomaterials*. 2015;2015:1-22.
171. Hariharan S, Bhardwaj V, Bala I, Sitterberg J, Bakowsky U, Kumar MNVR. Design of Estradiol Loaded PLGA Nanoparticulate Formulations: A Potential Oral Delivery System for Hormone Therapy. *Pharmaceutical Research*. 2006;23(1):184-95.
172. Khemani M, Sharon M, Sharon M. Encapsulation of Berberine in Nano-Sized PLGA Synthesized by Emulsification Method. *ISRN Nanotechnology*. 2012;2012:187354.
173. Panda BP, Krishnamoorthy R, Shivashekaregowda NKH, Patnaik S. Influence of Poloxamer 188 on Design and Development of Second Generation PLGA Nanocrystals of Metformin Hydrochloride. *Nano Biomedicine and Engineering*. 2018;10(4):334-43.
174. Chen G, Wen J. Poly(lactic-co-glycolic acid) based double emulsion nanoparticle as a carrier system to deliver glutathione sublingually. *Journal of Biomedicine*. 2018;3:50-9.
175. Tefas LR, Tomuță I, Achim M, Vlase L. Development and optimization of quercetin-loaded PLGA nanoparticles by experimental design. *Clujul Med*. 2015;88(2):214-23.
176. Lalani J, Rath M, Lalan M, Misra A. Protein functionalized tramadol-loaded PLGA nanoparticles: preparation, optimization, stability and pharmacodynamic studies. *Drug Development and Industrial Pharmacy*. 2013;39(6):854-64.
177. Maaz A, Abdelwahed W, Tekko I, Trefi S. Influence of nanoprecipitation method parameters on nanoparticles loaded with gatifloxacin for ocular drug delivery. *Int J Acad Sci Res*. 2015;3(1):1-12.
178. Sharma D, Maheshwari D, Philip G, Rana R, Bhatia S, Singh M, et al. Formulation and Optimization of Polymeric Nanoparticles for Intranasal Delivery of Lorazepam Using Box-Behnken Design: in vitro and in vivo evaluation. *BioMed Res Int*. 2014;2014:1-14.

179. Draheim C, De Crécy F, Hansen S, Collnot E-M, Lehr C-M. A Design of Experiment Study of Nanoprecipitation and Nano Spray Drying as Processes to Prepare PLGA Nano- and Microparticles with Defined Sizes and Size Distributions. *Pharmaceutical Research*. 2015;32(8):2609-24.
180. Suksiriworapong J, Rungvimolsin T, A Ag, Junyaprasert VB, Chantasart D. Development and characterization of lyophilized diazepam-loaded polymeric micelles. *AAPS PharmSciTech*. 2014;15(1):52-64.
181. Cheng C-Y, Wang J-Y, Kausik R, Lee KYC, Han S. Nature of Interactions between PEO-PPO-PEO Triblock Copolymers and Lipid Membranes: (II) Role of Hydration Dynamics Revealed by Dynamic Nuclear Polarization. *Biomacromolecules*. 2012;13(9):2624-33.
182. El Sayeh F, Abou El Ela A, Abbas Ibrahim M, Alqahtani Y, Almomen A, Sfouq Aleanizy F. Fluconazole nanoparticles prepared by antisolvent precipitation technique: Physicochemical, in vitro, ex vivo and in vivo ocular evaluation. *Saudi Pharmaceutical Journal*. 2021;29(6):576-85.
183. Tefas LR, Tomuță I, Achim M, Vlase L. Development and optimization of quercetin-loaded PLGA nanoparticles by experimental design. *Medicine and Pharmacy Reports*. 2015;88(2):214-23.
184. Mehrotra A, P JK. Preparation and Characterization and Biodistribution Studies of Lomustine Loaded PLGA Nanoparticles by Interfacial Deposition Method. *Journal of Nanomedicine & Nanotechnology*. 2015;6(6):1.
185. Nirachonkul W, Ogonoki S, Thumvijit T, Chiampanichayakul S, Panyajai P, Anuchapreeda S, et al. CD123-Targeted Nano-Curcumin Molecule Enhances Cytotoxic Efficacy in Leukemic Stem Cells. *Nanomaterials*. 2021;11(11):2974.
186. De Menezes TI, De Oliveira Costa R, Sanches RNF, De Oliveira Silva D, Santos RLSR. Preparation and characterization of dithiocarbazate Schiff base-loaded poly(lactic acid) nanoparticles and analytical validation for drug quantification. *Colloid and Polymer Science*. 2019;297(11-12):1465-75.
187. Liu W-Y, Lin C-C, Hsieh Y-S, Wu Y-T. Nanoformulation Development to Improve the Biopharmaceutical Properties of Fisetin Using Design of Experiment Approach. *Molecules*. 2021;26(10):3031.
188. Sahoo SK, Panyam J, Prabha S, Labhasetwar V. Residual polyvinyl alcohol associated with poly (d,l-lactide-co-glycolide) nanoparticles affects their physical properties and cellular uptake. *Journal of Controlled Release*. 2002;82(1):105-14.
189. Wilson BK, Prud'homme RK. Nanoparticle size distribution quantification from transmission electron microscopy (TEM) of ruthenium tetroxide stained polymeric nanoparticles. *Journal of Colloid and Interface Science*. 2021;604:208-20.
190. Swider E, Maharjan S, Houkes K, van Riessen NK, Figdor C, Srinivas M, et al. Förster Resonance Energy Transfer-Based Stability Assessment of PLGA Nanoparticles in Vitro and in Vivo. *ACS Applied Bio Materials*. 2019;2(3):1131-40.
191. Oliveira CL, Veiga F, Varela C, Roleira F, Tavares E, Silveira I, et al. Characterization of polymeric nanoparticles for intravenous delivery: Focus on stability. *Colloids and Surfaces B: Biointerfaces*. 2017;150:326-33.
192. Papagiannopoulos A, Vlassi E, Pispas S, Houston JE. Association and Internal Morphology of Self-Assembled HPPhOx/BSA Hybrid Nanoparticles in Aqueous Solutions. *The Journal of Physical Chemistry B*. 2018;122(29):7426-35.

193. Drasler B, Sayre P, Steinhäuser KG, Petri-Fink A, Rothen-Rutishauser B. In vitro approaches to assess the hazard of nanomaterials. *NanoImpact*. 2017;8:99-116.
194. Park MVDZ. The status of in vitro toxicity studies in the risk assessment of nanomaterials. *Nanomedicine*. 2009;4(6):669-85.
195. Owens DE, Peppas NA. Opsonization, biodistribution, and pharmacokinetics of polymeric nanoparticles. *International Journal of Pharmaceutics*. 2006;307(1):93-102.
196. Li S-D, Huang L. Pharmacokinetics and Biodistribution of Nanoparticles. *Molecular Pharmaceutics*. 2008;5(4):496-504.
197. Vranic S, Boggetto N, Contremoulins V, Mornet S, Reinhardt N, Marano F, et al. Deciphering the mechanisms of cellular uptake of engineered nanoparticles by accurate evaluation of internalization using imaging flow cytometry. *Particle and Fibre Toxicology*. 2013;10(1):2.
198. Kakinoki A, Kaneo Y, Ikeda Y, Tanaka T, Fujita K. Synthesis of Poly(vinyl alcohol)-Doxorubicin Conjugates Containing cis-Aconityl Acid-Cleavable Bond and Its Isomer Dependent Doxorubicin Release. *Biological and Pharmaceutical Bulletin*. 2008;31(1):103-10.
199. Dumortier G, Grossiord JL, Agnely F, Chaumeil JC. A Review of Poloxamer 407 Pharmaceutical and Pharmacological Characteristics. *Pharmaceutical Research*. 2006;23(12):2709-28.
200. Bodratti AM, Alexandridis P. Amphiphilic block copolymers in drug delivery: advances in formulation structure and performance. *Expert Opinion on Drug Delivery*. 2018;15(11):1085-104.
201. Viegas TX, Henry RL. Osmotic behavior of poloxamer 407 and other non-ionic surfactants in aqueous solutions. *International Journal of Pharmaceutics*. 1998;160(2):157-62.
202. Information NCfB. Poloxamer 407  
<https://pubchem.ncbi.nlm.nih.gov/substance/347911166>: DrugBank; 2023 [cited 2023 06.12.2023]. Available from: <https://pubchem.ncbi.nlm.nih.gov/substance/347911166>.
203. Grabowski N, Hillaireau H, Vergnaud J, Tsapis N, Pallardy M, Kerdine-Römer S, et al. Surface coating mediates the toxicity of polymeric nanoparticles towards human-like macrophages. *International Journal of Pharmaceutics*. 2015;482(1):75-83.
204. G. Moloughney J, Weisleder N. Poloxamer 188 (P188) as a Membrane Resealing Reagent in Biomedical Applications. *Recent Patents on Biotechnology*. 2012;6(3):200-11.
205. Olbrich C, Schöler N, Tabatt K, Kayser O, Müller RH. Cytotoxicity studies of Dynasan 114 solid lipid nanoparticles (SLN) on RAW 264.7 macrophages—impact of phagocytosis on viability and cytokine production. *Journal of Pharmacy and Pharmacology*. 2010;56(7):883-91.
206. Chamchoy K, Pakotiprapha D, Pumirat P, Leartsakulpanich U, Boonyuen U. Application of WST-8 based colorimetric NAD(P)H detection for quantitative dehydrogenase assays. *BMC Biochemistry*. 2019;20(1).
207. Alkholief M, Kalam MA, Anwer MK, Alshamsan A. Effect of Solvents, Stabilizers and the Concentration of Stabilizers on the Physical Properties of Poly(D,L-lactide-

- co-glycolide) Nanoparticles: Encapsulation, In Vitro Release of Indomethacin and Cytotoxicity against HepG2-Cell. *Pharmaceutics* [Internet]. 2022; 14(4):[870 p.].
208. Frasco MF, Almeida GM, Santos-Silva F, Pereira MDC, Coelho MAN. Transferrin surface-modified PLGA nanoparticles-mediated delivery of a proteasome inhibitor to human pancreatic cancer cells. *Journal of Biomedical Materials Research Part A*. 2015;103(4):1476-84.
  209. Joseph A, Simo GM, Gao T, Alhindi N, Xu N, Graham DJ, et al. Surfactants influence polymer nanoparticle fate within the brain. *Biomaterials*. 2021;277:121086.
  210. Tiwari S, Gupta P, Anees M, Kaur H, Kharbanda S, Singh H. Pluronic modified PLA based hybrid block copolymeric nanoformulation enhanced anti-cancer therapeutic efficacy of Epirubicin. *European Polymer Journal*. 2023;193:112084.
  211. Raudszus B, Mulac D, Langer K. A new preparation strategy for surface modified PLA nanoparticles to enhance uptake by endothelial cells. *International Journal of Pharmaceutics*. 2018;536(1):211-21.
  212. Mr S, Nallamuthu I, Singait D, Anand T. Toxicological evaluation of PLA/PVA-naringenin nanoparticles: In vitro and in vivo studies. *OpenNano*. 2022;7:100061.
  213. Bernard M, Jubeli E, Pungente MD, Yagoubi N. Biocompatibility of polymer-based biomaterials and medical devices – regulations, in vitro screening and risk-management. *Biomaterials Science*. 2018;6(8):2025-53.
  214. Zhang JM, An J. Cytokines, inflammation, and pain. *Int Anesthesiol Clin*. 2007;45(2):27-37.
  215. Ilić K, Kalčec N, Krce L, Aviani I, Turčić P, Pavičić I, et al. Toxicity of nanomixtures to human macrophages: Joint action of silver and polystyrene nanoparticles. *Chemico-Biological Interactions*. 2022;368:110225.
  216. Cicchese JM, Evans S, Hult C, Joslyn LR, Wessler T, Millar JA, et al. Dynamic balance of pro- and anti-inflammatory signals controls disease and limits pathology. *Immunol Rev*. 2018;285(1):147-67.
  217. JOHN M, LIM S, SEYBOLD J, JOSE P, ROBICHAUD A, O'CONNOR B, et al. Inhaled Corticosteroids Increase Interleukin-10 but Reduce Macrophage Inflammatory Protein-1  $\alpha$ , Granulocyte-Macrophage Colony-stimulating Factor, and Interferon-  $\gamma$  Release from Alveolar Macrophages in Asthma. *American Journal of Respiratory and Critical Care Medicine*. 1998;157(1):256-62.
  218. Giambartolomei GH, Dennis VA, Lasater BL, Murthy PK, Philipp MT. Autocrine and Exocrine Regulation of Interleukin-10 Production in THP-1 Cells Stimulated with *Borrelia burgdorferi* Lipoproteins. *Infection and Immunity*. 2002;70(4):1881-8.
  219. Truong N, Cottingham AL, Dharmaraj S, Shaw JR, Lasola JJM, Goodis CC, et al. Multimodal nanoparticle-containing modified suberoylanilide hydroxamic acid polymer conjugates to mitigate immune dysfunction in severe inflammation. *Bioengineering & Translational Medicine*. 2024;9(1):1-17.
  220. Meena J, Kumar R, Singh M, Ahmed A, Panda AK. Modulation of immune response and enhanced clearance of *Salmonella typhi* by delivery of Vi polysaccharide conjugate using PLA nanoparticles. *European Journal of Pharmaceutics and Biopharmaceutics*. 2020;152:270-81.
  221. Zucker RM, Ortenzio JN, Boyes WK. Characterization, detection, and counting of metal nanoparticles using flow cytometry. *Cytometry Part A*. 2016;89(2):169-83.

222. Duong HTT, Marquis CP, Whittaker M, Davis TP, Boyer C. Acid Degradable and Biocompatible Polymeric Nanoparticles for the Potential Codelivery of Therapeutic Agents. *Macromolecules*. 2011;44(20):8008-19.
223. Samadi Moghaddam M, Heiny M, Shastri VP. Enhanced cellular uptake of nanoparticles by increasing the hydrophobicity of poly(lactic acid) through copolymerization with cell-membrane-lipid components. *Chem Commun (Camb)*. 2015;51(78):14605-8.
224. Zahr AS, Davis CA, Pishko MV. Macrophage Uptake of Core-Shell Nanoparticles Surface Modified with Poly(ethylene glycol). *Langmuir*. 2006;22(19):8178-85.
225. Kannan S, Kolhe P, Raykova V, Glibatec M, Kannan RM, Lieh-Lai M, et al. Dynamics of cellular entry and drug delivery by dendritic polymers into human lung epithelial carcinoma cells. *J Biomater Sci Polym Ed*. 2004;15(3):311-30.
226. Juneja R, Roy I. Surface modified PMMA nanoparticles with tunable drug release and cellular uptake. *RSC Adv*. 2014;4(84):44472-9.
227. Lobatto ME, Binderup T, Robson PM, Giesen L, Calcagno C, Witjes JJ, et al. Multimodal Positron Emission Tomography Imaging to Quantify Uptake of <sup>89</sup>Zr-Labeled Liposomes in the Atherosclerotic Vessel Wall. *Bioconjugate Chemistry*. 2019;31(2):360-8.
228. Hou S, Sikora KN, Tang R, Liu Y, Lee Y-W, Kim ST, et al. Quantitative Differentiation of Cell Surface-Bound and Internalized Cationic Gold Nanoparticles Using Mass Spectrometry. *Acs Nano*. 2016;10(7):6731-6.
229. Reifarth M, Schubert US, Hoepfner S. Considerations for the Uptake Characteristic of Inorganic Nanoparticles Into Mammalian Cells—Insights Gained by TEM Investigations. *Advanced Biosystems*. 2018;2(8).
230. Briley-Saebo K, Bjørnerud A, Grant D, Ahlstrom H, Berg T, Kindberg GM. Hepatic cellular distribution and degradation of iron oxide nanoparticles following single intravenous injection in rats: implications for magnetic resonance imaging. *Cell and Tissue Research*. 2004;316(3):315-23.
231. Ezhilarasan D, Shree Harini K. Nanodrug delivery: Strategies to circumvent nanoparticle trafficking by Kupffer cells in the liver. *Journal of Drug Delivery Science and Technology*. 2023;86:104731.
232. Gustafson HH, Holt-Casper D, Grainger DW, Ghandehari H. Nanoparticle uptake: The phagocyte problem. *Nano Today*. 2015;10(4):487-510.
233. Park EI, Mi Y, Unverzagt C, Gabius HJ, Baenziger JU. The asialoglycoprotein receptor clears glycoconjugates terminating with sialic acid alpha 2,6GalNAc. *Proc Natl Acad Sci U S A*. 2005;102(47):17125-9.
234. FDA. The Use of Bovine Milk-derived Lactoferrin [updated 12.09.2016. Available from: <https://www.fda.gov/media/124472/download>.
235. Rosa L, Cutone A, Lepanto M, Paesano R, Valenti P. Lactoferrin: A Natural Glycoprotein Involved in Iron and Inflammatory Homeostasis. *International Journal of Molecular Sciences*. 2017;18(9):1985.
236. Gupta AK, Curtis ASG. Lactoferrin and ceruloplasmin derivatized superparamagnetic iron oxide nanoparticles for targeting cell surface receptors. *Biomaterials*. 2004;25(15):3029-40.
237. Ashida K, Sasaki H, Suzuki YA, Lönnnerdal B. Cellular internalization of lactoferrin in intestinal epithelial cells. *BioMetals*. 2004;17(3):311-5.

238. McAbee DD, Jiang X, Walsh KB. Lactoferrin binding to the rat asialoglycoprotein receptor requires the receptor's lectin properties. *Biochem J.* 2000;348 Pt 1(Pt 1):113-7.
239. D'Souza AA, Devarajan PV. Asialoglycoprotein receptor mediated hepatocyte targeting — Strategies and applications. *Journal of Controlled Release.* 2015;203:126-39.
240. Mishra N, Yadav NP, Rai VK, Sinha P, Yadav KS, Jain S, et al. Efficient hepatic delivery of drugs: Novel strategies and their significance. *BioMed Res Int.* 2013;2013.
241. Bennett DJ, McAbee DD. Identification and Isolation of a 45-kDa Calcium-Dependent Lactoferrin Receptor from Rat Hepatocytes. *Biochemistry.* 1997;36(27):8359-66.
242. Agwa MM, Sabra S. Lactoferrin coated or conjugated nanomaterials as an active targeting approach in nanomedicine. *International Journal of Biological Macromolecules.* 2021;167:1527-43.
243. Asthana S, Gupta PK, Jaiswal AK, Dube A, Chourasia MK. Targeted chemotherapy of visceral leishmaniasis by lactoferrin-appended amphotericin B-loaded nanoreservoir: in vitro and in vivo studies. *Nanomedicine.* 2015;10(7):1093-109.
244. Hu K, Li J, Shen Y, Lu W, Gao X, Zhang Q, et al. Lactoferrin-conjugated PEG-PLA nanoparticles with improved brain delivery: In vitro and in vivo evaluations. *Journal of Controlled Release.* 2009;134(1):55-61.
245. Erickson HP. Size and shape of protein molecules at the nanometer level determined by sedimentation, gel filtration, and electron microscopy. *Biol Proced Online.* 2009;11:32-51.
246. Bi C, Wang A, Chu Y, Liu S, Mu H, Liu W, et al. Intranasal delivery of rotigotine to the brain with lactoferrin-modified PEG-PLGA nanoparticles for Parkinson's disease treatment. *International Journal of Nanomedicine.* 2016;11(null):6547-59.
247. Hu K, Shi Y, Jiang W, Han J, Huang S, Jiang X. Lactoferrin conjugated PEG-PLGA nanoparticles for brain delivery: Preparation, characterization and efficacy in Parkinson's disease. *International Journal of Pharmaceutics.* 2011;415(1):273-83.
248. Plaut AG, Geme JS. Chapter 805 - Lactoferrin. In: Rawlings ND, Salvesen G, editors. *Handbook of Proteolytic Enzymes (Third Edition)*: Academic Press; 2013. p. 3635-40.
249. Bourbon AI, Martins JT, Pinheiro AC, Madalena DA, Marques A, Nunes R, et al. 6 - Nanoparticles of lactoferrin for encapsulation of food ingredients. In: Jafari SM, editor. *Biopolymer Nanostructures for Food Encapsulation Purposes*: Academic Press; 2019. p. 147-68.
250. Wei M, Xu Y, Zou Q, Tu L, Tang C, Xu T, et al. Hepatocellular carcinoma targeting effect of PEGylated liposomes modified with lactoferrin. *European Journal of Pharmaceutical Sciences.* 2012;46(3):131-41.
251. Li H, Tong Y, Bai L, Ye L, Zhong L, Duan X, et al. Lactoferrin functionalized PEG-PLGA nanoparticles of shikonin for brain targeting therapy of glioma. *International Journal of Biological Macromolecules.* 2018;107:204-11.
252. Kowalczyk P, Kaczyńska K, Kleczkowska P, Bukowska-Oško I, Kramkowski K, Sulejczak D. The Lactoferrin Phenomenon—A Miracle Molecule. *Molecules.* 2022;27(9):2941.

253. Kumari S, Kondapi AK. Lactoferrin nanoparticle mediated targeted delivery of 5-fluorouracil for enhanced therapeutic efficacy. *International Journal of Biological Macromolecules*. 2017;95:232-7.
254. Harris RL, van den Berg CW, Bowen DJ. ASGR1 and ASGR2, the Genes that Encode the Asialoglycoprotein Receptor (Ashwell Receptor), Are Expressed in Peripheral Blood Monocytes and Show Interindividual Differences in Transcript Profile. *Mol Biol Int*. 2012;2012:283974.
255. Elzoghby AO, Abdelmoneem MA, Hassanin IA, Abd Elwakil MM, Elnaggar MA, Mokhtar S, et al. Lactoferrin, a multi-functional glycoprotein: Active therapeutic, drug nanocarrier & targeting ligand. *Biomaterials*. 2020;263:120355.
256. Saraswat A, Vemana HP, Dukhande VV, Patel K. Galactose-decorated liver tumor-specific nanoliposomes incorporating selective BRD4-targeted PROTAC for hepatocellular carcinoma therapy. *Heliyon*. 2022;8(1):e08702.
257. Park J-K, Utsumi T, Seo Y-E, Deng Y, Satoh A, Saltzman WM, et al. Cellular distribution of injected PLGA-nanoparticles in the liver. *Nanomedicine: Nanotechnology, Biology and Medicine*. 2016;12(5):1365-74.
258. Weber C, Coester C, Kreuter J, Langer K. Desolvation process and surface characterisation of protein nanoparticles. *International Journal of Pharmaceutics*. 2000;194(1):91-102.
259. Hassanin I, Elzoghby A. Albumin-based nanoparticles: a promising strategy to overcome cancer drug resistance. *Cancer Drug Resist*. 2020;3(4):930-46.
260. Qi J, Yao P, He F, Yu C, Huang C. Nanoparticles with dextran/chitosan shell and BSA/chitosan core—Doxorubicin loading and delivery. *International Journal of Pharmaceutics*. 2010;393(1):177-85.
261. Rohiwal SS, Satvekar RK, Tiwari A, Raut A, Kumbhar SG, Pawar SH. Investigating the Influence of Effective Parameters on Molecular Characteristics of Bovine Serum Albumin Nanoparticles. *Applied Surface Science*. 2015(334):157-64.
262. Galisteo-González F, Molina-Bolívar JA. Systematic study on the preparation of BSA nanoparticles. *Colloids and Surfaces B: Biointerfaces*. 2014;123:286-92.
263. Rahimnejad M, Najafpour G, Bakeri G. Investigation and modeling effective parameters influencing the size of BSA protein nanoparticles as colloidal carrier. *Colloids and Surfaces A: Physicochemical and Engineering Aspects*. 2012;412:96-100.
264. Zhou L, Wang K, Wu Z, Dong H, Sun H, Cheng X, et al. Investigation of Controllable Nanoscale Heat-Denatured Bovine Serum Albumin Films on Graphene. *Langmuir*. 2016;32(48):12623-31.
265. Nguyen HH, Ko S. Preparation of Size-Controlled BSA Nanoparticles by Intermittent Addition of Desolvating Agent. 2010:231-4.
266. Marty JJ, Oppenheim RC, Speiser P. Nanoparticles--a new colloidal drug delivery system. *Pharm Acta Helv*. 1978;53(1):17-23.
267. Jun JY, Nguyen HH, Paik S-Y-R, Chun HS, Kang B-C, Ko S. Preparation of size-controlled bovine serum albumin (BSA) nanoparticles by a modified desolvation method. *Food Chemistry*. 2011;127(4):1892-8.
268. Amighi F, Emam-Djomeh Z, Labbafi-Mazraeh-Shahi M. Effect of different cross-linking agents on the preparation of bovine serum albumin nanoparticles. *Journal of the Iranian Chemical Society*. 2020;17(5):1223-35.



269. Barbinta-Patrascu M-E, Iftimie S, Cazacu N, Stan DL, Costas A, Balan AE, et al. Bio-Entities Based on Albumin Nanoparticles and Biomimetic Cell Membranes: Design, Characterization and Biophysical Evaluation. *Coatings*. 2023;13(4):671.
270. FDA SCOGS 2023 [updated 17.10.2023. Available from: <https://www.cfsanappsexternal.fda.gov/scripts/fdcc/?set=SCOGS>.
271. Wang Y, Chen S, Yang X, Zhang S, Cui C. Preparation Optimization of Bovine Serum Albumin Nanoparticles and Its Application for siRNA Delivery. *Drug Des Devel Ther*. 2021;15:1531-47.
272. Rohiwal SS, Tiwari AP, Verma G, Pawar SH. Preparation and evaluation of bovine serum albumin nanoparticles for ex vivo colloidal stability in biological media. *Colloids and Surfaces A: Physicochemical and Engineering Aspects*. 2015;480:28-37.
273. Liu S, Liu M, Xiu J, Zhang T, Zhang B, Cun D, et al. Celastrol-loaded bovine serum albumin nanoparticles target inflamed neutrophils for improved rheumatoid arthritis therapy. *Acta Biomaterialia*. 2023;15(174):345-57.
274. Dumetz AC, Snellinger-O'brien A M, Kaler EW, Lenhoff AM. Patterns of protein protein interactions in salt solutions and implications for protein crystallization. *Protein Sci*. 2007;16(9):1867-77.
275. Parmar AS, Muschol M. Hydration and Hydrodynamic Interactions of Lysozyme: Effects of Chaotropic versus Kosmotropic Ions. *Biophysical Journal*. 2009;97(2):590-8.
276. Annunziata O, Payne A, Wang Y. Solubility of Lysozyme in the Presence of Aqueous Chloride Salts: Common-Ion Effect and Its Role on Solubility and Crystal Thermodynamics. *Journal of the American Chemical Society*. 2008;130(40):13347-52.
277. Solanki R, Rostamabadi H, Patel S, Jafari SM. Anticancer nano-delivery systems based on bovine serum albumin nanoparticles: A critical review. *International Journal of Biological Macromolecules*. 2021;193:528-40.
278. Lankoff A, Sandberg WJ, Wegierek-Ciuk A, Lisowska H, Refsnes M, Sartowska B, et al. The effect of agglomeration state of silver and titanium dioxide nanoparticles on cellular response of HepG2, A549 and THP-1 cells. *Toxicology Letters*. 2012;208(3):197-213.
279. Wu Y, Gu J, Zhang S, Gu Y, Ma J, Wang Y, et al. Iodinated BSA Nanoparticles for Macrophage-Mediated CT Imaging and Repair of Gastritis. *Analytical Chemistry*. 2021;93(16):6414-20.
280. Jose P, Sundar K, Anjali CH, Ravindran A. Metformin-Loaded BSA Nanoparticles in Cancer Therapy: A New Perspective for an Old Antidiabetic Drug. *Cell Biochemistry and Biophysics*. 2015;71(2):627-36.
281. Woods A, Patel A, Spina D, Rizzo-Vasquez Y, Babin-Morgan A, de Rosales RTM, et al. In vivo biocompatibility, clearance, and biodistribution of albumin vehicles for pulmonary drug delivery. *Journal of Controlled Release*. 2015;210:1-9.
282. Schildberger A, Rossmanith E, Eichhorn T, Strassl K, Weber V. Monocytes, Peripheral Blood Mononuclear Cells, and THP-1 Cells Exhibit Different Cytokine Expression Patterns following Stimulation with Lipopolysaccharide. *Mediators of Inflammation*. 2013;2013:1-10.
283. Ahmed LB, Milić M, Pongrac IM, Marjanović AM, Mlinarić H, Pavičić I, et al. Impact of surface functionalization on the uptake mechanism and toxicity effects

- of silver nanoparticles in HepG2 cells. *Food and Chemical Toxicology*. 2017;107:349-61.
284. Thao LQ, Lee C, Kim B, Lee S, Kim TH, Kim JO, et al. Doxorubicin and paclitaxel co-bound lactosylated albumin nanoparticles having targetability to hepatocellular carcinoma. *Colloids and Surfaces B: Biointerfaces*. 2017;152:183-91.
285. Ray S, Mishra A, Mandal TK, Sa B, Chakraborty J. Optimization of the process parameters for the fabrication of a polymer coated layered double hydroxide-methotrexate nanohybrid for the possible treatment of osteosarcoma. *RSC advances*. 2015;5(124):102574-92.
286. Lu B, Lv X, Le Y. Chitosan-Modified PLGA Nanoparticles for Control-Released Drug Delivery. *Polymers (Basel)*. 2019;11(2).
287. Mu JZ, Tang LH, Alpers DH. Asialoglycoprotein receptor mRNAs are expressed in most extrahepatic rat tissues during development. *Am J Physiol*. 1993;264(4 Pt 1):G752-62.
288. Pazdzior R, Kubicek S. PlateFlo - A software-controllable plate-scale perfusion system for culture of adherent cells. *HardwareX*. 2021;10:e00222.

## **Chapter 8: SUPPLEMENTARY FIGURES**

Fluorescent microscopy images

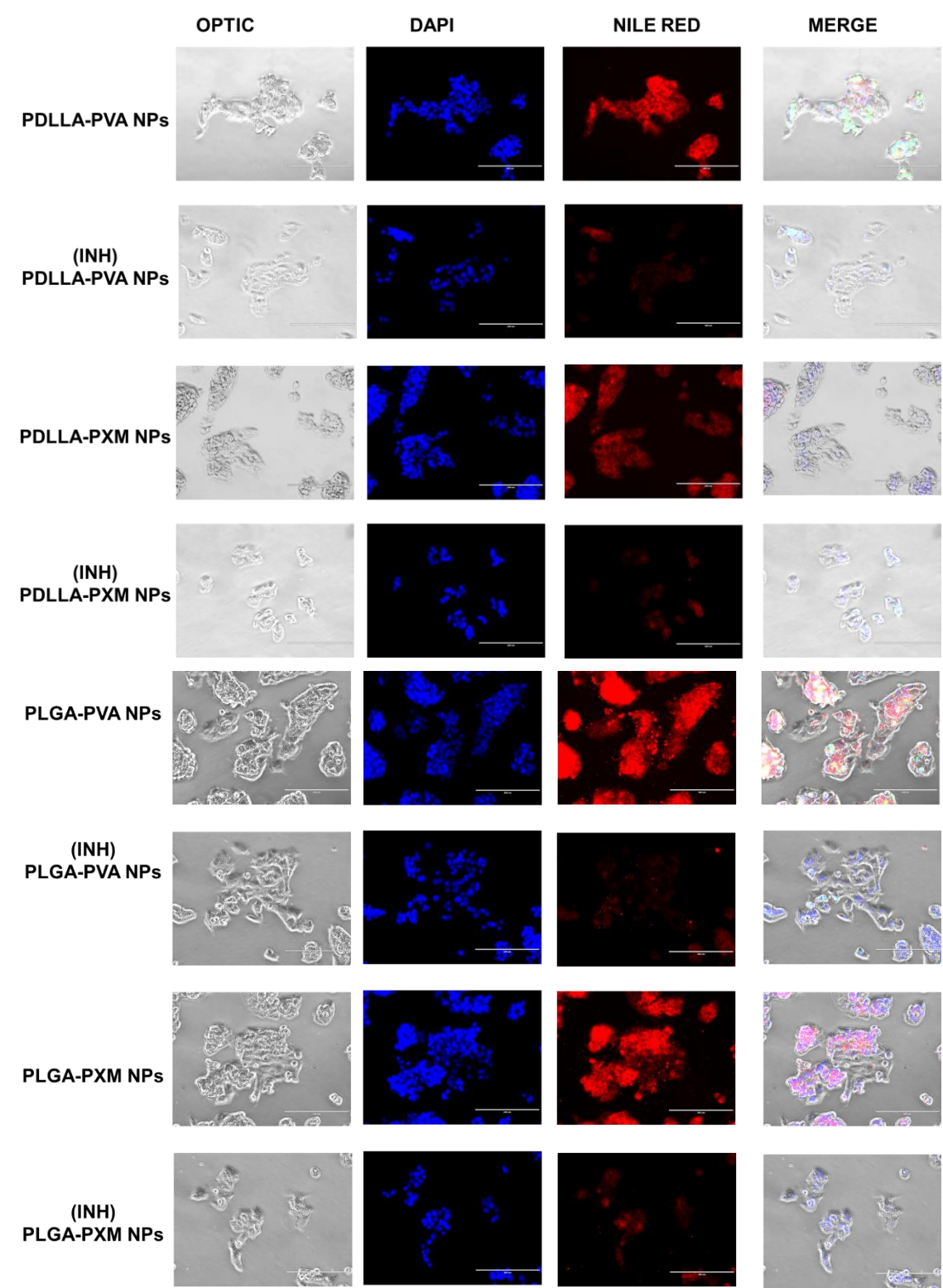


**Figure S 1 HEP-G2 fluorescent microscopy images.** Cells were treated with PDLLA and PLGA NPs for one hour (bars represent 200  $\mu$ m length)

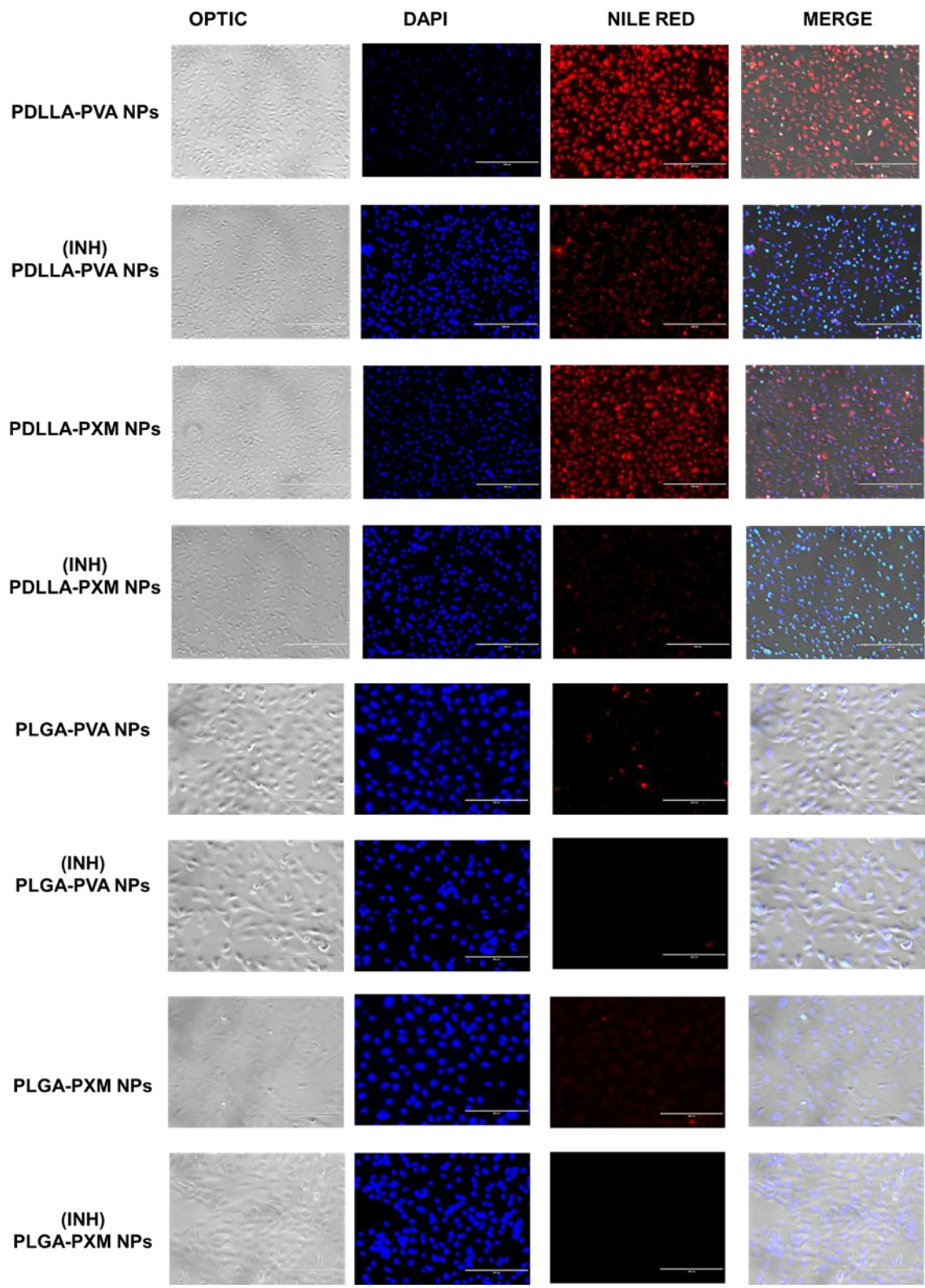


**Figure S 2 HMEC-1 fluorescent microscopy images.** Cells were treated with PDLLA (bars represent 200  $\mu\text{m}$  length) and PLGA NPs for one hour (bars represent 400  $\mu\text{m}$  length).



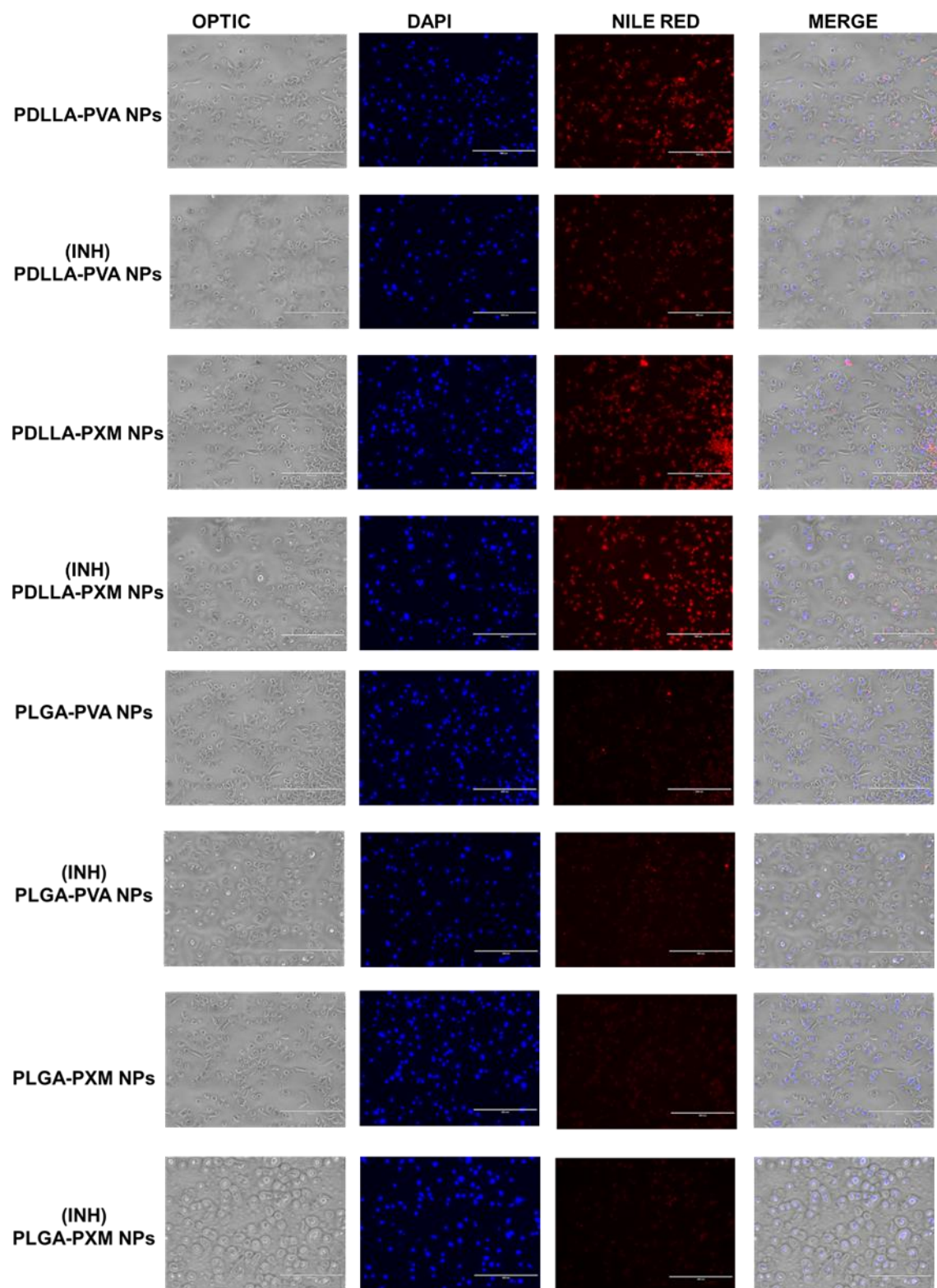


**Figure S 3 DTHP-1 fluorescent microscopy images.** Cells were treated with PDLLA and PLGA NPs for one hour (bars represent 200  $\mu$ m length)

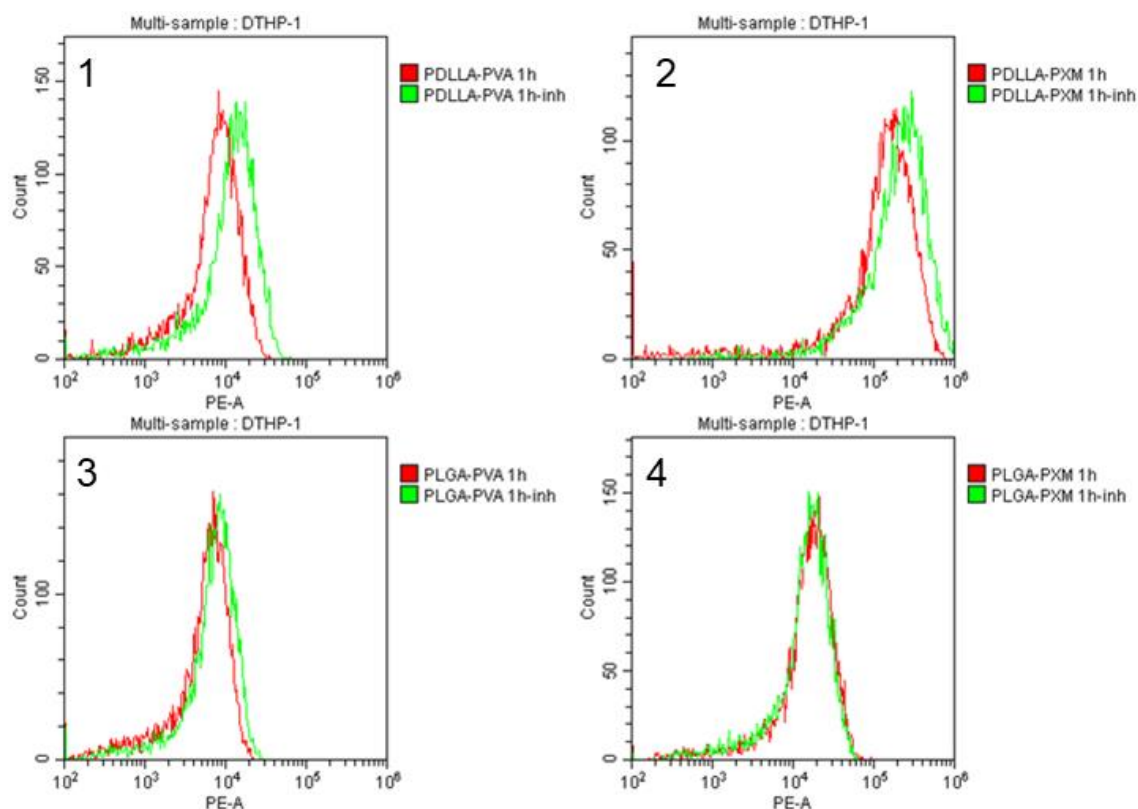


**Figure S 4. Uptake on NPs by DTHP-1 cells.** Uptake of PDLLA and PLGA NPs was assessed in the absence and presence of sodium azide by flow cytometry at 1h. (1) PDLLA-PVA, (2) PDLLA-PXM, (3) PLGA-PVA, (4) PLGA-PXM. Addition of  $\text{NaN}_3$  did not decrease NP uptake by DTHP-1 cells according to flow cytometry.